Biochar as a support for nanocatalysts and other reagents: Recent advances and applications

Renata Pereira Lopes, Didier Astruc

Biochar as a support for nanocatalysts and other reagents: recent advances and applications.

Renata Pereira Lopes[a,b] and Didier Astruc[b]

[a]Department of Chemistry, Universidade Federal de Viçosa, Viçosa/MG, Brazil, 36570-900

[b]Université de Bordeaux, ISM, UMR CNRS 5255, Talence 33405 Cedex, France

renata.plopes@ufv.br

didier.astruc@u-bordeaux.fr

Abstract

The transformation and use of the biomass are of fundamental energetic and ecological interest. The general objective of this review is to provide an overview of biochar (a major biomass product) as a support for nanocatalysts and other reagents, its mode of coordination and activation with nanoparticles and applications. This includes the physico-chemical characteristics of biochar, the advances in its production processes, and its activation and functionalization in order to improve its physical and chemical characteristics and applications as support in catalysis and environmental decontamination. Biochar is a by-product produced by carbonization of biomass. In this process, the products of interest are syngas and bio-oil, due to their high calorific value and their diverse applications. However, biochar has interesting characteristics. It can be used as support, allowing to disperse nanoparticles of the catalysts, such as those of the transition metals: Fe, Ag, Ni, Pd, etc., bimetallic compositions such as Ru/Re, Fe/Ni, etc. and metal oxides such as Fe_3O_4, CO_3O_4, CuO, TiO_2, etc., increasing the reactivity of the system, minimizing the leaching of the catalysts and allowing their re-use. These materials can be employed in the degradation of contaminants in aqueous systems, soil and sediments, tar reforming reactions and synthesis of fine chemicals. This review will serve as the basis for new research aiming to add value to this important resource.

Keywords: Sustainability, biomass, biochar, catalyst support, metal catalyst, nanocatalysis.

Contents

1 List of abbreviations

AOPs	Advanced oxidation processes
BC	Biochar
CQDs	Carbon Quantum Dots
FRs	Free radicals
HMF	hydroxymethylfurfural
HP	Hydrogen peroxide
HTC	Hydrothermal carbonization
NPs	Nanoparticles
nZVI	Nano-Zero-valent Iron
PMS	Peroxymonosulfate anion
PS	Persulfate anion
ZVI	Zero Valent Iron

2

1. Introduction

Due to the growing environmental pollution, practices are being encouraged all over the world to minimize the impacts caused by man. One of the bottlenecks to ensure the sustainable use of natural resources is mainly the use of fuels to generate energy. In this sense, the use of biomass from agro industry waste for energy generation has been extensively studied in recent years.

In Brazil, agribusiness in 2019 represented 21.4% of the total Brazilian Gross Domestic Product [1]. Although it is important to a country's economy, agribusiness generates a large amount of waste. The annual biomass waste generated in the world is in the order of 140 Gt [2]. These residues resulting from agro-industrial activities are generated in the processing *inter alia* of leather, fibers, food, wood, sugar and alcohol production. The composition of agricultural residues is similar to other lignocellulosic materials: cellulose (40–50%), hemicellulose (20–30%), lignin (20–25%) and ash (1–5%) [3], [4]. Many of these residues represent safety and environmental liabilities. In order to guarantee the sustainability of the process, research has been directed towards guaranteeing zero waste. The development of technologies oriented towards a circular economy in agribusiness is one of the strategic directions in the sustainability of these productive chains [5]. In this sense, the production of energy from biomass is a practice that has been widely studied.

The waste biomass is a clean, sustainable and renewable energy source and is obtained by residues from agricultural production, processing industries and social activities being available in large quantities [6], [7], [8]. The use of biomass residues has a win-win effect for carbon sequestration and water pollution control [9]. Energy recovery from these residues has become an important alternative to replace conventional fossil fuels like coal [10]. Among the processes for obtaining bio-oil from biomass, pyrolysis is the most commonly used. This occurs, because pyrolysis has increased attention as an acceptable route for waste disposal due to product selectivity, process scalability and versatility [11]. In this process, syngas, bio oil and biochar are generated. Depending on temperature and residence time, maximum gas or liquid yields are produced. Slow-conventional pyrolysis is applied to produce high charcoal yields, while fast or flash pyrolysis is associated with a high reduction in the solid yield [3].

Bio-oil, also called pyrolysis oil or liquid fraction converted from biomass, can replace heavy fuel oil, light fuel oil or natural gas in a wide variety of equipment

installations, including boilers, turbines and gas and other heating and power generation devices [12]. The significant amount of biochar produced during the process of obtaining bio-oil is one of the obstacles to the industrialization of biomass thermal conversion technology [13]. In general, the biochar is treated inappropriately as an industrial waste; however, its use for immobilization of organic carbon is beneficial for mitigating the greenhouse effect [14], [15]. Thus, the production of new value-added biochar products is very important for economy and management of energy resources.

Although the main element present in the structure of the biochar is carbon (C), its elemental composition tends to vary according to the production conditions of the biochar and the raw material used to produce it [16]. In general, biochar contains, in addition to carbon (C), hydrogen (H), oxygen (O) and small amounts of nitrogen (N) and sulfur (S) [17]. In addition, biochar contains stacks of graphite agglomerates that contain layers of graphene and graphene oxide (GO) whose edge carbons are reactive because they present groups such as -COOH; -OH and -O-, acting as CO_2 binding sites [18]. There are two factors that can impact the biochar surface property: (1) the type of biomass feedstock and (2) the carbonization approach that transfers biomass into biochar [19].

Biochar was introduced in daily life with the main function of soil alteration, due to its positive role in carbon sequestration, in reduction in greenhouse gas emissions and improvement of soil fertility [20]. Its use dates from 100-450 BC by the Amazon tribes making the “terra preta”, from Portuguese, which means black earth [21]. In the soil, the biochar reduces soil acidity, adsorbs and immobilizes nutrients and reduces greenhouse gas emissions (N_2O, up to 80%, and CH_4) from plants [18], [22]. Nowadays, biochar can be used for catalyst production [23], biodiesel production [24], and mainly, as soil additives [25]. The use as an adsorbent material for water and air pollutants is due to its main characteristics that are, as a general rule, large specific surface area, extensive microstructure, porous structure, functional groups of the surface, high nutrient content and great water storage capacity [26], [27], [28]. Besides, they have high chemical stability that allows them to operate in corrosive environments and good electrical conductivity [29], [30].

Other applications of biochar have also been studied, such as its uses for the production of fuel cells [31], [32], [33], supercapacitors [34], [35] and as support in catalysis for the production of new composites as metallic nanoparticles (NPs) [36], [37], [38].

Catalysts based on metallic and bimetallic NPs and their oxides are very efficient in reactions of economic interest, such as fine chemistry [39], [40], [41] or in the removal of contaminants [42], [43], [44], [45]. However, one of their disadvantages is their strong aggregation. Thus, depositing them on a support significantly improves their efficiency.

Studies involving biochar have been reported for decades, and as of 2010, as shown in Fig. 1, the number of publications increased considerably, reaching 3115 publications in 2019, according to data extracted from the Web of Science database in April/2020. Its use as a support in catalysis has increased more modestly, and in 2019 the number of publications was 196 publications as can be seen in the insert in Fig. 1. Other applications of biochar can also be viewed, such as catalysis, photocatalysis and persulfate activation. It is believed that the number of publications involving the use of biochar as a support in catalysis will increase considerably in the next years. This is because biochar can disperse and stabilize engineered NPs to further enhance their stability and mobility.

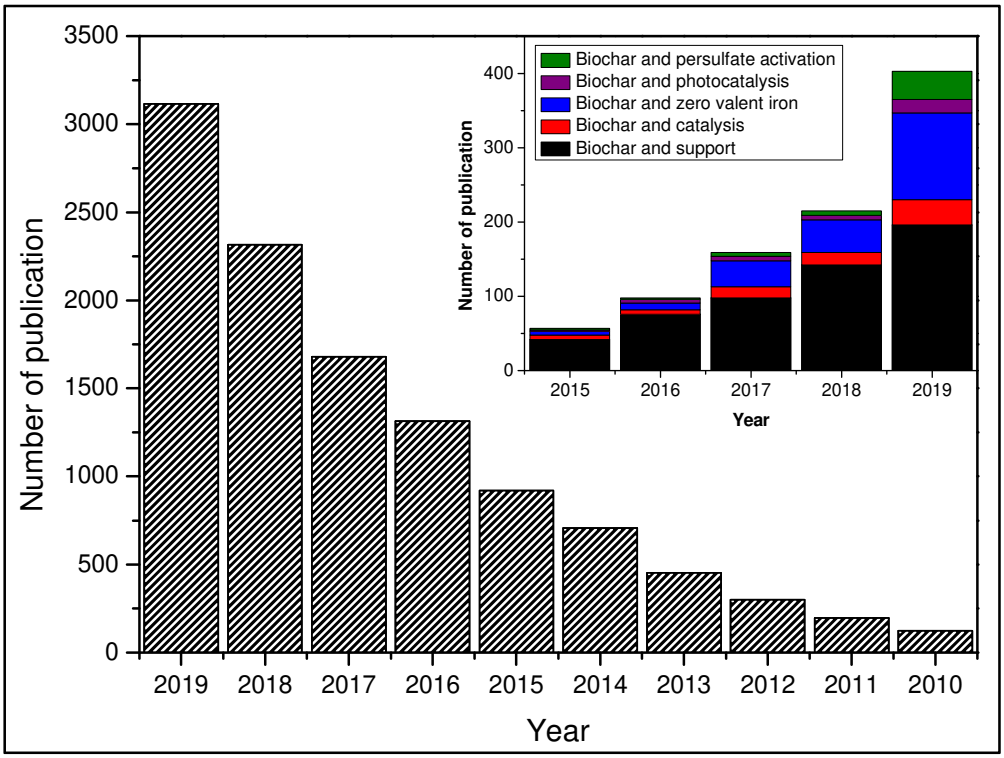

Fig.1. Database: Web of Science, search day: 04/14/2020. Search terms: "Biochar" Insert: Search terms: "Biochar and support"; "Biochar and catalysis", "Biochar and zero valent iron", "Biochar and photocatalysis" and "Biochar and persulfate activation"

The general objective of this review is to provide an overview of the biochar's physical-chemical characteristics, advances in biochar production processes, activation

and functionalization of biochar in order to improve its physical and chemical characteristics, and applications as a support for different catalysts and reagents used in different types of reactions and environmental decontaminations. The use of biochar as a support for metallic NPs and their oxides for the remediation of contaminants in aqueous systems and sediments, activation of oxidants such as peroxide and persulfate and photocatalysis are discussed as well as other applications such as the synthesis of fine chemicals and tar reforming. This review will serve as base for new research aiming to add value to this important resource that is produced in large quantities in the world.

2. Biochar

After oxygen, carbon is the most abundant element in the biosphere, being used by nature as a basis for the storage of renewable energy in the form of carbohydrates [46]. Carbon-based materials have been recognized with the highest scientific awards, including the 1996 Nobel Prize in Chemistry (fullerenes), the 2008 Kavli Prize for Nanoscience (carbon nanotubes) and the 2010 Nobel Prize in Physics (graphene) [46].

Unlike commercial carbon materials (activated carbon, graphene and carbon nanotubes) whose source materials are restricted to some agricultural products, biochar can be produced from practically all biomass, from organic raw materials to organic waste [47]. As previously mentioned, the production of energy from agribusiness residues leads to three products: syngas, bio oil and biochar. The characteristics and main processes for obtaining the biochar are discussed in the following sections.

2.1. Biochar characteristics

Generally, the raw material used to produce biochar from agro-industrial residues consists mainly of hemicellulose, cellulose and lignin as well as some inorganic minerals [6]. Biomass such as *inter alia* sugarcane bagasse, coffee straw, soy straw, rice straw, corn cob can be cited as examples. The structure and physicochemical properties of biochar, which are closely dependent on the conditions of the process, affect the way in which it interacts with organic and inorganic compounds [48]. According to Ahmed (2016) the biochar quality characteristics will change along several dimensions according to final pyrolysis temperature, heating rate

and residence time [49]. In these processes Hierarchical Porous Carbon are generated that refers to carbon materials with two or more different pore sizes, integrating the advantages of micropores, mesopores and macropores [50]. It is important to mention that macropores and mesopores contribute to the rapid transport of ions through the channels of micropores [51]. The type of feedstock material is an important factor that determines the final application, because its properties are affected by the nature of the original material [52]. Organic matter undergoes thermal decomposition with moisture loss at temperatures up to about 120 °C [53]. Hemicellulose decomposes at 220-330 °C, cellulose at 315-400 °C, while lignin gradually decomposes in the temperature range 150-600 °C [54], [55].

Biochar is considered as a highly aromatic compound, containing layers of graphene and graphite structures, randomly arranged [56]. The ordered basal carbons of the aromatic leaf have high concentrations of delocalized π electrons and are therefore considered as Lewis bases [48]. Biochar generally has less aromaticity and hydrophobicity than activated carbon, because it contains more non-carbonized organic matter [57]. The aromaticity of biochar produced depends on the conditions of synthesis. In their work, Park et al. (2019) found that the production of biochar from Debarked loblolly pine (Pinus taeda) at a higher temperature (700 °C) in a nitrogen atmosphere containing 7% oxygen in the pyrolysis stage favored the production of clusters containing a higher number of carbons (C59) [58], as shown in Fig. 2.

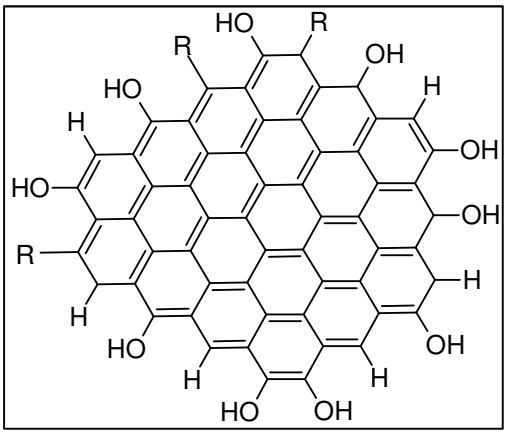

Fig. 2. Minimum estimated number of carbons in an aromatic cluster (C59), pyrolysate at 700 °C under an N_2 atmosphere (93%) containing 7% CO_2. Adapted from: Impact of oxidative carbonization on structure development of loblolly pine-derived biochar investigated by nuclear magnetic resonance spectroscopy and X-ray photoelectron spectroscopy, 96, Park, J. *et al.* Copyright (2019), with permission from Elsevier, License number: 4856490763912, https://doi.org/10.1016/j.diamond.2019.05.001 [58].

Xiao and Chen (2017) proposed a quaternary structure for biochar that includes heterogeneous phases, graphene-like aggregates, nanosized aromatic clusters and

atomic arrangements, as shown in Fig. 3. This quaternary model illustrates biochar structures of the macro to atomic scale [59].

The carbonization promotes the formation of some functional groups on biochar surface such as hydroxyl (OH), carbonyl (CO) and carboxyl ((CO)OH) [60]. Therefore, infrared analysis of the biochar shows characteristic bands of these organic groups, as indicated in Table 1. For C1s X-ray photoelectron spectroscopy (XPS) peaks appear at 284.7 eV, 286.0 eV, and 287.2 eV that are attributed to C–C, CO and CO-= [61],[62]. X-Ray Diffraction (DRX) analysis shows biochar diffraction peaks at 23.3-26.4° and 42.5-44°, that represent (002) and (100) diffraction planes of graphite [63], [64], [65].

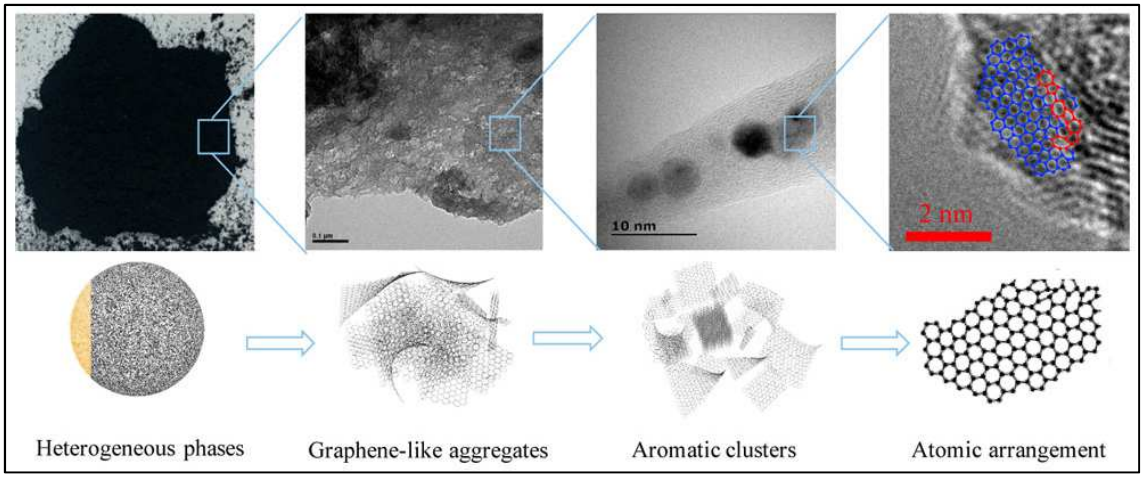

Fig. 3. Quaternary structure of biochar. Reproduced from: A direct observation of the fine aromatic clusters and molecular structures of biochars, 51, Xiao, X. et al. Copyright (2017), with permission from ACS, https://pubs.acs.org/doi/10.1021/acs.est.6b06300. Further permission related to this material excerpted should be directed to the ACS [59].

Table 1. Main bands of organic groups found in biochar

Wave number (cm^{-1})	Vibration type	Ref.
3400-3431	Stretching of O-H	[66],[67],[61],[68],[65]
2930 and 2890	asymmetric and symmetric stretches of aliphatic C-H	[67], [65]
2372	Stretching of $-CH_2$	[66]
1590-1703	Carbonyl/carboxyl C=O stretching vibration	[67], [61], [65]
1621-1643 and 1388-1420	Vibration of C=C	[66], [67], [68]
1033-1103	Vibration of C-O	[66],[67],[61],[68],[65]

The Raman spectra of biochar samples present a D band at 1341-1360 cm^{-1} due stemming from the breathing mode of A1g symmetry that is forbidden in perfect graphite and only becomes active in the presence of disorders often referred to

amorphous carbon, and a G band at 1580-1594 cm^{-1} that represent the in-plane bond-stretching motion of pairs of sp^2 carbon atoms in chains and rings demonstrating the existence of graphitic carbon [69], [59]. The ratio of the intensity of these two peaks (I_D/I_G) represents the degree of disorder of carbon materials [66], [63], [65]. Sun et al. (2020) observed that the I_D/I_G ratio of BC500 considerably increased from 0.737 to 1.150 after CO_2 activation from 950 °C, Fig. 4 [63].

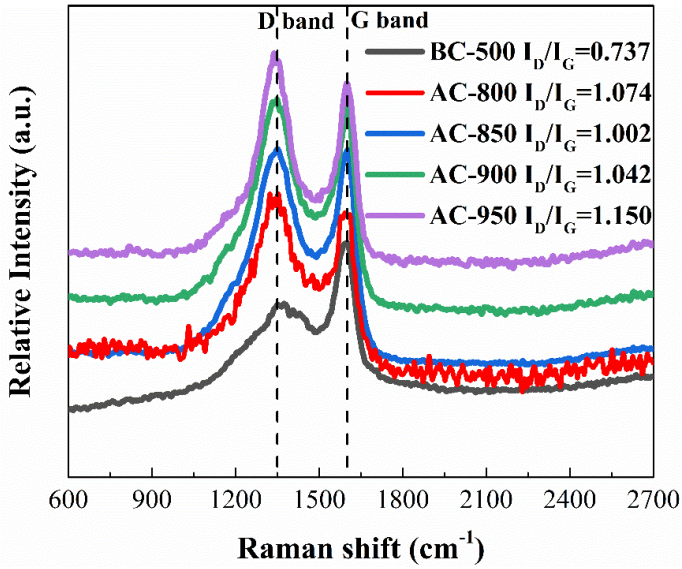

Fig 4. Raman spectra of the five biochar (BC) activated by CO_2 atmosphere at different temperatures. Reproduced from: Activation of persulfate by CO_2-activated biochar for improved phenolic pollutant degradation: performance and mechanism, 380, Sun, C. *et al.* Copyright (2020), with permission from Elsevier, License number: 4843540842806, https://doi.org/10.1016/j.cej.2019.122519 [63].

Zhang et al. (2018) proposed the contribution of the ice-type adlayer (agglomerates of water) to the aromatic surface of the biochar as acceptors of H of ionizable organic pollutants (IOPs) in the adsorption process. According to the authors, when biochar is in water, each water molecule turns a hydrogen atom pointing to an aromatic ring (H ⋯ π interactions), Fig. 5a. Another hydrogen atom bonds to the oxygen atom of a lateral water molecule due to Polarization-Assisted or σ-Bond Cooperative H-Bond (PAHB), Fig. 5b. Therefore, these water molecules and the coronene form a complex with six adsorption sites, which leads to the electronegative oxygen atom (H acceptor), Fig. 5c. This complex is linked to H donor by H bonds of IOPs (Ionizable Organic Products). Then, the hydrogen atom of the IOP considered to be hydrogen donor is linked to the oxygen atom of the complex by polarization-assisted H bond, Fig. 5d and 5e [70].

Another interesting feature is the presence of free radicals (FRs) in materials obtained through combustion. Fang et al. (2015) found that suspensions of biochar are

capable of generating hydroxyl radicals without the addition of H_2O_2. According to the authors, (i) the free radicals (FRs) present in biochar suspensions transfer electrons to O_2 to form $^{\bullet}O_2^-$; (ii) $^{\bullet}O_2^-$ accepts an electron from FR to produce H_2O_2; (iii) H_2O_2 reacts with FRs to form $^{\bullet}OH$ radical through a single electron transfer process, as shown in the Eq. 1-4 [22].

$$O_2 + e^- \rightarrow {}^{\bullet}O_2^- \quad \text{(Eq. 1)}$$

$$H^+ + {}^{\bullet}O_2^- \rightarrow HO_2^{\bullet} \quad \text{(Eq. 2)}$$

$$2HO_2^{\bullet} \rightarrow H_2O_2 + O_2 \quad \text{(Eq. 3)}$$

$$H_2O_2 + e^- + H^+ \rightarrow {}^{\bullet}OH + H_2O \quad \text{(Eq. 4)}$$

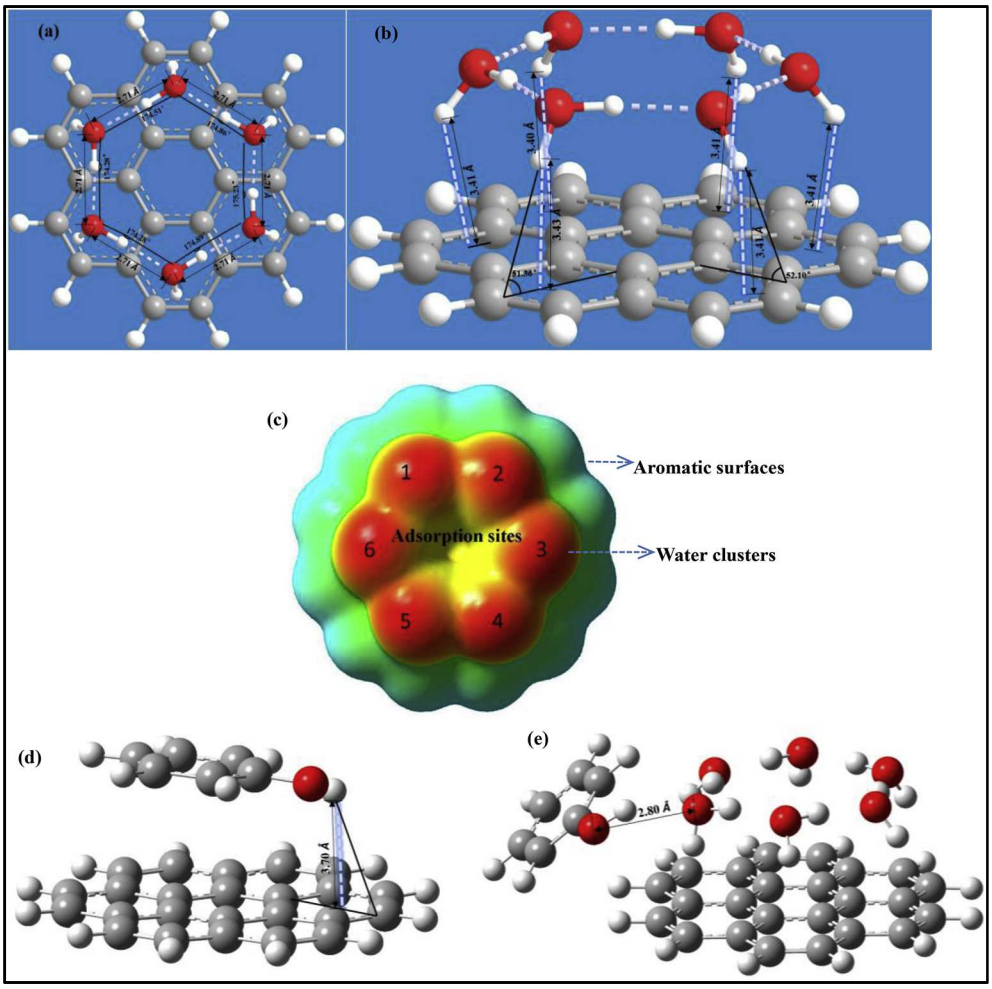

Fig. 5. Structural details of the complex of coronene with a cyclic chair water clusters (a, b, and c), phenol adsorbed on a coronene (d), and phenol adsorbed on the complex (e). Reproduced from: Water clusters contributed to molecular interactions of ionizable organic pollutants with aromatized biochar via π-PAHB: Sorption experiments and DFT calculations, 240, Zhang, K. *et al.* Copyright (2018), with permission from Elsevier, License number: 4843540657075, https://doi.org/10.1016/j.envpol.2018.04.083 [70].

Wenmei et al. (2020) investigated the formation of persistent free radicals (PFRs) in rice husk biochar by monitoring the pyrolysis kinetics of the material. These authors found that lignin started to pyrolyze at a lower temperature than cellulose and hemicellulose, and lignin was the main factor for the generation of PFRs. The breakdown of chemical bonds contributed only slightly to the formation of PFRs. The reconfiguration of carbonaceous structures is a more important contributor to the formation of PFRs, whereas the crosslinking between different compositions and the interactions between inorganic chemical and mineral compositions play a significant role in the generation and stabilization of PFR in biochar [6].

Recently, biochar has been used as electron-transfer catalyst in redox reactions of environmental relevance [71]. The electron-transfer mode of biochar occurs by three types of active redox structures: the quinones that accept electrons (oxidants), the polycondensed aromatic structures of biochar (oxidants) and the phenolic portions (reducing agents) that donate electrons [72], [71].

2.1.1. Carbon Quantum Dots

In the syntheses of biochar by hydrothermal carbonization (HTC) from biomass, a great attention has been given to solid products, whereas the pale yellow liquid, a by-product of the synthesis, has always been considered as a waste and discarded [73], [74]. HTC will be discussed in the next items. However, Wu et al. (2014) found that this liquid contains abundant carbon NPs similar to quantum dots, with excellent photoluminescence and high quantum yield (~20%) [73], [74]. Carbon Quantum Dots (CQDs), a relatively new type of zero-dimensional carbon-based material [75], include carbon NPs with a diameter less than 10 nm, containing several functional groups, such as hydroxyl, epoxy and carboxylic acid on their surface [76]. CQDs have several applications due to their distinctive thermal, optical, chemical, electronic and mechanical properties, non-blinking luminescence, and magnificent compatibility, flexibility in surface modification and nominal toxicity [77], [78], [79]. In addition, CQDs have high solubility, excellent photostability, favorable biocompatibility and low toxicity [13],[78].

There are several methods for the synthesis of CQDs, such as graphite laser ablation [80], microwave heating of carbohydrates [81], hydrothermal carbonization of polymers [82] and plasma albumen pyrolysis [83], [79]. In addition, CQDs have largely been synthetized from biomass [84], [85], [86]. CQDs had been made earlier by other

methods. As this is not the focus of the present review, the reading of a recent mini review by Wang and coworkers is therefore recommended [87].

The CQDs have an absorption band between 210 and 400 nm in the UV-vis. region that is attributed to the complex electronic transition on the surface, the π conjugated aromatic system and the n-π* transition of carbonyl and other oxygen-containing groups [88], [73], [85], [86], [79]. The excitation and emission fluorescent peak occurs at approximately 350 and 450 nm, respectively [88], [85], [86], [79]. The surface charge of CQDs evaluated by Zeta potential presents negative values, which is assigned to the presence of highly hydrophilic hydroxyl and carboxyl group [77],[88]. Synthesized CQDs have relatively stable fluorescence intensity under neutral conditions [75], [77]. The CQD synthesis process involves four stages including dehydration, polymerization, aromatization and carbonization (passivation) [73], [78], as shown in Fig. 6. In their work, Liu et al. (2020) verified that the optical properties were closely related to sp^2 C, N-doped surface states, and the synergy among them [78].

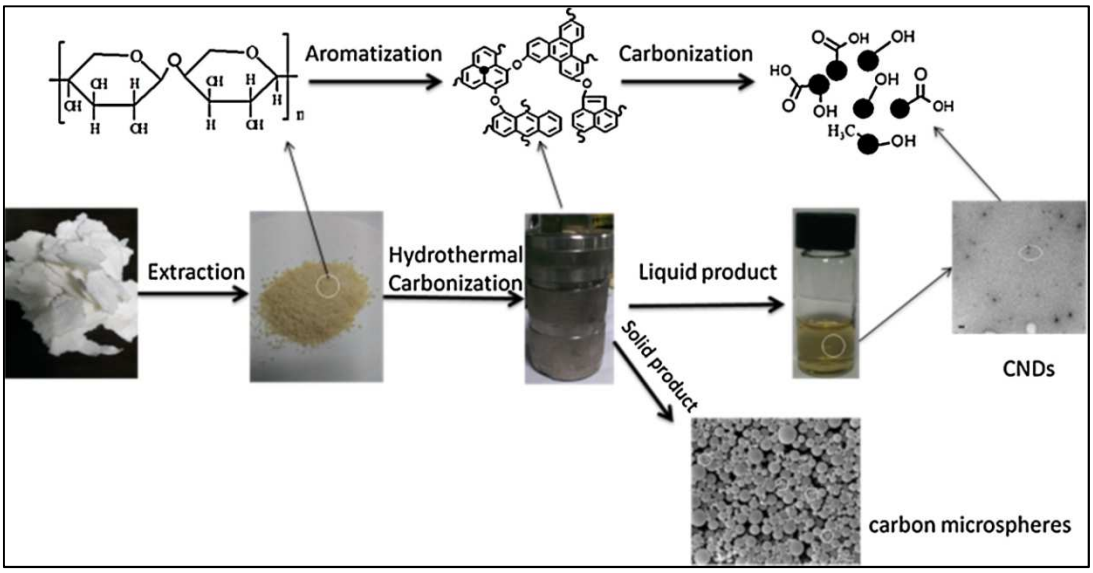

Fig. 6. Scheme of Carbon Quantum Dots synthesis. Reproduced from: Pentosan-derived water-soluble carbon nano dots with substantial fluorescence: properties and application as a photosensitizer, 315, Qiong, W. *et al.* Copyright (2014), with permission from Elsevier, License number: 4843550159542, https://doi.org/10.1016/j.apsusc.2014.06.127 [73].

Ziqi et al. (2020) synthesized CQDs from waste palm powders in the presence of thionyl chloride as a dopant through a one-stage hydrothermal treatment, which showed excellent photocatalytic property in the degradation of rhodamine B and methylene blue [79]. Wu and collaborators (2014) synthesized CQDs/TiO_2 composites by the sol-gel method and applied them to the photocatalytic degradation of methylene

blue. The oxygen-containing groups of the CQDs act as photosensitizers, absorbing photons that excite electrons from HOMO to LUMO. Free electrons are transferred to the TiO_2 conduction band, then react with oxygen (O_2) adsorbed on TiO_2 to produce active superoxide radical anion ($O_2^{\bullet-}$) [73].

Luo and coworkers (2020) also synthesized CQDs from chitosan by the solvothermal method, and they used them as photosensitizers of TiO_2 aiming at an application in photoelectrochemistry. According to the authors, the materials exhibited a higher photocurrent compared to the pristine TiO_2, with an even greater enhancement under visible-light illumination. This result was attributed to the synergism between CQDs and TiO_2, which forms a type II heterojunction, expanding the light response to the visible region [89]. Zhang et al. (2018) also synthesized CQDs from chitosan using the solvothermal method. The CQDs were covalently linked to an indium tin oxide (ITO) surface through a self-assembled silane monolayer, which showed a direct photoelectronic response. The photocurrent was attributed to the improved electron transfer process catalyzed by CQDs under illumination. The materials have potential for application as biocompatible and addressable electrochemical sensors in bioanalytical and bioimaging applications [90].

2.2. Biochar synthesis

The carbonization of biomass to produce biochar, among other products, is a complex process that includes many chemical reactions, including *inter alia* dehydration, decomposition, condensation and polymerization. [30]. This carbonization can occur by processes involving pyrolysis, gasification, flash carbonization and hydrothermal carbonization. Pyrolysis technologies are differentiated by the reaction time of the pyrolysis material (slow and fast) and the heating method (burning of fuels, by electrical heating, or by microwaves) [91]. The gasification uses high temperatures and some oxygen to produce a non-condensable gas rich in hydrogen and carbon dioxide [92]. Flash carbonization consists in processes at relatively low temperatures (≤ 400 °C) at short periods of time (between 5 to 10 minutes) in the presence of air [93].

Hydrothermal carbonization (HTC), also known as wet pyrolysis, is a thermochemical process performed by submerging biomass in water and then sealed in a confined system to be heated for several hours under saturated pressure [19], [94]. One of the advantages of HTC is the greater energy efficiency, due to higher solid yields without the need for intensive drying compared to dry pyrolysis [95]. The heat is transferred to the surface of the material by conduction, convection or radiation, and to

the interior of the material by thermal conduction [96]. During the HTC process, biomass undergoes thermal degradation in water and affects the physical-chemical properties of water, reducing its dielectric constant and making it a good solvent for non-polar substances [97]. HTC is carried out under relatively mild temperature (180-250 °C) and pressure conditions in a closed aqueous system, in which the pressure source is mostly related to steam [74], [98], [99], [100], [101]. In 2010, Titirici et al. published a detailed review of the various synthetic routes to carbon-based materials or composites through the HTC biomass process [102].

The carbonization by pyrolysis microwave has been highlighted [103]. The microwave carbonization process is different from microwave-assisted activation that will be discussed later. Compared to electric heating, microwave heating is advantageous in terms of speed, selectivity, flexibility and ease of control [104]. Microwave pyrolysis is thermal degradation in an inert environment using electromagnetic radiation as a heat source [53]. In furnace, surface heating of hearth wall does not guarantee a uniform temperature for different particle shapes and sizes of chars, generating a thermal gradient from the hot surface of the coal particle to its interior, preventing the effective removal of gaseous products into the environment, compromising the quality of the prepared activated carbons [105]. On the other hand, microwave pyrolysis results in materials that receive energy that is converted to heat, at a molecular level through dipolar rotation and ion conduction [106]. Dipole reorientation occurs millions of times in microwave absorbent compounds after exposition to microwave radiation; then, the heating results from friction and collisions between molecules in microwave absorbent compounds [107]. Thus, by microwave, the rapid thermal gradient from the interior of the char particle to its coal surface allows the microwave-induced reaction to proceed more quickly and effectively at a lower temperature, resulting in energy savings and decreasing processing time [105].

The yield of biochar can be affected by several factors, such as the biomass, carbonization process, and carbonization conditions used. For example, the pyrolysis temperature increase causes the thermal cracking of heavy hydrocarbons, which leads to a decrease in the yield of biochar. Some yields of biochar synthesized by different processes, besides feedstock, the process of obtaining and the general conditions for synthesis of biochar are indicated in Table 2.

Table 2. Yield of biochar synthesized by different processes

Feedstock	Process	General condition	Yield	Ref.
Arabica coffee husks	Pyrolysis	Heating ramp: 10 ºC min^{-1}; residence time: 4 h; Temperature: 350 and 600 ºC	36 and 33% for 350 and 600 ºC, respectively.	[108]
Pine nut shell	Pyrolysis	Temperature (400-700 ºC) and pressure (0.1-2.0 MPa) for 20 min under N_2 flow (80 mL min^{-1}).	~45 to 35% from 400 to 700 ºC. ~35 to 45% from 0.1 to 2.0 MPa.	[109]
Tea waste	Catalytic pyrolysis	Flow rates of CO_2: 200 mL min^{-1}. Biomass: 1.50 g; Heating rate of 10 °C min^{-1} from 200 to 720 °C. Ni/SiO_2 catalyst: 1.00 g.	34-35%	[110]
Coconut fiber (CF) and eucalyptus leave (EL)	HTC	10 g of biomass + 100 mL of deionized water; heating of autoclave 150-375 ºC.	90% (150 ºC) to 35.3 and 28.1% for CF and EL up to 375 ºC, respectively.	[111]
Eucalyptus sawdust	HTC	80 g of sawdust: distilled water (ratio 1: 7). Purge the reactor with N_2 for 5 min, stirring at 100 rpm. Heating 160 - 250 ° C for 1 h.	~70 to 35% from 160 to 250 ºC.	[112]
Fresh (FBPB) and dehydrated banana peel (DBPB)	HTC	5 g FBPB or 2.5 g DBPB + 50 mL of H_3PO_4 solution 20% (soaked for 2 h). The mixture was transferred to an autoclave and heated to 230 ° C for 2 h.	15.6* and 35.75 for FBPB and DBPB, respectively.	[113]

* the low yield was attributed to the amount of water in the sample.

2.2.1. Biochar activation

The adsorption behavior of biochar is the result of the cooperation between physical interaction and chemical reaction. The first depends largely on the surface area and porosity, whereas the second significantly depends on surface functional groups, due to chemical reactions occurring, including ion exchange, complexation, precipitation, electrostatic attraction and π interaction between biochar and the species to be adsorbed [97]. The properties of biochar are related to its surface characteristics, due to the oxygen-containing functional groups, mineral fractions and aromatic carbon present in its constitution [19].

However, the direct use of these biochar without any treatment is not straightforward due to their poor textural and physico-chemical properties [4]. Hydrophobicity, pore volume and functional groups of biochar can be altered by physical/chemical modifications, such as steam activation, chemical modification,

impregnation and heat treatment [57]. The biochar produced from thermal decomposition processes is often activated physically and chemically to increase its specific surface area, porosity, pore size distribution and attach various desired functional groups [106].

The physical activation involves carbonization and activation in a single step or two separate steps at a higher temperature under the gasification of gas atmosphere, such as carbon dioxide or water at 800-900 °C [114], [15]. The physical activation gives rise to carbons with porosity composed almost exclusively of micropores < 2 nm [29], whereas the chemical activation is more versatile, because it allows the synthesis of activated carbon with an adjustable porosity (made up of micropores and mesopores) [29][115]. Chemical activation is widely used due to its short activation time, low activation temperature and simple control process [116], [114], [117]. In the next items, some of these processes are described.

2.2.1.1. Chemical activation

Many compounds have been proposed for chemical activation, such acids (H_3PO_4, H_2SO_4, HNO_3 and HCl), alkaline chemicals (KOH and NaOH) and activating agents ($ZnCl_2$, K_2CO_3, $FeCl_3$, H_2O_2, O_3)[118], [8]. In fact, however, KOH, H_3PO_4 and $ZnCl_2$ are the most commonly used activators [8]. These chemicals are dehydrating agents that influence the pyrolytic decomposition and retard the formation of tars during the carbonization process [119]. In the activation process, doping with heteroatom, including *inter alia* N, P and S introduces functionality to biochar [120]. In general, a chemical activation process consists in carbon atoms slightly bound in the carbon structure that reacts with an oxidizing agent (OH^-, CO_3^{2-}; PO_4^{3-}; NO_3^-; etc.), in which carbon is released as CO or CO_2 producing a large number of pores that appears in the residual carbonaceous solid (Eq. 5) [29].

$$CO_3^{2-} + C \rightarrow 2CO + O^{2-} \qquad \text{(Eq. 5)}$$

The material activation by chemical compounds can be conducted before (one-step, also called one-pot)[115] or after (two-step, also called two-pot) the thermal treatment leading to biochar [121]. Both processes have pros and cons that must be evaluated for the intended purpose. In the biochar activation in two stages, the activating agent facilitates the removal of tarred substances in the pores of the material and acts as a model for the creation of microporosity during activation [121], [115]. On the other hand, catalytic pyrolysis of biomass in one-step improves the efficiency of decomposition and the quality of products [122].

2.2.1.1.1. Activation by H_3PO_4

Compared to other chemical activators, such as zinc chloride, hydroxide and nitric acid, H_3PO_4 undergoes less equipment corrosiveness, and the products obtained contain less harmful residues, and relatively low pyrolysis temperature; less pollution for the environment and low costs result thereof [97],[123]. The pretreatments using NaOH and HCl remove silica and ash from biochar thoroughly, which leads to cracks and pore opening [124]. The electronegativity of P is smaller compared to those of other heteroatoms, and the covalent radius is greater than that of N and S. Therefore, doping with phosphorus could improve the properties of biochar more effectively, increasing the number of acidic sites on the biochar surface and increasing its porosity [120].

Multiple micropores and mesopores form on biochar surface, because phosphoric acid and its derivative (polyphosphoric acid) react with the organic functional groups [125],[120]. Oxidation by the catalytic action of H_3PO_4 in the biochar modification process results in the fixation of oxygen-containing groups on the pore walls, which leads to a decrease in the size of the pores and/or to the transfer of some mesopores to micropores, increasing the biochar surface area [126]. The mechanism of formation of these micropores occurs by H^+ from H_3PO_4 that contribute to micropore generation via a H^+ catalysis process. This is due the organic phosphate bridge protection of the carbon skeleton from micropore collapse via the crosslinking of radical phosphate [47]. In another work, Chu et al (2020) evaluated the activation of biomass with H_3PO_4 before the pyrolysis stage in which these authors verified the contribution of cellulose and lignin to the formation of micropores. The activated materials have better structural characteristics, and the cellulose is the constituent that made the greatest contribution to the formation of micropores in relation to lignin [123].

The biochar functional group containing oxygen reacts with H_3PO_4 to generate water vapor to form the structure of the internal pores (Eq. 6) [127]. The H_3PO_4 catalysis leads to the oxidation and fixation of functional groups containing oxygen in the pore walls, leading to the reduction of the pore size or the transformation of the mesopores into micropores [127]. The reaction with H_3PO_4 promotes the formation of –COOH, –OH, C=C, aromatic structures and increased the formation of PO or P-OOH functional groups [127].

$$4H_3PO_4 + 10C \rightarrow P_4 + 10CO + 6H_2O \qquad \text{(Eq. 6)}$$

Shi et al. (2019) synthesized activated carbon from sucrose by *in situ* hydrothermal impregnation with H_3PO_4 and subsequent calcination at 500–900 °C. During the activation process, the decomposition of H_3PO_4 resulted in the formation of P_2O_5 and water. The P_2O_5 sublimation was responsible for the generation of pores in the material. Water molecules also contributed to the development of porosity through carbon gasification (Eq. 7). When a temperature of 900 °C was used, the surface area drastically increased to 1929 m^2 g^{-1}. At this temperature, P_2O_5 formed by the decomposition of H_3PO_4 acts as an oxidizing agent (Eq. 8) [128].

$$C + H_2O \rightarrow CO + H_2 \quad \text{(Eq. 7)}$$

$$P_2O_5 + 5C \rightarrow 2P + 5CO \quad \text{(Eq. 8)}$$

Oginni et al. (2019) compared the activation process in one or two stages. The materials obtained from the biomass in one-step were called Activated Carbon from Kanlow Switchgrass Biomass (KSBM) and Activated Carbon from Public Miscanthus Biomass (PMBM) and had a specific surface area of 1372.93 and 999.06 m^2g^{-1}, respectively. On the other hand, the biochar-derived activated carbons, formed in two-step, were denominated as Activated Carbon from Kanlow Switchgrass Biochar (KSBC) and Activated Carbon from Public Miscanthus Biochar (PMBC) and had a specific surface area of 697.96 and 161.97 m^2 g^{-1}, respectively. The adsorption capacity efficiency was evaluated in the caffeine and acetaminophen removal. The KSBM and PMBM were about 3–5 folds higher than KSBC and PMBC [121].

Zhou et al. (2019) synthesized biochar by Conventional Hydrothermal Carbonization (HTC). According to the authors, H_3PO_4 has a multifunctional property, as it serves as a catalyst for the decomposition process of organic matter, creating a liquid-air interface, as well as a phosphorus (P) donor. The biochar surface was further improved by the addition of Na_2CO_3 whose function was to neutralize biochar, removing the extra H_3PO_4, breaking the hydrogen bonds between surface functional groups (SFGs). These groups impede surface coordination and introduce carbonate anions that promote precipitation reactions with heavy metal ions [129].

Wu and colleagues (2019) synthesized activated biochar prepared by Pomelo Peel using H_3PO_4. According to the authors, the pores in the material are produced after etching of the biochar framework by H_3PO_4 oxidizing into carbonate and intercalating the phosphorus compounds [121].

2.2.1.1.2. Activation by alkaline compounds (NaOH and KOH)

NaOH accelerates the dissolution of condensed organic matter, such as lignin and celluloses, during the impregnation step, and it promotes a subsequent chemical reaction during the thermal activation stage [118]. The development of porosity in the material is attributed to activator's dehydration effect of NaOH, which breaks the C-O-C and C-C bonds of hydrochar. Thus, NaOH is reduced to metallic sodium Na, hydrogen gas, and sodium carbonate Na_2CO_3 according to Eq. 9 [130].

$$6\ NaOH + 2\ C \rightarrow 2\ Na + 3\ H_2 + 2\ Na_2CO_3 \qquad \text{(Eq. 9)}$$

Na_2CO_3 produced under thermal decomposition give gases (CO_2 and H_2O) that is responsible for burst precursors and results in wider holes [119].

A similar reaction occurs with KOH activation [131],[132]. Hydrogen, carbon monoxide, potassium vapor, and carbon dioxide are generated during sintering, which results in a large number of pores on the surface of biochar [116]. The addition of KOH first dehydrates cellulose, hemicellulose and lignin. The K^+ ions enter completely inside the material to generate the pore network (Eqs. 10-12) [133], [127].

$$4\ KOH + C \rightarrow K_2CO_3 + K_2O + 2\ H_2 \qquad \text{(Eq. 10)}$$

$$K_2CO_3 + 2\ C \rightarrow 2\ K + 3\ CO \qquad \text{(Eq. 11)}$$

$$K_2O + 2\ C \rightarrow 2\ K + CO \qquad \text{(Eq. 12)}$$

In the synthesis of micro-mesoporous carbon derived from castor bean peel proposed by Okonkwo et al. (2020), the nitrogen-rich spirulina extract was used to mediate KOH activation. The structural characteristics were greatly improved, which led to a specific surface area of 1527 $m^2\ g^{-1}$ [30]. Ismail et al. (2020) synthesized biochar from marc grape with KOH activation in two steps. The KOH/grape marc biochar ratio of 3 presented the highest specific surface area, i.e. 2473 $m^2\ g^{-1}$, high micropore volume (0.72 $cm^3\ g^{-1}$) and a pore diameter of 0.74 nm. The performance of the material was evaluated in the capture of CO_2, the excellent result being associated with the coexistence of high specific surface area, high microporosity and oxygenated functional groups on the surface [134].

Hsu et al. (2019) compared the efficiency of biochar from sorghum distiller grains activated by KOH and NaOH in the adsorption of ammoniacal nitrogen. Although the NaOH-activated biochar (132.8 $m^2\ g^{-1}$) had a higher specific surface area compared to KOH (117.7 $m^2\ g^{-1}$), this last one showed a higher adsorption efficiency. According to FTIR (Fourier-Transform Infrared Spectroscopy) results obtained by the

authors, the KOH-activated biochar has a much higher content of functional groups compared to the NaOH-activated biochar and, consequently, it has greater adsorption capacity [135].

KOH-activated biochar for different biomasses under optimal activation conditions showed different specific surface areas (m^2 g^{-1}): (1) biochar from rice husk and rice husk pellet: 1818.45 and 1320.45, respectively [136]; (2) from Sargassum and enteromorpha: 291.8 and 60.2, respectively [137]; (3) from millet straw and anthracite in Inner Mongolia, China: 1264.8 and 1424.1, respectively [138]; (4) from Lotus seedpod, by activation with KOH for one or two steps, were 227.20 and 364.30, respectively [139]; (5) from Taihu blue algae: 1657.8 [140]; from groundnut shell: 709 [141]; (6) from rice plant: 2329 [51], among others.

Liu et al. (2019) evaluated the activation of biochar from corn stalk by KOH and H_3PO4. The specific surface area for the biochar without activation (CSCB), activated by KOH (KOH-CSCB) and H_3PO_4 (H_3PO4-CSCB) were, respectively, 24.2543, 473.6432 and 2.8404 m^2 g^{-1}. The efficiency of the materials was evaluated in the adsorption capacity of methylene blue (MB), whose results were, respectively, 43.14, 230.39 and 406.43 mg g^{-1}. The efficiency of KOH-CSCB was mainly related to its porous structure. The efficiency of H_3PO_4-CSCB was mainly related to the functional groups of biochar containing oxygen and phosphorus, including -OH, -COOH, amino phosphonic acid functional group, and P-OH bond [127].

2.2.1.1.3. Activation by $ZnCl_2$

$ZnCl_2$ is a dehydrating agent that influences the thermal decomposition of biomass and inhibits the formation of tar, which results in the degradation of cellulosic material [142], [143], [144], [145]. Dehydration results in carbonization and aromatization of the carbon skeleton enabling the formation of pores in the material structure [142]. $ZnCl_2$ promotes depolymerization processes to produce strong carbonization, a strong breakdown of the liquid phase and, therefore, a greater formation of hydrogen [3]. In the presence of Zn, hydrogen is the largest gas product formed associated with other additives (LiCl, NaCl, KCl, $AlCl_3$), while methane and carbon monoxide production are less important [3]. Hydrogen is released from the aromatic/phenolic structure of the precursor, leaving active sites behind for reactions [145].

At high $ZnCl_2$ concentrations, some $ZnCl_2$ remains in the external part of the carbon particles, widens the porosity by a localized decomposition of the organic matter, and enhances the meso- and macropore formation [146], [147]. The increase in porosity and surface area after the process of chemical activation of $ZnCl_2$ may be related to the interstices left by $ZnCl_2$ incorporated in the carbon structure, which governs the porosity of carbon during heat treatment, leading to mesoporous materials [4]. $ZnCl_2$ has a relatively low melting and boiling point (263 and 732 °C, respectively), which forms molten salts during the pyrolysis process and distributed in the carbon structure [148]. According to Shi et al. (2020) the potential of the pyrolytic process of activation of the biochar derived from glue residue by $ZnCl_2$ can be summarized in Eq. 13-16 [148].

$$5\ ZnCl_2 + 10\ H_2O \rightarrow Zn_5(OH)_8Cl_2{\bullet}2H_2O + 8\ HCl \qquad \text{(Eq. 13)}$$

$$Zn_5(OH)_8Cl_2{\bullet}2H_2O \rightarrow ZnO + 2HCl + 5\ H_2O \qquad \text{(Eq. 14)}$$

$$2\ ZnO + SiO_2 \rightarrow Zn_2SiO_4 \qquad \text{(Eq. 15)}$$

$$3\ ZnO + 2\ C \rightarrow 3\ Zn\uparrow + CO\uparrow + CO_2\uparrow \qquad \text{(Eq. 16)}$$

Sun and co-workers (2018) evaluated the effect of $ZnCl_2$ activation of biochar from pine wood chips that was used to catalyze the pyrolysis of mixed plastic waste. According to the authors, $ZnCl_2$ treatment resulted in the formation of abundant acid sites, mainly Lewis acid sites, whose catalytic effect led to an increase in the content of aromatic hydrocarbons and a decrease in the content of alkene in plastic pyrolysis oil, as outlined in Fig. 7 [149].

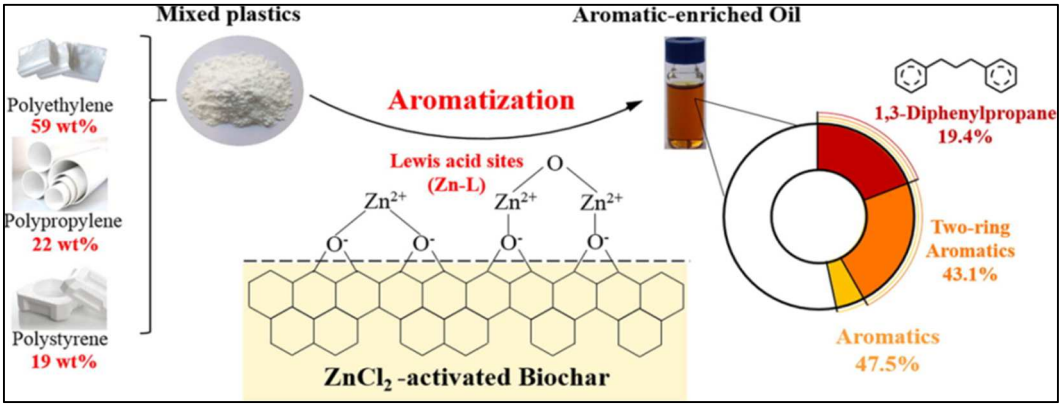

Fig. 7. Lewis acid scheme on the surface of the $ZnCl_2$ activated biochar. Reproduced from: Effect of $ZnCl_2$-activated biochar on catalytic pyrolysis of mixed waste plastics for producing aromatic-enriched oil, 81, Sun, K. *et al.* Copyright (2018), with permission from Elsevier, License number: 4844661221741, https://doi.org/10.1016/j.wasman.2018.09.054 [149].

Guo et al. (2019) compared biochar activation from rice husks (RHC) using different activating agents, H_3PO_4, KOH and $ZnCl_2$. The specific surface area ($m^2\ g^{-1}$) was RHC-$ZnCl_2$ (394.50)> RHC-KOH (390.59)> RHC-H_3PO_4 (346.30)> RHC (89.93). The catalytic performance of the materials was evaluated in the tar decomposition, with an efficiency obtained of 83.4, 91.6 and 94.2% for, respectively, RHC-$ZnCl_2$, RHC-H_3PO_4 and RHC-KOH [8].

Wang et al. (2020) synthesized biochar from corn cob activated with H_3PO4 (BC-H_3PO_4) or $ZnCl_2$ (BC-$ZnCl_2$), which had a high surface area of 680 and 790 $m^2\ g^{-1}$, respectively. BC-$ZnCl_2$ sample showed more functional groups than the BC-H_3PO_4 sample, wherein the acidic groups (carbonyl, carboxylic, lactones and phenol groups) content in the BC-$ZnCl_2$ and BC-H_3PO_4 samples were 0.98 and 0.69 mmol g^{-1}, respectively. The main mechanisms for removing metal ions include porous diffusion, electrostatic interactions and cation-π interactions [150].

2.2.1.2. Physical activation

Despite the low cost of physical activation, its effect on porous structures is much less important than that of chemical activation [151]. In the next items, some of these processes are described.

2.2.1.2.1. Activation by CO_2 and steam atmosphere

Activation by a CO_2 atmosphere is one of the most popular methods for producing activated carbon [152]. The physical activation of carbon materials by a CO_2 atmosphere at high temperatures is a simple method that increases the surface area and assists in the graphitization of crude biochar [63]. CO_2 is considered as a physical activation agent because it participates in pyrolysis through the reverse reaction of Boudouard, which decreases carbon yield and leads to successive removal of carbon from the pores (Eq. 17) [4]. For steam, the process is very similar (Eq. 18) [4]. The volatilization and conversion of the organic phase of the primitive hydrocarbons induces the increase of the pore volume, while the carbon skeleton retains the rudimentary porosity and the original structure [152].

$$C + CO_2 \rightleftharpoons 2\ CO \qquad \text{(Eq. 17)}$$

$$C + H_2O \rightleftharpoons CO + H_2 \qquad \text{(Eq. 18)}$$

Fang et al. (2016) synthesized biochar from walnut and peanut hulls physically activated by CO_2. The specific surface areas for the material activated at 900 °C with 2

h of activation were, respectively, 928 and 1308 m^2 g^{-1}. The materials were applied in the removal of methylene blue, lead, copper and cadmium by those who showed high removal rates [95].

Cuong et al. (2019) synthesized biochar from rice husks through alkaline leaching and physico-chemical activation processes. The authors used a KOH: biochar ratio of 3 and activated at 800 °C for 0.5 h under a CO_2 atmosphere. The biochar had a specific surface area of 2330 m^2 g^{-1}, and it was used to remove Cu(II) with an adsorption capacity greater than 265 mg g^{-1} [51].

Braghiroli and collaborators (2019) produced biochar physically activated with CO_2 atmosphere or steam and chemical activation with KOH impregnation. For biochar from white birch, the specific surface areas were 1700, 881 and 590 m^2 g^{-1} for KOH, CO_2 and steam, respectively. For biochar from black spruce, the specific surface areas were 1662, 735 and 412 m^2 g^{-1} for KOH, CO_2 and steam, respectively. The Cu^{2+} adsorption mechanisms involved physical and chemisorption for CO_2-activated biochar, while the chemisorption for KOH-activated biochar was probably due to the high proportion of functional groups connected to its surface [153].

Zhang et al. (2019) produced biochar derived from pig manure residues activated by KOH, CO_2 and H_3PO_4, which had a specific surface area of 2335.9, 700.1 and 500.7 m^2 g^{-1}, respectively. The materials were applied to the removal of methylene blue, obtaining removals of 717.0, 73.9 and 65.1 mg g^{-1} for KOH, H_3PO_4 and CO_2, respectively [117].

Yek and coworkers (2020) obtained biochar from orange peel by microwave heating pyrolysis and activation by steam or CO_2 in a single step. The total process time was 15 min, which is an advantage over the conventional pyrolysis method, whose time varies between 1 to 7 h. The use of CO_2 and steam as an activating agent increases the surface area of the carbonized product, whose results were, respectively, 158.5 and 305.1 m^2 g^{-1}. The materials were applied to the removal of the Congo red dye, which led to the removal of 136 and 91 mg g^{-1} for the material activated by steam and CO_2, respectively [53].

2.2.1.2.2. Activation by ultrasonic waves and microwave irradiation

Cavitation under ultrasound consists of three steps: nucleation, growth of bubbles and water bubbles with high energy and pressure, which increases the temperature by producing microjets within the liquid [154]. The generation of microjets,

shock waves and highly pressurized overheated regions, that is, hot spots, divides larger particles into smaller particles, cleans smooth surfaces and increases the porosity of solid surfaces [155]. Ultrasound is able to remove fine mineral particles in the porous biochar and to improve the desired reactions due to increased mass transfer in aqueous solution [18]. The physical effects of ultrasound on plant materials were identified as erosion (of the plant structure), fragmentation (reduction of particle size), sonocapillary effect (increased penetration of solvent into the channels and pores of plant material), local shear stress (flow and micro-flow effects), detexturation (destruction of plant structures) and sonoporation [48].

Sonication increases the porosity of the material due to the exfoliation of the graphical layers of the biochar and the leaching of ash from the pores formed during the thermochemical decomposition of biomass by pyrolysis [156], [154]. The cavitation effect of the ultrasound produces a uniform suspension of the biochar, activates the binding sites and leads to a better graft of the functional groups [154]. Therefore, combined processes using ultrasound aid chemical activation, because ultrasonic waves improve the mass transfer and dispersion of solid particles, allow the nucleation, growth and collapse of cavitation bubbles, thus improving the chemical attack on the biochar surface [157].

Sajjadi et al. (2020) found that physical activation combined with acid treatment and functionalization with urea grafted more functional groups containing nitrogen onto the surface of the biochar, leading to complete adsorption of heavy metal ions. Overall, a 40% increase (from 110.13 to 154.96 m^2 g^{-1}) in the microporous area and a 23% reduction (from 13.50 to 9.89 m^2 g^{-1}) in the mesoporous surface area were obtained after 0.5 min of ultrasound. The microporous increase is attributed to the formation of microjets and shock waves induced by ultrasound, which causes the generation of new pores, the opening of blocked pores and the exfoliation of the graphical structure of the biochar, as shown in Fig. 8 [155].

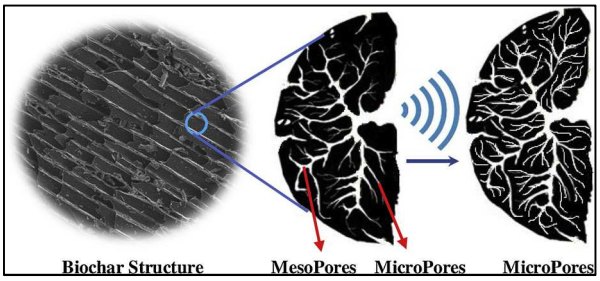

Fig. 8. The impact of short-term ultrasound activation on micro-porosity of biochar. Reproduced from: Engineering Low-temperature acoustic-based activation of biochar for enhanced removal of heavy metals, 34, Sajjadi B. *et al.* Copyright (2020), with permission from Elsevier, License number: 4896510793009, https://doi.org/10.1016/j.jwpe.2020.101166 [155].

Microwave activation is considered as a clean and effective modification method that increases the pore structure of the sample [158]. In the microwave activation process, the material already carbonized is subjected to microwave heating for a short period of time. In this stage, chemical activating agents are used to obtain a more porous structure and increase of the number of sorption surface sites [159]. Microwave-assisted heating allows for internal and volumetric heating compared to conventional heating, which causes different pore structures and surface areas [160].

Liu et al. (2018) obtained different biochars from rice husks that underwent chemical and physical activation assisted by microwaves. Different activating agents such as HNO_3, H_3PO_4, $ZnCl_2$, H_2SO_4, H_2O_2 were evaluated, which resulted, respectively, in specific surface areas of 66.00, 45.16, 31.30, 22.73 and 11.50 $m^2\ g^{-1}$. These results were significantly larger than those obtained for biochar without activation (1.72 $m^2\ g^{-1}$). The materials were applied to the *in situ* remediation of Cd in sediments, which led to excellent results [160].

2.2.2. Biochar functionalization

The functionalization of the biochar surface is an important factor that assists in the adsorption performance, improving the soil environment, promoting crop growth and mitigating carbon dioxide, as well as the surface area [161]. The surface of the biochar is modified to improve the desirable physicochemical characteristics, through an appropriate choice of activation procedures [48]. For example, Narayanan et al. (2018) synthesized a functionalized catalyst derived from coconut shell, equipped with CQDs. The treatment with concentrated sulfuric acid led to the anchoring of $-SO_3H$ and -COOH groups on the surface of carbon species that reacted to form amidoalkyl naphthols as shown in Fig. 9 [162]. Another interesting application was the functionalization of carbon-based materials formed by HTC from glucose performed by Urakami and coworkers (2013). The method consisted of a Diels-Alder cycloaddition reaction of furan fractions present on the surface of an HTC material with the maleimide groups from a maleimide-protected poly (ethylene glycol) (Me-PEG-MI) [163].

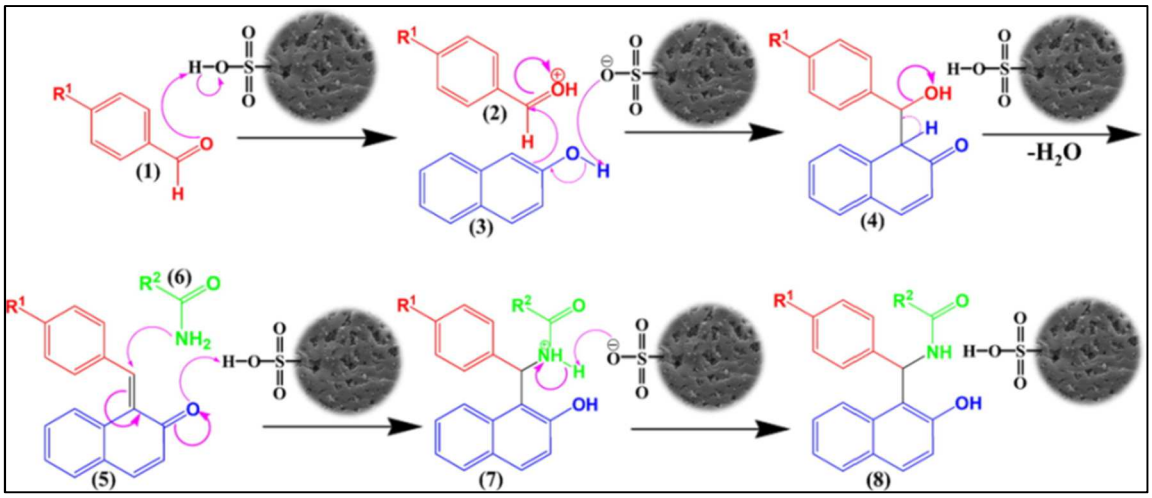

Fig. 9. Proposed mechanism for the synthesis of amidoalkyl naphthols over biochar-based catalyst. Reproduced from: Functionalized carbon dot adorned coconut shell char derived green catalysts for the rapid synthesis of amidoalkyl naphthols, 520, Divya P. *et al.* Copyright (2018), with permission from Elsevier, License number: 4843560656508, https://doi.org/10.1016/j.jcis.2018.02.077 [162].

Others important functionalization processes are described in the next items.

2.2.2.1. Amino functionalization of biochar

The incorporation of heteroatoms into the carbon lattice increases the degree of charge delocalization, breaking the structure inertia of the sp^2-hybridized carbon network [164]. Nitrogen doping is one of the most promising approaches. Amino-functionalized adsorbents capture heavy metal ions through the formation of stable chelate complexes and/or strong electrostatic interactions [165], [161]. Treatment of biochar with ammonia and amines (both photochemically and non-photochemically) leads to aminolysis of the surface [11]. Guang and Hong (2014) introduced an innovative method for amino-functionalization of biochar. In general, a method for amino-functionalization of biochar consists of a first nitration step involving its impregnation with sulfuric and nitric acid, both concentrated. After washing the material and drying, an amount of sodium hydrosulfite is added to the nitrated beaker, as shown in the scheme of Fig. 10 [166].

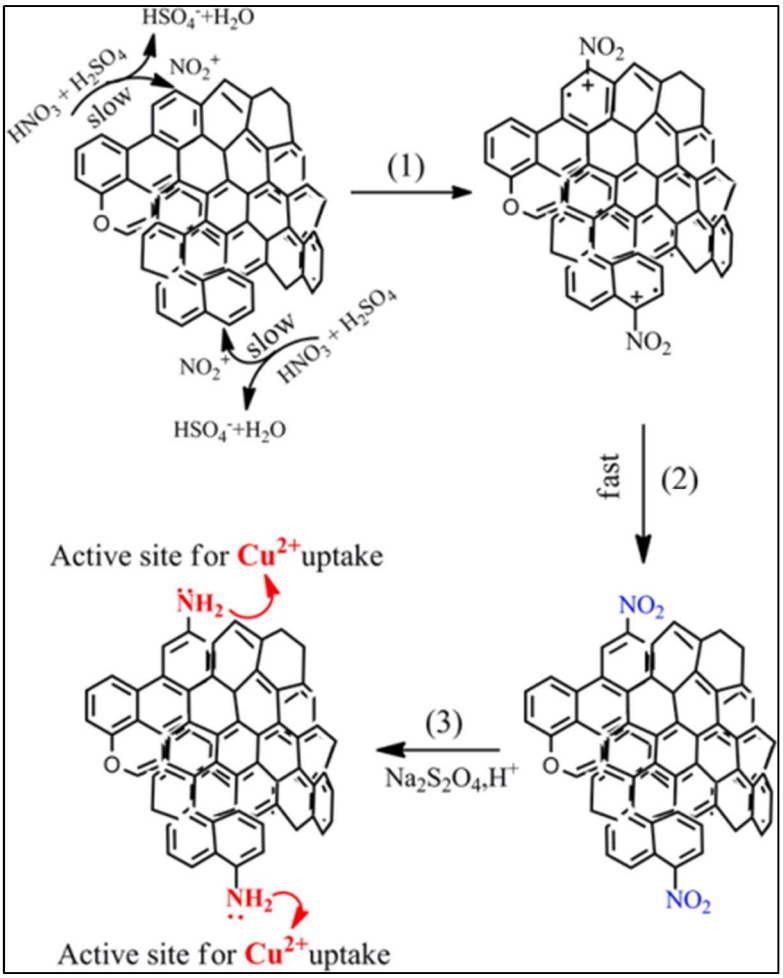

Fig. 10. Schematic amino-modification of biochar. Reproduced from: Amino modification of biochar for enhanced adsorption of copper ions from synthetic wastewater, 48, Guang-Xi Yang and Hong Jiang, Copyright (2014), with permission from Elsevier, License number: 4843560847487, https://doi.org/10.1016/j.watres.2013.09.050 [166].

Bamdad et al. (2018) functionalized biochar with 3-aminopropyltrimethoxysilane (APTES) [167]. Therefore, the authors prepared a suspension of biochar in distilled water, with pH between 3 and 4, and slowly added APTES. After sonication, the reaction was carried out under reflux at 70 °C, as shown in the diagram in Fig. 11. Tang and workers (2019) synthesized biochar derived from sewage sludge functionalized using a similar process employing previously pyrolyzed biochar (500 °C) plus hexadecyl trimethyl ammonium chloride and ammonia followed by addition of ethyl tetraethyl orthosilicate (TEOS). The system was stirred in N_2 atmosphere, and the gray precipitate, after washing and drying, was calcined under N_2. Amino-functionalization was obtained by mixing this solid with APTES whose mixture was refluxed (95 °C, 24 h under N_2 flow). This material was used to remove Cu (II), providing satisfactory results.

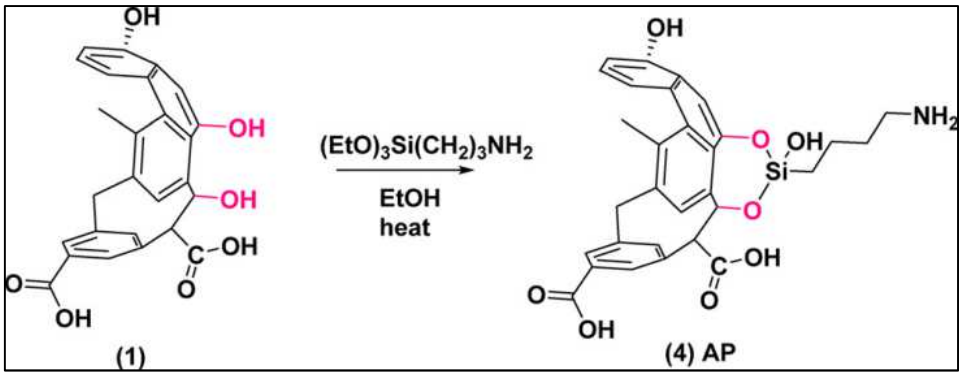

Fig. 11. Modification of the biochar surface with APTES under reflux at 70 °C. Reproduced from: Nitrogen Functionalized Biochar as a Renewable Adsorbent for Efficient CO_2 Removal, 32, Bamdad *et al.* Copyright (2018), with permission from American Chemical Society, https://doi.org/10.1021/acs.energyfuels.8b03056 [167].

Wang et al (2019) synthesized biochar derived from the Pinus sylvestris biomass doped with N as a catalyst for CO_2 methanation. The authors used urea as a precursor to nitrogen and $NaHCO_3$ as an activator. The material with biomass pyrolysis temperature at 600 °C presented optimized catalytic performances with the highest content of pyridine-N. They concluded that the introduction of nitrogen, pyridinic-N, pyrrolic-N and graphitic-N atoms in the catalyst support improves the catalytic performance of CO_2 methanation, mainly due to the influence of pyridinic-N [135].

Cai et al. (2019) obtained a biochar from magnetic amino-functionalized peanut husks by the hydrothermal one-step method. The method performs carbonization, magnetization and amino-functionalization simultaneously in a one-step process. The material was used to remove Cr(VI), bringing up satisfactory results. The removal of Cr(VI) involves a redox reaction, forming Cr(III), and electrostatic attraction [168].

Bao et al. (2018) used partial oxidation of biochar, from raw corn cobs, by H_2O_2, which was used in order to promote partial oxygenation of biochar in order to increase its cation exchange capacity, due to the formation of oxygen functional groups, particularly the groups (-COOH) on the surface of the biochar. The BC-COOH amination was performed by an immersion method, using urea and finalization with the use of diethylenetriamine. The material was applied to remove Hg(II), obtaining satisfactory results [169].

2.2.2.2. Magnetic functionalization

Biochar is a fine powder that is difficult to separate from the aqueous system. The magnetization of these material improves its application and re-use because it can be facially separated from the system by an external magnetic field to perform the

solid-liquid separation [170]. Biochar is magnetized by the introduction of a magnetic material, such as iron, cobalt [171], [172] or nickel [132]. However, among ferromagnetic materials, iron is most widely used for magnetizing biochar. The principal magnetization process involves chemical co-precipitation, thermal decomposition, hydrothermal synthesis, pyrolysis and microwave assisted heating [173].

In the pyrolysis process, the iron preloading on biomass before the thermal treatment is converted to Fe_3O_4 according to Equations 19-22 [174].

$$Fe^{3+} + 3\ H_2O \rightarrow Fe(OH)_3 + 3\ H^+ \quad \text{(Eq. 19)}$$

$$Fe(OH)_3 \xrightarrow{\Delta} FeO(OH) + H_2O \quad \text{(Eq. 20)}$$

$$2\ FeO(OH) \xrightarrow{\Delta} Fe_2O_3 + H_2O \quad \text{(Eq. 21)}$$

$$9\ Fe_2O_3 + (H_2, CO, C) \rightarrow 6\ Fe_3O_4 + (H_2O, CO_2, CO)\uparrow \quad \text{(Eq. 22)}$$

Mubarak and collaborators (2016) synthesized magnetic biochar upon microwave assisted heating. The magnetic biochar showed excellent ferromagnetic property with a saturation magnetization of 8.16 and 4.20 emu/g using microwave and conventional heating, respectively [173].

Han and co-workers (2020) synthesized magnetic bioactivated carbon from lignin. According to the authors, a ferrous salt is incorporated into the carbon matrix during the process of fusing lignin, and it is decomposed and reduced to Hagg iron carbide (Fe_5C_2) during the carbonization process. Afterwards, the Hagg iron carbide is exposed and oxidized to form magnetite (Fe_3O_4) during the steam activation process. Pyrolysis steam is not only an activating agent for the generation and enlargement of pores, but it is also effective for the oxidation of reduced iron species. The best magnetic saturation was 12.05 emu/g [175].

Spinel ferrite, with the general formula of AFe_2O_4 (A = Mn, Zn, Ni, Co, Fe, among others) has excellent structural stability and magnetic property due to the variable valence of iron [176]. In this sense, Zhai and collaborators (2020) synthesized the photocatalyst biochar@$CoFe_2O_4$/Ag_3PO_4 for the degradation of bisphenol A under irradiation with visible light [177]. The material was synthetized *via* a one-pot method by co-precipitation followed by heating in an autoclave and pyrolysis. The saturation magnetic strength of the biochar@$CoFe_2O_4$/Ag_3PO_4 was 17.30 emu/g, which met the requirements to separate from suspension easily only by the additional magnetic field after being used in the photocatalytic process.

Jiang and coworkers (2019) synthetized magnetic biochar-supported noble-

metal NPs such as Pd@Fe-BC, Pt@Fe-BC and Ag@Fe-BC (BC = biochar, that were applied in *p*-nitrophenol reduction for recovery of the excessive reductants in the form of H_2 [178]. After pyrolysis, magnetite (Fe_3O_4) was found in all materials, with mean Pd, Pt and Ag NP size of 2.15, 3.60 and 19.62 nm, respectively. The order of reactivities was Pd@Fe-BC > Pd@Fe-BC > Pd@Fe-BC, which was attributed to the relative sizes of these NPs. The synergic effect was proven by the authors where biochar and Fe_3O_4 acted as accelerators of the noble metal NP catalysis to produce active hydrogen. The magnetic separation allowed the recuperation and reuse of the material for five times with high efficiency.

In a previously work, Jiang et al. (2018) described the study of *p*-nitrophenol reduction by Pd@Fe_3O_4/BC, the synthesis of the material being similar to that described above [174]. The great contribution of this work consisted in the model of reduction by the material, which attributed the excellent catalytic activity to the distinct electronic structure of the Pd modified by Fe species, mediated by the key functions present in the biochar (C–O, C=O, COOH and OH). Metallic Pd, Pd oxides, Fe(II), and Fe(III) coexist in Pd@Fe_3O_4/BC, which has been proven by XPS analysis. The reaction model proposes: (1) the adsorption on the catalyst surface of BH_4^- that loses an electron forming hydrogen atoms on Pd NPs; (2) the 4-NP, in the form of nitrophenolate ion, is reversible adsorbed on the catalyst surface, and (3) the hydrogen atoms and electrons are transferred from hydrogen for 4-NP, followed by any steps of dehydro-deoxygenation until the formation of 4-aminophenol, as shown in Fig. 12.

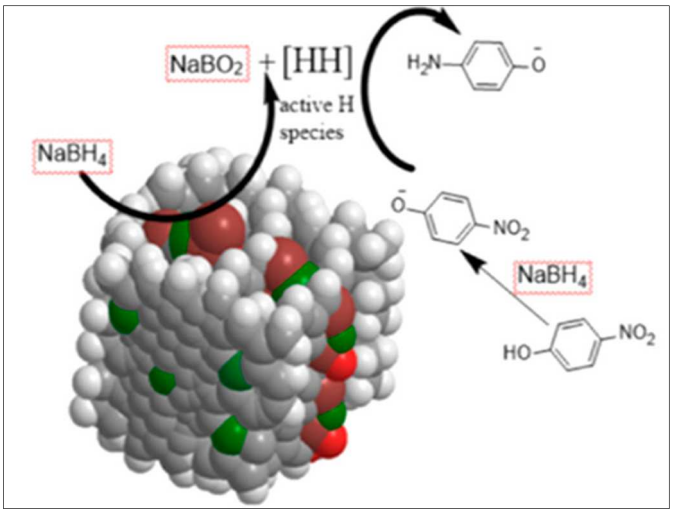

Fig. 12. Possible pathway of 4-nitrophenol reduction by Pd@Fe_3O_4/biochar Reproduced from: Enhancing the catalytic activity and stability of noble metal nanoparticles by the strong interaction of magnetic biochar support, 57, Jiang, S. *et al.* Copyright (2018), with permission from American Chemical Society, https://doi.org/10.1021/acs.iecr.8b02777 [174].

Li et al. (2019) [179] synthesized Ag NPs loaded on a polydopamine-coated magnetic biochar catalyst (MC-PDA-Ag). The feedstock used was pine sawdust that was preloaded with iron and pyrolysate under N_2. The material was dispersed into dopamine hydrochloride, previously dissolved into Tris-HCl (10 mmol L^{-1}, pH = 8.5). The AgNPs were produced using Tollens' reagent (silver ammonia solution). Besides a binder medium to connect the matrix of magnetic biochar and AgNPs, polydopamine served as a reducing agent for the reduction of Ag^+ to Ag^0. The synthetic route is shown in Fig. 13. The material was applied to the reduction of organic dyes (methylene blue, rhodamine B and methyl orange) satisfactorily. The material was separated by magnetization and reused in five successive cycles, maintaining cycle stability and high reactivity.

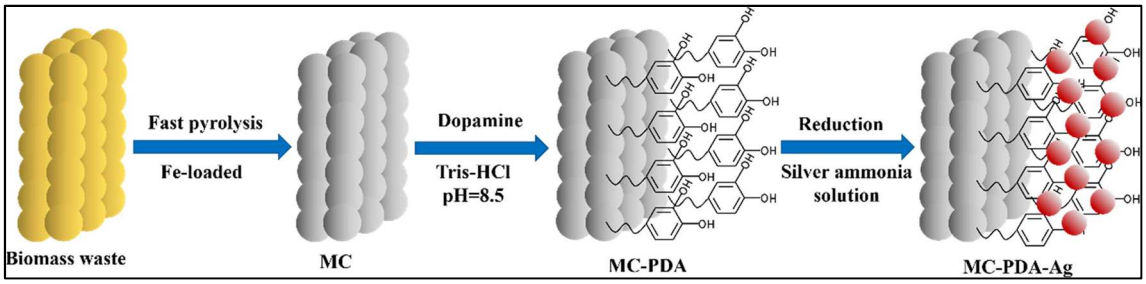

Fig. 13. Synthetic route to NPs loaded on a polydopamine-coated magnetic biochar catalyst (MC-PDA-Ag). Reproduced from: Preparation of silver-nanoparticle-loaded magnetic biochar/poly(dopamine) composite as catalyst for reduction of organic dyes, 555, Li, H. *et al.* Copyright (2019), with permission from Elsevier, License number: 4843650301201, https://doi.org/10.1016/j.jcis.2019.08.013 [179].

Zahedifar et al. [76] synthesized nanomagnetic biochar dots-coated AgNPs (BCDs-Ag/MNPs) using a green process. The biochar was produced from leaves and stems feedstock that were pyrolyzed at 450 °C. Biochar dots were formed using an acid process involving a mixture of concentrated HNO_3 and H_2SO_4 (1: 3, v/v), followed by sonication for 3h and heating at 100 °C for 24h. The synthesis of amino-functionalized magnetic NPs (PEI-Fe_3O_4) was performed by the co-precipitation method. The synthesis of BCDs coated with Fe_3O_4 magnetic NPs were synthesized by coupling the amino and carboxyl groups on the CQD surface. Finally, the plant extract of Atlantic Pistachio leaves was used for the synthesis of BCDs-Ag/MNPs.

3. Biochar as a support of nanocatalysts and other reagents

There are two types of catalysts, unsupported and supported. An unsupported catalyst comprises only active material, such as metal complexes and metal compounds such as oxides that are used in the desired reaction [180]. On the other hand, a supported catalyst consists of small amounts of active material on the surface of a support material called a catalyst support [180]. The use of heterogeneous

catalysts is interest due to their non-toxicity, ease of handling and reuse [162]. Although many nanoparticle suspensions are highly efficient, their application in reaction systems is seriously compromised due to their ease of aggregation. Therefore, this support presents advantages in catalysis because it allows to stabilize fragile suspensions of nanoparticles without deactivating them. Some examples of catalyst supported on different supports are: Cu supported on octahedral molecular sieves of manganese oxide [181]; ruthenium(II) complexes supported on magnetic NPs [182]; Mn–Fe NPs supported on reduced graphene oxide (rGO) nano-sheets [183], among others.

Ali and coworkers (2014) summarized, in their review, some advantages and disadvantages of some main materials (alumina, silica, zeolite and carbon) used as catalyst supports in oxidation reactions [184]. There are a few disadvantages for each of these materials and, therefore, the choice of a particular support depends mainly on its availability and ease of obtaining. In particular, the use of biochar has been widely studied as a support for various catalysts and reagents [185], [186], [187]. Biochar has proven to be an effective support due to its high specific surface area, stability and many active sites on the surface [188]. Besides, biochar prevents NP agglomeration and improve their reactivity [14]. Leaching metal ions are adsorbed and immobilized by biochar through complexation or electrostatic adsorption [189]. Another advantage is the ease of obtaining, as it is formed as a by-product of the production of biofuels from biomass.

Recent use of biochar as a stabilizer of metal-organic frameworks (MOFs) has shown its great versatility [190]. Several researchers have integrated transition metals into the carbon template, such as graphene sheet, to produce MOFs, and reported that the carbon template effectively stabilized the metal derivatives [191]. MOFs have been applied in several fields due to their unique characteristics, such as large specific surface areas and uniform distribution of active sites [192]. In this sense, Navarathna and collaborators (2020) synthesized MIL-53-Fe MOF/Magnetic Magnetite/Biochar composites and evaluated its efficiency in the photocatalytic degradation of Rhodamine B. According to the authors, biochar contributes to the dispersion of MOF, minimizing the aggregation of NPs, provides extra stability to MOF and serves as a secondary adsorption site for heavy metals, oxy anions and organic contaminants [190].

Recent studies have indicated that metal-modified biochar composites provided more active sites and modify the electrical charge, facilitating the removal of contaminants [193]. In the next sections, this theme is discussed in more details.

3.1. Metallic NPs and their bimetallic compositions

Zero Valent Iron (ZVI) is an effective reagent for wastewater remediation, due to its good activity, low cost, high surface activity, magnetic recovery property and low toxicity for the environment [194]. Besides, iron is the fourth most abundant element on earth, and it is a reactive metal with a standard redox potential of –0.44 V, thus also a good reducing agent [195]. ZVI has been widely used for the removal of environmental contaminants, as azo dye methyl orange [196], amoxicillin and ampicillin antibiotics [197], and 2,4,6-trinitrotoluene [198], among others. ZVI commonly used for applications is of macroscopic dimension, however, and the action mode involves the large surface of the ZVI sample. On the other hand, at the nanoscale, the lifetime of ZVI does not allow crossing a sufficiently long distance in large water areas to reach the target contaminant, because nano ZVI is too reactive. Let us focus on the nanoscale, for which nano-Zero-valent will now be abbreviated as nZVI. According to Raman and Kanmani (2016), the toxicity of nZVI nanoparticles (NPs) is smaller than that of carbon nanotubes, nanodiamond, nano TiO_2, nano ZnO, and also no toxic effect is reported on humans [199]. The nZVI NPs have spherical shape and their diameter size as bare is typically less than 100 nm. In aqueous solutions, all nZVI NPs react with water and oxygen to form an outer iron (hydr)oxide layer [200].

Under acidic conditions:

$$2Fe + 4H^+(aq) + O_2(aq) \rightarrow 2Fe^{2+} + 2H_2O \qquad E=+1.67\ V \qquad \text{(Eq. 23)}$$

$$2Fe^{2+} + 4H^+(aq) + O_2(aq) \rightarrow 4Fe^{3+} + 2H_2O \qquad E=+0.46V \qquad \text{(Eq. 24)}$$

Under neutral or alkaline conditions:

$$2Fe + 2H_2O \rightarrow 2Fe^{2+} + H_2(g) + 2OH^- \qquad E=-0.39\ V \qquad \text{(Eq. 25)}$$

$$2\ Fe^{2+} + 2H_2O \rightarrow 2Fe^{3+} + H_2(g) + 2OH^- \qquad E=-1.60\ V \qquad \text{(Eq. 26)}$$

Iron has a sufficiently negative redox potential (Eq. 23-26) [201], under acid or alkaline conditions, to reduce various molecules, but efficiency and potential applications depend on the type of size (*vide supra*).

nZVI have some limitations such as easy precipitation, passivation, poor mass and electron transfer [202], [203]. In addition, the lack of durability and the mechanical resistance presented by FeNPs also impair their practical applications [204]. To overcome these limitations, depositing nZVI on various supports has been widely used, such as clays [205], [206], [204], [207], zeolites [208], [209], [210], chitosan [211], [212] among others. However, biochar deserves to be highlighted due to the previously

mentioned advantages. Furthermore, supporting nZVI in biochar facilitates adsorption and further degradation of the molecule of interest. Wu and co-workers (2019) verified that the π–π interaction, hydrophobic interaction and reduction process contributed to the phenanthrene removal process by modified biochar-supported nZVI [213].

According to Lyu et al. (2020), biochar/Fe composites can be divided into three types, based on their different functional applications. The first includes composites for reduction purposes, such as nZVI/BC. The second includes compounds for the purposes of adsorption. The third includes BC/Fe composites used as activators in advanced oxidation processes (AOPs), such as persulfate oxidation [214].

The synthesis of nZVI is performed by different methods, but the chemical method using $NaBH_4$ solution is the most widely employed one due its advantages such as speed, simplicity and ease of synthesis, particularly on a laboratory scale [215]. However, the toxicity of sodium borohydride and the production of flammable hydrogen gas are some limitations of the synthesis [216]. Thus, biochar has numerous advantages, because it can function as a support and assist in the iron reduction process to produce nZVI, eliminating the use of auxiliary reducers. In the carbothermic process, ZVI is synthesized from an Fe-rich precursor that is mixed with biomass and subsequently co-melted under low oxygen conditions at high temperature [217],[218]. The synthesis of Fe-biochar composites *via* a one-step pyrolysis pretreated with an iron precursor at high temperature allows coupling the adsorptive, reducing and complexing characteristics of biochar and Fe in a single material [219]. The biomass, in addition to being able to be transformed for the production of the biochar support, contains groups that can be used in the green iron reduction process to generate Fe^0, as shown in Equations 27-30 [14].

$$Fe_3O_4 + 2\ C \rightarrow 3\ Fe^0 + 2\ CO_2 \quad \text{(Eq. 27)}$$

$$2\ Fe_2O_3 + 3\ C \rightarrow 4\ Fe^0 + 3\ CO_2 \quad \text{(Eq. 28)}$$

$$Fe_2O_3 + 3\ H_2 \rightarrow 2\ Fe^0 + 3\ H2O \quad \text{(Eq. 29)}$$

$$Fe_2O_3 + 3\ CO \rightarrow 2\ Fe^0 + 3\ CO_2 \quad \text{(Eq. 30)}$$

However, the iron source must be carefully selected for a particular purpose. For example, Kong et al. (2018) synthesized flour carbon (FC)-supported nano-flake Fe (Fe-FC). The authors found that FeS was formed by carbothermic reduction from ferrous sulfate ($FeSO_4$) under a reducing atmosphere [220]. Lawrinenko et al. (2017) uses $FeCl_3$ as an iron precursor for the production of ZVI supported in biochar by the

carbothermic method using different biomasses. They found that different biomasses produce different materials, because, in addition to ZVI, other compounds are formed in the process. For example, the association of silicon (Si) and phosphorus (P) with Fe resulted in the formation of fayalite, phosphates and phosphides of Fe, which limited the efficiency of ZVI production and/or facilitated its corrosion. In addition, chlorine is significantly volatilized in high temperature pyrolysis [221]. On the other hand, magnetite (Fe_3O_4) is available in abundance, and it can be obtained at low cost in large quantities. It reduces the problematic discharge of harmful gases in the pyrolysis effluent [222]. The synthesis of the Fe-biochar compost, however, is also carried out in two-steps, (1) biomass pyrolysis and (2) reduction of iron precursor ions with a reducing agent [223].

Doping a nZVI surface with another metal such as Ni, Pd, Ag, etc., to synthesize bimetallic NPs can increase or modulate its reactivity and reduce the nZVI agglomeration [224]. Due to the empty electron orbitals of transition metals, they accept electrons and activate the hydrogen molecule [224]. In typical bimetallic iron-based system, nanoscale zero-valent iron serves as a reducing agent, while noble metals or transition metals serve as catalysts [225]. Besides biomass use, that is a waste from agribusiness, alternative materials can be used as an iron source, such as the experiments by Li and collaborators (2017), who synthesized BC@Fe/Ni from steel pickling liquor and cane bagasse [226].

Biochar has also been widely used as a support for noble metals for different applications. For example, the use of biochar/gold composites has been used in the development of electrodes for the detection of hydroquinone and catechol isomers [227], [228]. Biochar from chicken manure was used as a heterogeneous support for Pd immobilization as a biocatalyst in Suzuki-Miyaura and Heck-Mizoroki reactions [229]. Lobos et al. (2016) obtained a biochar from pyrolysis of cellulose and used it as an alternative support of Cu-Ru@Pt core-shell NPs for the electro-oxidation of methanol [230].

Liu and collaborators (2016) synthesized Ag@biochar by carbothermic reduction of Ag^+ by biomass and applied the material in the catalytic reduction of Cr(VI) in the presence of HCOOH. The process occurs in steps: (1) decomposition of HCOOH to generate CO, Eq. 31; (2) CO activation by Ag NPs to form an activated Ag-carbonyl complex, which adsorb Cr(VI) to generate an Ag-carbonyl-Cr complex; (3) under acidic conditions, Cr(VI) reduction by CO to Cr (III) that undergoes several stages of

oxygenation-reduction reactions to form the final product, Cr(III), Eq. 32 [231]. The scheme of reactions is shown in Fig. 14.

$$HCOOH \rightarrow H_2O + CO \quad \text{(Eq. 31)}$$

$$2CrO_4^{2-} + 10H^+ + 3CO \rightarrow 2Cr^{3+} + 3CO_2 + 5H_2O \quad \text{(Eq. 32)}$$

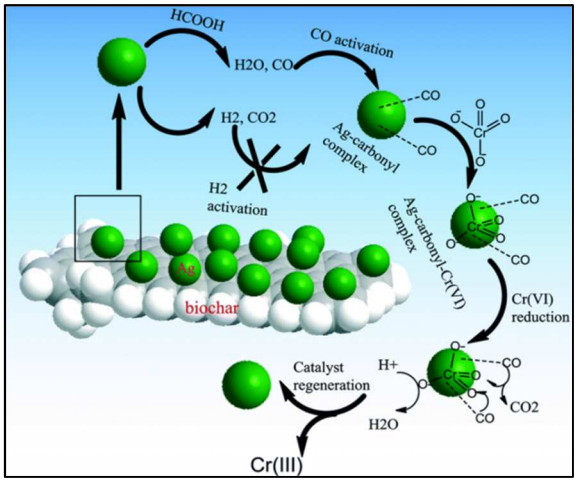

Fig. 14. Schematic Cr(VI) reduction on the Ag@biochar catalyst. Reproduced from: One-pot high-yield synthesis of Ag nanoparticle-embedded biochar hybrid materials from waste biomass for catalytic Cr(VI) reduction, 3, Liu, W. J. *et al.* Copyright (2016), with permission from Royal Society of Chemistry, https://doi.org/10.1039/c6en00109b [231].

p-nitrophenol (PNP) is a nitro-aromatic compound that plays an important role in the field of industrial chemistry; it is generally produced as a by-product of *inter alia* pharmaceuticals, agrochemicals, urethanes, and dyes, in addition to areas of toxic organic species [232]. Sohyun et a. (2019) synthesized nitrogen-doped Cu-biochar and applied it to the catalytic reduction of PNP (conditions: [PNP] = 0.35 mM, N-Cu-biochar = 0.25 g L^{-1}, [$NaBH_4$] = 30 mM, k_{app} : 0.0057 s^{-1} [47].

Some applications related to different metals and its bimetallic compositions supported on biochar are shown in Table 3. Briefly, in this table are described the reagents that were supported, the feedstock used and biochar process of obtaining, environmental application, material reuse and leaching study.

Although comparing the efficiency of different materials is difficult due to the different conditions used in the experiments, five works with different materials used as a support for ZVI (montmorillonite, porous silica, alginate sphere, cationic resin beads, oak wood biochar) have been selected. All materials were used to remove hexavalent chromium and the main results are briefly described in Table 4. As can be seen, biochar showed similar results to the other supports. The great advantage over other supports is that biochars are easy to obtain.

Table 3. Some environmental applications of different metals its bimetallic compositions supported on biochar.

Metallic catalyst	Biomass/ activation agent	NPs obtaining process	Contaminant removal application	Number of material cycles (% of removal)	Leaching study	Ref.
nZVI	Rice husk	One-step carbothermic reduction	Remediation of soils polluted with Cr(VI)	Unrealized	Unrealized	[14]
Ag/Fe	Sawdust/NaOH	Chemical reduction with $NaBH_4$	Removal of carbon tetrachloride in aqueous system.	1°(100) and 3°(80)	[Fe]=20.76; [Ag]=20.76 mg/L (pH 3.0) [Fe]=0.17; [Ag]=0.04 mg/L (pH 9.0)	[57]
nZVI	Sewage sludge	Chemical reduction with $NaBH_4$	Removal of Sb(III)	Unrealized	Unrealized	[72]
Ni/Fe	Sugarcane bagasse	Chemical reduction with $NaBH_4$	Remediation of soil contaminated with decabromodiphenyl	Unrealized	Unrealized	[189]
Ni/Fe	Sugarcane bagasse	Chemical reduction with $NaBH_4$	Removal of decabromodiphenyl in aqueous system.	Unrealized	BC@Ni/Fe: [Ni]=2.72 (10 min); [Ni]=0.48 (60 min); [Ni]≅0 mg/L (180 min) Ni/Fe: [Ni]=1.29 (10 min); [Ni]=3.09 mg/L (180 min)	[224]
Ag/Fe	Sawdust/NaOH	Chemical reduction with $NaBH_4$	Removal of cephalexin aqueous system.	Unrealized	Unrealized	[225]
Fe/Ni	Sugarcane bagasse	Chemical reduction with $NaBH_4$	Removal of nitrate in aqueous system.	Unrealized	Unrealized	[226]
Co/Fe	Sawdust/NaOH	Chemical reduction with $NaBH_4$	Degradation of cefotaxime in aqueous system.	Unrealized	[Co]= 0.01; [Fe]=0.20 mg/L (pH 5) [Co]=7.3×10^{-3}; [Fe]= 0.18 mg/L (pH 7) [Co]= 4.9×10^{-3}; [Fe]= 0.12 mg/L (pH 9)	[233]
Ni/Fe	Wheat straw/HCl	Chemical reduction with $NaBH_4$	Removal of 1,1,1-trichloroethane in aqueous system.	Unrealized	Unrealized	[234]

nZVI	Starch	Carbothermic reduction	Removal of uranium in aqueous system.	Unrealized	Unrealized	[235]
Magnetic ZVI	Peanut hull	Carbothermic reduction	Removal of Cr(VI) and trichloroethylene in aqueous system.	Unrealized	Unrealized	[236]
ZVI	Red oak (RO) and switchgrass (SG)	Carbothermic reduction	Removal arsenic in aqueous system.	RO: 1°(81.8) and 16°(44.8) SG: 1°(50.97) and 16°(36.3) *	[Fe]≅0 (Data not shown)	[237]
ZVI	Rice straw	Carbothermic reduction	Removal of 2,4,6-trinitrotoluene; hexahydro-1,3,5-trinitro-1,3,5-triazine; 2,4-dibromophenol and 2,4-difluorophenol in aqueous system.	Unrealized	Unrealized	[238]
Sulfidated-Fe^0	Seaweed (*Ulva prolifera*)	Hydrothermal Carbonization	Removal of tetrabromobisphenol A in aqueous system.	1° (1.45) and 6° (1.17 mg g^{-1})**	Unrealized	[239]
Fe/Pd	Rice straw/HCl, NaOH, HF, H_2O_2, HNO_3 and $KMnO_4$	Chemical reduction with KBH_4	Removal of 1,2,4-trichlorobenzene in aqueous system.	Unrealized	Unrealized	[240]
nZVI	Sewage sludge	Carbothermic reduction	Removal of Cr(VI) in aqueous system.	Unrealized	Unrealized	[241]
Pd/Fe	Corn straw	Chemical reduction with $NaBH_4$	Removal of trichlorobenzene in aqueous system.	Unrealized	Unrealized	[242]
nZVI-Si/Pd	Rice straw	Chemical reduction with KBH_4	Removal of Cr(VI) in aqueous system.	Unrealized	Unrealized	[243]

*Column leaching experiment; **Adsorption capacity

Table 4. Comparison of Zero-Valent Iron (ZVI) supports for Cr(VI) removal in aqueous system reactions.

Support material	General synthesis conditions of the material	General conditions of reaction	Efficiency	Ref.
Montmorillonite (Fe in Mt-nZVI)	(1) ZVI were synthesized via chemical reduction by $NaBH_4$. (2) ZVI and montmorillonite suspensions were, separately, sonicated to ensure dispersion of the particles (15 min). (3) Mixing both suspensions, stirring for 12 h.	$[Cr(VI)]_{initial}$= 20 mg L^{-1}; pH = 5.5, reaction time = 240 min, Fe in Mt-nZVI= 2.75 g L^{-1}	q_e[a] = 31.65 mg g^{-1} and removal of 99.75%.	[244]
Porous silica (NZVI@QIOS)	(1)[b] Preparation of aqueous solution of PVAL (15 g/L) and n-hexane solution of LPO (42.2 g/L). (2) Addition of MMA (0.448 M), TEOS (0.124 M) and PDMS (22.7 g/L) in LPO solution. (3) Addition of this last mix in PVAL solution. (4) System agitation by 3h at 70 ºC, under N_2 atmosphere. (5) The solid particles obtained, including TEOS, were added to an aqueous solution of IPA (429.6 g/L), HCl (79.6 g/L) and DI water, and then a sol-gel reaction continued for a certain time. Calcination at 500 ºC for 5 h. (6) Ethanol solution of $FeCl_3$ (90 g/L) was added to porous silica materials. (7) The mixture was heated at 80 ºC for 2 h to ethanol elimination. (8) $NaBH_4$ ($NaBH_4$:$FeCl_3$=1:10) was slowly added by 15 minutes.	$[Cr(VI)]_{initial}$= 25 mg L^{-1}; pH = 6.0, reaction time = 60 min, NZVI@QIOS = 1 g L^{-1}	Removal of 96.5%.	[245]
Alginate sphere (alginate-nZVI sphere)	(1) sodium alginate solution (2% (w/v)) was dropped into the $CaCl_2$ solution (5% (w/v)) and the Ca(II)-alginate spheres were formed by rapid gelation. (2) the incorporation of Fe^{3+} ions, $FeCl_3$ solution (2% (w/v)), was made over night, and the spheres were filtrated. (3) Addition of $NaBH_4$ (0.2 M) for 10 min under N_2 atmosphere. (4) The material was washed with acetone and freeze-dried for 48 h by using a freeze dryer.	$[Cr(VI)]_{initial}$= 20 mg L^{-1}; pH = 5.3, reaction time = 48 h, alginate-nZVI sphere ~ 5 g L^{-1}	Removal of 98.2%.	[246]
Cationic resin beads (R-nFe)	Resin: Dowex 50WX2 Na^+. 20 g of Dowex 50WX2 resin was added to $FeCl_3$ (200 mL, 0.05 M). (2) System agitation for 4 h (3) the resin was washed with deionized water (DI); Add the latter material to 150 ml of polyphenol solution (gallic acid) and 100 ml of DI, and stir the suspension for 20 h. The resin containing nZVI was filtered, subjected to washing steps and subjected to	$[Cr(VI)]_{initial}$= 15 mg L^{-1}; pH = 3.2, reaction time = 1 h, R-nFe = 4 g L^{-1}	Removal of 96.1%.	[247]

	lyophilization.			
Oak wood biochar (TP-nZVI-OB)	(1) $FeCl_3$ solution (49.25 g L^{-1}) was added to an amount of biochar (2.0 g); Fe/C of 2:1, which was subjected to agitation for 2 hours. Tea polyphenols (10 g L^{-1}) was added to the suspension. The mixture was kept under stirring for an additional 30 min. The samples obtained were vacuum filtered, washed and vacuum dried at 50 ° C overnight.	$[Cr(VI)]_{initial}$= 50 mg L^{-1}; pH = 2.0, reaction time = 720 min, TP-nZVI-OB = 1 g L^{-1}	Removal of 99.9%.	[248]

[a] q_e denotes the amount of Cr(VI) adsorbed at equilibrium. [b] PVAL (polyvinyl alcohol); LPO (lauroyl peroxide); MMA (Methyl methacrylate); TEOS (tetraethyl orthosilicate) PDMS (methacryloxypropyl-terminated polydimethylsiloxane) and IPA (isopropyl alcohol).

3.2. Activators of oxidizing agents

The main components of biochar are graphene pieces or carbon quantum dots that stabilize transition metal nanoparticles and transition metal oxide nanoparticles by π-bonding to their surface. Peripheral OH and CO_2H groups bind the nanoparticles by H-bonding and O-metal site bonding that contribute to this stabilization, but leave a large number of open free sites for interaction with- and catalytic activation of substrates. This situation creates electronic delocalization at the biochar-nanoparticle interacting surface that is favorable for activation by inner-sphere electron transfer processes leading to the formation of free radicals (FRs). Yang and co-workers (2015) reported the degradation of *p*-nitrophenol by FRs employing biochar from pine. The signs of FRs increased when the biomass was pyrolyzed from 200 to 500 ° C, but decreased at 700 ° C. The authors also found that coating biochar with tamic acid inhibited the generation of $^{\bullet}OH$, but did not inhibit the formation of FRs. The addition of *t*-butyl alcohol also inhibited the $^{\bullet}OH$ generation and decreased *p*-nitrophenol (PNP) degradation, which was associated with a competition between PNP and $^{\bullet}OH$ for the biochar surface. Degradation by-products were determined by GC-MS, such as catechols and hydroquinone [249].

Advanced Oxidative Processes (AOPs) are characterized by the *in-situ* generation of free radicals with sufficient potential for instance to degrade various persistent contaminants. The common AOPs mainly include O_3/UV, UV/H_2O_2, H_2O_2/O_3, Fenton, Fenton-like reactions and photocatalytic degradation that are characterized by the production of hydroxyl radicals [250]. Recently, persulfate-based AOPs (PS) has stood out due to its strong oxidizing ability, principally, because sulfate radicals ($SO_4^{\bullet-}$, E° = 2.5-3.1 V) has more positive redox potential than hydroxyl radicals ($^{\bullet}OH$, E° = 1,8-2,7 V) [251]. Compared to H_2O_2, solid sodium persulfate ($Na_2S_2O_8$) is more stable, costs less and is easier to transport and store [63]. The $SO_4^{\bullet-}$ radical anion preferentially attacks organic compounds through electron transfer reactions, while $^{\bullet}OH$ more likely do that through by capturing hydrogen or addition reactions; thus, $SO_4^{\bullet-}$ exhibits better selectivity towards organic pollutants than $^{\bullet}OH$ [252].

The persulfate (PS) or peroxymonosulfate (PMS) anion (Fig. 15) contains an O-O bond; it is an oxidizing agent with a relatively strong oxidizing property [253] [164]. $SO_4^{\bullet-}$ can be produced by activating PMS or PS. PMS is more susceptible to activation due to the asymmetry of its molecular structure [254].

Fig. 15. Structural formula (a) persulfate (PS) (b) peroxymonosulfate (PMS) anions

The sulfate radical has a high redox potential, high stability and a relatively long half-life of ~ 30-40 µs, which is much longer than that of the hydroxyl radical (10^{-3} µs)[188]. The conversion of persulfates to $SO_4^{\bullet-}$ requires some type of activating agent, including transition metals, high temperatures, UV irradiation, ultrasound and microwave irradiation, among others [255]. Recent studies show that persistent free radicals (PFRs) in biochar activates hydrogen peroxide [256] and PS [257] to generate hydroxyl radical and radical sulfate, respectively.

According to Fang et al., for the PRFs formation, (1) the phenolic lignin in the biomass is pyrolyzed to form condensed structures with abundant portions of phenol or quinone, (2) a phenol group transfers one electron to transition metals, pre-existing in the biomass, (3) this is accompanied by the formation of PFRs linked to the surface of biochar, as shown in Fig. 16. Finally, the PFRs in the biochar react directly with H_2O_2 by transferring a single electron forming $^{\bullet}OH$ [256].

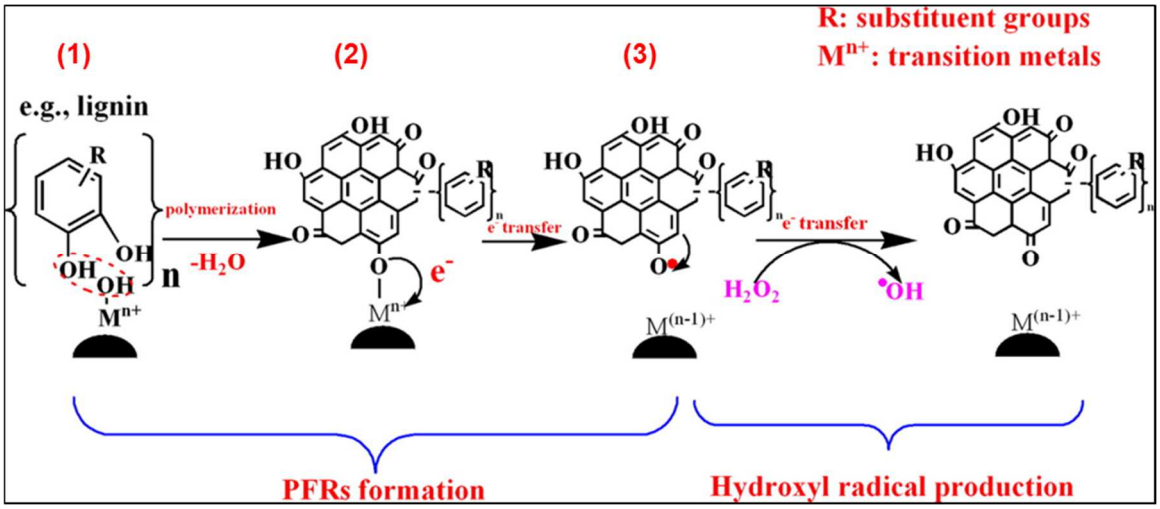

Fig. 16. Proposed Mechanisms of PFR formation and H_2O_2 activation by biochar. Reproduced from: Key Role of Persistent Free Radicals in Hydrogen Peroxide Activation by Biochar: Implications to Organic Contaminant Degradation, 48, Guodong, F. *et al.* Copyright (2014), with permission from American Chemical Society, https://doi.org/10.1021/es4048126 [256].

Functional groups such as -COOH and -OH on the surface of biochar act as electron transfer mediators to activate persulfate, (Eqs. 33-34) [251], [258], [259], [66], [260].

$$BC\text{-}OOH + S_2O_8^{2-} \rightarrow BC\text{-}OO^{\bullet} + SO_4^{\bullet-} + HSO_4^- \quad \text{(Eq. 33)}$$

$$BC\text{-}OH + S_2O_8^{2-} \rightarrow BC\text{-}O^{\bullet} + SO_4^{\bullet-} + HSO_4^- \quad \text{(Eq. 34)}$$

Carbonaceous materials containing sp^2 hybridized graphical structures have a large number of free flowing π electrons (C-π) [65]. The basic locations on the carbon surface accelerate the decomposition of H_2O_2 into hydroxyl and perhydroxyl radicals (Eqs. 35-36) [260], [261].

$$C\text{-}?? + H_2O_2 \rightarrow C\text{-}??^+ + OH^- + {}^{\bullet}OH \quad \text{(Eq. 35)}$$

$$C\text{-}??^+ + H_2O_2 \rightarrow C\text{-}?? + HO_2^{\bullet} + H^+ \quad \text{(Eq. 36)}$$

Similar mechanisms have been proposed for the biochar-persulfate system (Eq. 37)[260]. Semiquinone radical anion ($SQ^{\bullet-}$) is generated by reversible reduction of quinone or quinone moieties on humic/fulvic-acid (HA/FA≡Q), which decomposes the PS with the generation of radicals, carrying out the degradation of organics [69].

$$C\text{-}?? + S_2O_8^{2-} \rightarrow C\text{-}??^+ + SO_4^{2-} + SO_4^{\bullet-} \quad \text{(Eq. 37)}$$

$SO_4^{\bullet-}$ is the dominant radical species in acidic and neutral conditions, whereas ${}^{\bullet}OH$ plays an important role under alkaline conditions [251]. In alkaline conditions, the generated $SO_4^{\bullet-}$ reacted with OH^- to produce HSO_4^-, according to Eq. 38-39 [258], [259], [65], [262].

$$SO_4^{\bullet-} + OH^- \rightarrow {}^{\bullet}OH + SO_4^{2-} \quad \text{(Eq. 38)}$$

$$^{\bullet}OH + SO_4^{\bullet-} \rightarrow HSO_4^- + 0.5O_2 \quad \text{(Eq. 39)}$$

In addition, ${}^{\bullet}OH$ radicals can still react with OH^- to form H_2O, Eq. 40 [259].

$$^{\bullet}OH + OH^- + e^- \rightarrow O^{2-} + H_2O \quad \text{(Eq. 40)}$$

In acidic conditions (pH < 2), however, the efficiency decreases because of the electron competition, as can be seen in the Eqs. 41-42 [259].

$$2H^+ + 2e^- \rightarrow H_2 \quad \text{(Eq. 41)}$$

$$S_2O_8^{2-} + e^- \rightarrow SO_4^{2-} + SO_4^{\bullet-} \quad \text{(Eq. 42)}$$

The efficiency of the process is dependent of the PS concentration. High concentrations, however, limit the efficiency of the activation process, as indicated in Eqs. 43-44 [263], [264].

$$SO_4^{\bullet-} + SO_4^{\bullet-} \rightarrow S_2O_8^{2-} \quad \text{(Eq. 43)}$$

$$SO_4^{\bullet-} + S_2O_8^{2-} \rightarrow S_2O_8^{\bullet-} + SO_4^{2-} \quad \text{(Eq. 44)}$$

A similar process occurs with excess hydrogen peroxide, as shown in Eq. 45-46 [265].

$$H_2O_2 + {}^{\bullet}OH \rightarrow HO_2^{\bullet} + H_2O \quad \text{(Eq. 45)}$$

$$HO_2^{\bullet} + {}^{\bullet}OH \rightarrow O_2 + H_2O \quad \text{(Eq. 46)}$$

Yua et al. (2020) used biochar from shrimps to activate persulfate in the 2,4-dichlorophenol removal process. The authors evaluated different pyrolysis temperatures in the synthesis process (400, 600 and 800 °C). The materials at 400 °C (PSS-400) showed a carbon structure with sp^3 hybridization, dominated by high disorder, while at 800 °C (PSS-800) it showed the existence of graphitic carbon (sp^2 hybridization). The catalytic efficiency of the material PSS-800 was 29 times larger than that of PSS-400. For PSS-400, the mechanism was dominated by free radicals, while for PSS-800 the mechanism was non-radical, that is, there was a direct transfer of two electrons. The authors concluded that porosity and carbon configuration were two critical factors in the degradation process [266]. Zhou et al. (2020) also observed this non-radical phenomenon in his work that dealt with persulfate activation by swine bone char-derived hierarchical porous in the degradation of 2,4-dichlorophenol [66].

Pi et al. (2019) found that, in addition to the radicals $SO_4^{\bullet-}$ and ${}^{\bullet}OH$, $^1O_2$ and $O_2^{\bullet-}$ also participate in the process of tetracycline degradation by magnetite supported on biochar [264]. The species $^1O_2$ is formed through the recombination of $O_2^{\bullet-}$ and the reaction of ${}^{\bullet}OH$ and $O_2^{\bullet-}$ based on Eqs. 47-48 [264].

$$O_2^{\bullet-} + O_2^{\bullet-} + 2H^+ \rightarrow {}^1O_2 + H_2O_2 \quad \text{(Eq. 47)}$$

$$O_2^{\bullet-} + {}^{\bullet}OH \rightarrow {}^1O_2 + OH^- \quad \text{(Eq. 48)}$$

The use of biochar as a support prevents leaching of free metal ions. This species causes secondary pollution of heavy metals, which represents serious problems *inter alia* for humans [267]. In addition, leaching of these metals disables the catalyst in successive processes. On the other hand, biochar allows a fast migration of electrons and accelerates electron transfer of the catalyst due to its exclusive electronic

structure [268]. In this sense, several studies have used biochar as a support for various compounds to activate oxidizing species. For example, Rong et al. (2019) used magnetic γ-Fe_2O_3 supported on biochar from banana peels to activate persulfate in the degradation of bisphenol A in aqueous system. The authors verified that, in addition to $SO_4^{\bullet-}$ and $^{\bullet}OH$, $O_2^{\bullet-}$ is one of the species responsible for degradation [269].

Zhu et al. (2020) synthesized BC@nZVI/Ni and applied it to the activation of persulfate for norfloxacin degradation. Under the used conditions, the degradation efficiency of BC@nZVI/Ni was higher than that of nZVI/Ni, by 67.8 and 80.5%, respectively. These results suggested that the degradation of norfloxacin was mainly due to the oxidation of radicals generated by the BC@nZVI/Ni/PS system [251].

Mian et al. (2019) synthesized MnOx supported on biochar derived from sewage sludge incorporated with agar, activated with NH_4OH and pyrolyzed at 800 °C to act as a catalyst for the decomposition of peroxymonosulfate (PMS) for the production of sulfate radicals ($^{\bullet}SO_4^-$). The authors evaluated the efficiency of the catalyst in the degradation of the acid orange 7 and rhodamine B dye. The efficiency of the material was associated with the presence of manganese oxides in different oxidation states, while activation with NH_4OH increased the amount of N hetero atoms, area specific surface and microporosity. A non-radical process governed by N-carbon should play the primary role in acid orange 7 degradation instead of radical-induced catalysis [191].

Some applications related to metal nanoparticles and oxides supported on biochar as activators of oxidizing agents are described in Table 5. In this table, briefly, the materials that were used, the oxidizing agent used, application, reuse of the material and leaching study are described.

As indicated in Table 6, the biochar showed characteristics similar to graphene oxide (GO) in the sulfadiazine degradation in aqueous systems. As previously reported for other materials, the advantage of biochar over GO is due to its ease of obtaining, which occurs as a by-product of biofuel production from biomass carbonization.

Table 5. Various materials supported in biochar to activate persulfate (PS) or peroxymonosulfate (PMS) or hydrogen peroxide (HP)

Material	Activated agent	Application	Number of material cycles (% of removal)	Leaching study	Ref.
$MnFe_2O_4$- Biochar from stems, leaves and corn cores	PMS	Removal of orange II in aqueous system.	1° (100); 2° (50) and 3° (46) [a]	[Fe]<40 and [Mn]<70 µg/L for the three cycles. [a]	[50]
Co_3O_4-Biochar	PMS	Degradation of ofloxacin in aqueous system.	1-3° (100); The degradation rate has been decreased.	[Co]≅1.5 mg/L	[252]
Fe_3O_4-Biochar	PMS	Degradation of *p*-hydroxybenzoic acid in aqueous system [b].	1° (100); 2° (71) and 3° (65)	Unrealized	[254]
ZVI supported on biochar from rice straw.	PS	Oxidation of phenol in aqueous system.	Unrealized	Unrealized	[260]
Cu supported on biochar from corn stalks.	PS	Removal of tetracycline in aqueous system.	Unrealized	Unrealized	[263]
Magnetic $MnFe_2O_4$/biochar (photo-Fenton system)	HP	Degradation of tetracycline in aqueous system.	1° (95); 2° (94); 3° (92) and 4° (90)	[Fe] and [Mn]<0.2 mg/L.	[265]
Fe-hydrochar	HP	Removal of several estrogens (E1, E2 and E3) in aqueous system.	1° (94.6) and 5° (81.5) [c]	[Fe]=0.017 (pH 3.5), [Fe]=0.011 mg/L (pH 4.1) and [Fe] not detected (pH ≥ 5.1) [c].	[267]
Co_3O_4-Biochar	PMS	Degradation of chloramphenicols (chloramphenicol, florfenicol and thiamphenicol) in aqueous system.	1° (97.8) and 10° (85) [d]	Unrealized	[268]
ZVI-sludge derived biochar.	PS	Degradation of acid orange and landfill leachate as target pollutants in aqueous system.	1° (0.0718); 2° (0.0655) and 3° (0.0502 min^{-1}) [e]	$[Fe]_{total}$=4.43 ppm (pH 9.13) and $[Fe]_{total}$=22.12 ppm (pH 2.01).	[270]

Nano Co_9S_8 and CoO encapsulated by nitrogen and sulfur co-doped sludge-derived biochar (Co_9S_8@N-S-BC).	PMS	Degradation of sulfamethoxazole in aqueous system.	1° (100); 5° (92.8)	[Co]= 0.11, 0.10, 0.08, 0.07 and 0.06 mg/L for the five cycles, respectively.	[271]
Iron-doped graphitic biochar from peanut shell.	PS	Removal of 17β-estradiol in aqueous system.	1° (100); 2° (88.8); 3° (30.2) and 4° (17.3)	[Fe]< 0.65 mg/L.	[272]
nZVI-Biochar from sorghum stalk.	PS	Degradation of decabromodiphenyl ether in soil.	Unrealized	Unrealized	[273]
Magnetite NPs (Fe_3O_4) supported on rice husk biochar.	PS	Removal of phthalate esters in marine sediments.	Unrealized	Unrealized	[274]
nZVI-Biochar *from miscanthus floridulus*	HP	Removal of ciprofloxacin in aqueous system.	Unrealized	Unrealized	[275]
Fe-Mn binary oxides-biochar (photo-Fenton system)	HP	Degradation of naphthalene in aqueous system.	1° (82.2), 2° (75.3), 3° (72.2) and 4° (71.0)	[Fe]=0.55 and [Mn]=2.03 mg/L.	[276]
CuO-Biochar	PMS	Removal of Methylene Blue (MB), Acid Orange 7, Rhodamine B, Atrazine and Ciprofloxacin in in highly saline aqueous systems.	1° (100); 4° (97.84) [f]	[Cu]=0.013, 0.011, 0.009 and 0.010 mg/L for the four cycles, respectively [f]	[277]
$CoFe_2O_4$-Biochar	PMS	Degradation of dimethyl phthalate in aqueous system.	Removal> 90% in the five cycles evaluated	Unrealized	[278]
CoO-Biochar	PMS	Removal of tetracycline in aqueous system.	1- 8° (>93), 10° (80)	Unrealized	[279]
nZVI-Biochar from cornstalk	HP	Removal of sulfamethazine in aqueous system.	1° (70.04); 2° (53.28) and 3° (38.02)	Unrealized	[280]

[a] Study performed only for steams; [b] The optimized condition was applied to the degradation of bisphenol A, ciprofloxacin, orange II and tartrazine; [c] For the conditions 0.5 g/L of the catalyst, 10 μM E2 and 5 mM H_2O_2.; [d] Study performed only for chloramphenicol; [e] Rate constants were (k). [f] Study performed only for methylene blue

Table 6. Comparison of biochar and graphene oxide-based supports for Zero-Valent Iron (ZVI) used in sulfadiazine (SDZ) degradation mediated by Fenton-like reaction using hydrogen peroxide

Material	Syntheses do material	General degradation conditions	Main results	Ref.
Three-dimensional graphene network	(1) The graphene oxide (GO) was obtained from graphite by Hummer method; (2) A suspension of 0.8 g of GO plus 100 mL of water was subjected to US by 2 h; (3) The system was stirred with KBH_4 (3.24 g) for 24 h, under Ar atmosphere. (4) 50 mL of $FeSO_4 \cdot 7H_2O$ (50 mM) was added dropwise (1 mL min^{-1}) to the system under constant stirring for 1 h, under air protection; (5) The material was washed with water and dried in a vacuum freeze dryer.	Material dose: 0.5 g L^{-1}; 10 mL of SDZ (10 mg L^{-1}), pH = 3.0. When used, the $[H_2O_2]$ = 3 mM.	(1) 11% removal of SDZ was attributed to surface adsorption; (2) under an argon atmosphere, 44% of SDZ removal was mainly attributed to adsorption and surface reduction; (3) in the presence of dissolved oxygen, 81% removal of SDZ was attributed to oxidation of $^{\bullet}OH_{ads}$; (4) in the presence of H_2O_2, there was 98% due more generation $^{\bullet}OH$.	[281]
Biochar (BC) from cornstalk	Biochar was produced by pyrolysis at 700 ºC. (2) BC (nZVI:BC 1:7) was added to 100 mL of $FeCl_3 \cdot 6H_2O$ (0,05 M) for 24 h (3) purged with N_2, and stirred for 30 min (4) 100 mL of $NaBH_4$ (0.2 M), was added dropwise to the suspension, followed by stirring for 30 min. Solid products washed with water and vacuum dried at 60 ºC for 8 h.	Material dose: 1.2 g L^{-1}; 10 mL of SDZ (10 mg L^{-1}), pH = 3.0. $[H_2O_2]$ = 20 mM.	73% removal, whose main contribution was attributed to •OH. BC allowed a uniform distribution of nZVI, played an important role in SDZ adsorption, H_2O_2 activation, and relief of nZVI passivation.	[280]

3.3. Photocatalysis using semiconductors

Since the discovery of water electrolysis by TiO_2 by Fujishima and Honda (1972) [282], many works have been developed using this semiconductor for different applications including photocatalysis. A photocatalyst is defined as a substance that is activated by adsorbing a photon and is capable of accelerating a reaction without being consumed [283]. Semiconductors can be used as photocatalysts that are activated when a photon with energy of *hv* matches or exceeds the bandgap energy, E_b, of the semiconductor (Fig. 17). This photolytic process generates the electron-hole pair, that is, an electron, e^-_{CB}, is promoted from the valence band, VB, into the conduction band, CB, leaving a hole, h^+_{VB} behind [284]. The electron-hole pair allows a series of reductive and oxidative reactions, as shown in Equations 49-51. As can be seen, photocatalysis uses water or oxygen to produce an oxidant/reductant that uses less energy compared to the chemical-consumption process [9].

$$TiO_2 + hv \rightarrow TiO_2(e^-_{CB} + h^+_{VB}) \quad \text{(Eq. 49)}$$

$$h^+ + H_2O_{ads} \rightarrow {}^{\bullet}OH + H^+ \quad \text{(Eq. 50)}$$

$$e^- + O_{2ads} \rightarrow O_2^{\bullet -} \quad \text{(Eq. 51)}$$

The scheme of electron-hole pair formation in a semiconductor is shown in the Fig. 17.

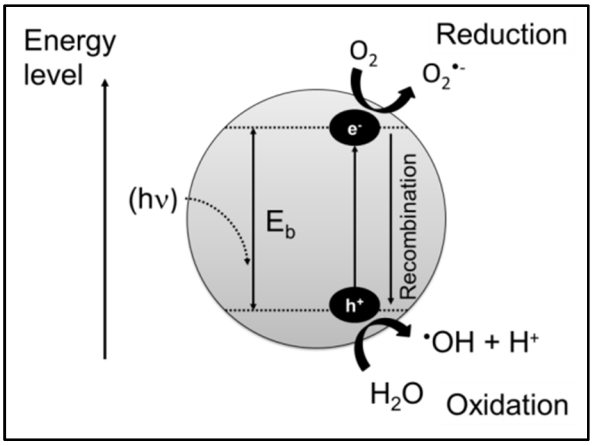

Fig. 17. Scheme of electron-hole pair formation in a semiconductor. Adapted from: Recent developments in photocatalytic water treatment technology : A review, Water Res. 44, Nan, M. *et al.* Copyright (2010), with permission from Elsevier, License number: 4897180681151, https://doi.org/10.1016/j.watres.2010.02.039. [285].

The TiO_2 semiconductor has been used in heterogeneous photocatalysis because of its properties such as chemical stability, low cost, and low toxicity [286]. However, TiO_2 undergoes rapid deactivation in practical applications due to low quantum efficiency and fast electron orifice recombination [192]. Other semiconductors

such as ZnO [287], [9], Fe_2O_3, CdS and ZnS are also widely used. In recent years, research on new semiconductors acting as photocatalysts has been extensively explored. The combination of various semiconductors results in different types of heterostructures. Heterostructures, such as the p-n type, Z-scheme and Schottky junction are commonly used in photocatalysis [288]. The construction of heterostructures has been considered as a promising method, because these structures prominently improve the separation of photoinduced charges and extend the light response range when coupling with narrow bandgap semiconductors [289]. For further discussion, reviews on this area are available [290–292].

Powdered semiconductors have some limitations in practical photocatalytic applications mainly due to the difficult separation of the aqueous phase, and they can still cause secondary pollution [293]. In addition, other disadvantages include the low usage of light, easy agglomeration and difficulty of separation from the aqueous phase to limit its application under visible irradiation because of its large band gap (3.2 eV for TiO_2, for example) and fast electron-hole recombination [294]. Biochar plays a vital role in improving electron transport due to the dense carbon layer, electron storage through oxidation and reduction of biochar quinone groups, charge separation through heterojunction between biochar and NPs, and enhancement of active sites by functional biochar surface groups [295]. Besides, larger surface area, H bond and electron donor-receptor π-π between the pollutant and biochar promote adsorption reaction [296]. Thus, biochar acts as a support to allow semiconductor particles to grow on the surface in a dispersed state, reducing the possibility of particle aggregation [297].

Lu et al. (2019) synthetized TiO_2 supported on biochar from nut shells. The efficiency of the material was used in the degradation of methyl orange. Methyl orange and intermediates were adsorbed by biochar due to the porous structure as well as the functional biochar groups. Under ultraviolet light, TiO_2 is photoexcited generating the electron-hole pair. The presence of biochar was fundamental to inhibit the recombination of the electron-hole pairs [298]. Others works employing TiO_2 supported on biochar for photodegradation are described in the literature, for the degradation of sulfamethoxazole [296],[299], amoxicillin [300], safranine [301] and Reactive Brilliant Blue KN-R [302]. The doping of TiO_2 with noble metals (Schottky junction, Fig. 18) supported on biochar is also described, as Ag/TiO_2-biochar that was used in methyl orange removal [303]. Heterostructures involving TiO_2 and biochar are also gaining

prominence, and for instance biochar-doped TiO_2/CuO was used in the degradation of ammonia [293].

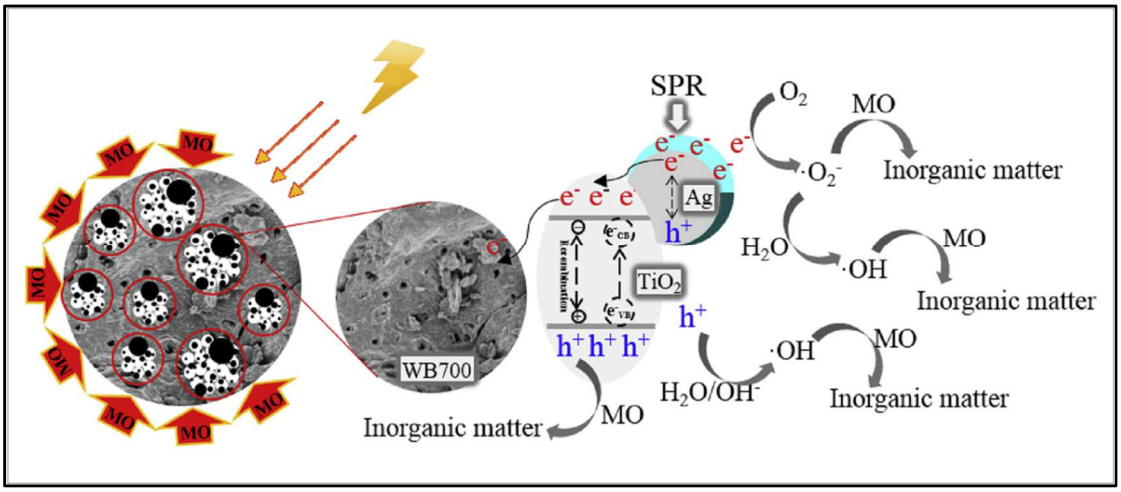

Fig. 18. Scheme of catalytic degradation of methyl orange (MO) by Ag/TiO_2-biochar. Reproduced from: Photocatalytic degradation of methyl orange by Ag/TiO2/biochar composite catalysts in aqueous solutions, 114, Shan, R. *et al.* Copyright (2020), with permission from Elsevier, License number: 4843651310688, https://doi.org/10.1016/j.mssp.2020.105088 [303].

ZnO is one of the most commonly used semiconductors due to its high chemical stability, low cost, low toxicity, and high oxidation properties; however; it has low photocatalytic efficiency [304]. To overcome these challenges, the construction of ZnO semiconductor heterostructures has been evaluated in order to improve semiconductor photocatalytic activity [305]. Chen et al. (2019) synthesized the composite ZnO/biochar nanocomposites from jute by a green method, in one pot, in which these authors used $Zn(OAc)_2$ and pyrolysis in an atmosphere of N_2 at 700 ° C. Above 250 °C, zinc acetate began to melt, decomposing at 318 °C, to form ZnO (Eq. 52). The material was applied to remove methylene blue in aqueous systems, and under optimized conditions the degradation and mineralization were 99 and 93%, respectively [9]. Other works involving ZnO-biochar has been developed, such as ZnO/biochar from carboxymethyl cellulose for methylene blue degradation [287]. Zhang et al. (2020) obtained γ-Fe_2O_3-ZnO-biochar nanocomposites for rhodamine B removal [306].

$$Zn(OOCCH_3)_2 + 4\ (\text{-O-}) \rightarrow ZnO + 4\ CO_2 + 3\ H_2O \qquad \text{(Eq. 52)}$$

Lanthanum manganite ($LaMnO_3$) crystallizes in the perovskite structure; it is known for its interesting electrical, magnetic and structural properties [307], and its use as a photocatalyst is known [308]. Hu et al. (2019) synthesized $LaMnO_3$ NPs (LMO) supported on N-doped biochar from soybean waste (PCB). The presence of PBC increases the oxygen vacancy in $LaMnO_3$, increasing the level of donors and decreasing the band difference in such a way that it can use sunlight more efficiently.

LMO-PCB was applied in the degradation of Direct Green. Some photo-generated electrons are removed by the N-graphitic mediator, which suppresses the recombination of pair electron-hole, while some electrons react with oxygen to produce $O_2^{\bullet-}$ in the conduction band. Pyridinic-N and pyrrolic-N act as active sites, in which oxygen is reduced to $O_2^{\bullet-}$ when it reacts on the plane. Finally, h^+ react with H_2O or OH^- to form $^{\bullet}OH$ radicals [297] (Fig. 19).

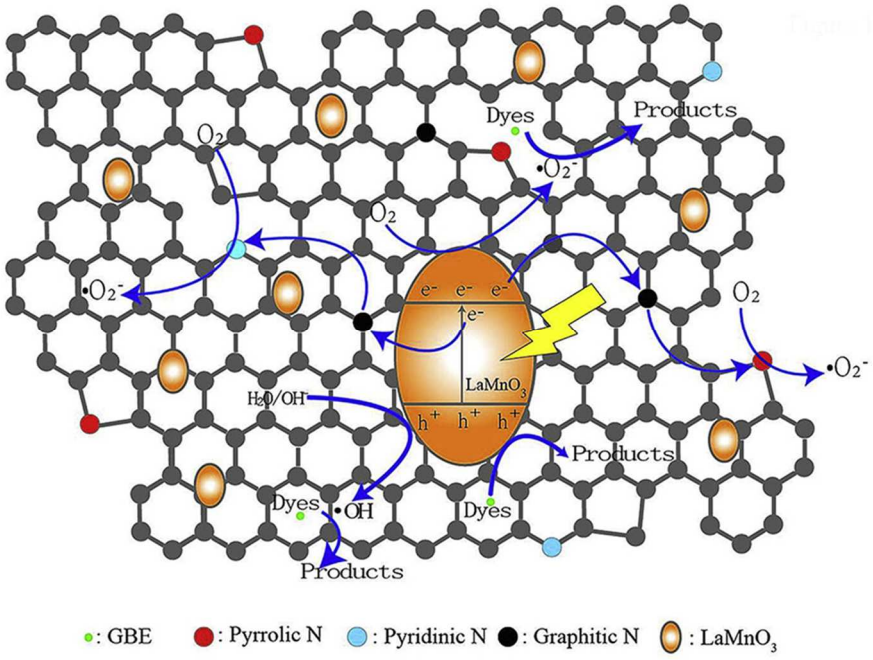

Fig. 19. Scheme of mechanism that occurs in the $LaMnO_3$/N doped porous carbon. Reproduced from: $LaMnO_3$ nanoparticles supported on N doped porous carbon as efficient photocatalyst, 159, Hu, J. *et al.* Copyright (2019), with permission from Elsevier, License number: 4843660035630, https://doi.org/10.1016/j.vacuum.2018.10.021 [297].

Low-cost graphitic carbon nitride (gC_3N_4) is gaining great prominence due to the rapid response to visible light, low bandgap energy (2.8 eV) and low cost [309]. This material is a new organic semiconductor induced by visible light, free of metals, with good chemical stability and suitable band positions [310]. However, the practical photocatalytic applications of gC_3N_4 are limited by the rapid recombination of photo-induced electron-hole pairs and the poor response of visible light [309]. Li and Lin (2020) obtained K-doped g-C_3N_4 supported on biochar from corn straw. The introduction of potassium effectively inhibited the growth of gC_3N_4 grains, reduced the energy of the gap band and increased the range of response to visible light [310].

Other recent works are described in Table 7. In this table the semiconductors used, the bandgap energy of the material and the range of the electromagnetic spectrum used, and application and reuse of the material and leaching study are briefly described.

As shown in Table 8, biochar showed characteristics similar to multiwalled carbon nanotubes (MWCNTs) and graphene oxide (GO) used as support for the semiconductor TiO_2 in the photocatalytic degradation of methylene blue (MB) in aqueous system. It is important to mention that for these materials with adsorbent characteristics, an MB adsorption-desorption equilibrium step is necessary.

Table 7. Use of various photocatalysts supported on biochar

Semiconductor	Bangap energy (eV) and electromagnetic spectrum range used in catalysis	Application	Number of material cycles (% of removal)	Leaching study	Ref.
Biochar@$ZnFe_2O_4$/BiOBr Z-scheme heterojunction	B_g: 2.02; Visible light irradiation (λ > 420 nm)	Degradation of ciprofloxacin in aqueous system.	4 cycles with removal >70%.	Unrealized.	[311]
BiOBr supported on biochar from wood flour waste	$B_g \cong$ 2.70; Visible light was a 200 W LED lamp	Rhodamine B dye and Cr(VI) removal in aqueous system.	Unrealized.	Unrealized.	[312]
Biochar–based heterojunction photocatalyst Bi_2S_3/BiOBr/BC	$B_g \cong$ 1.69; 50 W energy–saving visible LED light (dominant wavelength: 475 nm)	Diclofenac removal in aqueous system.	4 cycles with removal >82.64%.	Unrealized.	[313]
Hematite/biochar from Salacca skin waste	B_g: 2.21; 20-W UVB lamp	Degradation methylene blue in aqueous system.	The k slightly decreasing 1-2° and remains constant until 10th cycle.	1° cycle ≅ 5.5% of Fe (% in relation to Fe_{Total} in the catalyst; 5° cycle <0.5% and 6-10° ≅ 0	[314]
Biochar-TiO_2 composite	B_g: 2.60-2.70; 500 W visible light.	Degradation of methylene blue (MB) in simulated wastewater.	Unrealized.	Unrealized.	[315]
Bi_2WO_6 supported on biochar from pine modified with urea (n-biochar).	B_g: 2.28; (λ> 420 nm) - visible-light irradiation (500 W Xe lamp).	Rhodamine B dye and Cr(VI) removal in aqueous system.	1° (100) and 4° (98.4)	Unrealized.	[316]
Bi/Bi_2O_3 supported on biochar	B_g [a]; UV/Vis irradiation (500 W Xe lamp (λ> 350-700 nm)	Degradation of estrone in aqueous system.	1° (94.7) and 4° (82.9)	The bismuth concentration varies between 9.2- 6.1 µg/L in the 5 cycles.	[317]
$CuWO_4$ supported on biochar	B_g: 1.86; (λ > 400 nm) visible-light irradiation from tungsten lamp (150 mW/cm^2)	Photocatalytic degradation of ciprofloxacin, methylene blue and rhodamine-B in aqueous system and electro-oxidation of methanol.	1° (97), 2° (93), 3° (90), 4° (86) e 5° (79) [b].	Unrealized.	[318]
Zn-Co-LDH supported on biochar	B_g: 1.83; 10 W UV-B light irradiation source	Degradation of gemifloxacin in aqueous system.	5 cycles with removal >85%.	Unrealized.	[319]
Fe@Zn@biochar from corn stalks	B_g [a]; 260 ± 10 Lux of light intensity	Cr(VI) removal in aqueous and soil system.	Unrealized.	Unrealized.	[320]
Cu_2O-CuO@biochar	B_g: 1.70 and 2.10 for CuO and Cu_2O, respectively; 10 W UV-B light irradiation.	Degradation of reactive Orange in aqueous system.	5 cycles with removal >85%.	Unrealized.	[321]

CdSe quantum dots supported on biochar from bamboo	B_g [a]; (λ > 420 nm) visible-light irradiation from 250W Xe lamp.	Degradation of tetracycline in aqueous system.	4 cycles with removal ≅70%.	Unrealized.	[322]
Biochar quantum-dot/$Bi_4Ti_3O_{12}$ nanosheets	B_g: 2.36; 300 W Xenon irradiation lamp with a filter cutting off 400 nm light.	Degradation of tetracycline in aqueous system.	4 cycles with removal ≅80%.	Unrealized.	[323]
Carbon quantum dots CQDs/Cu_2O nanocomposite	B_g: 1.91; Visible-light irradiation from Halogen lamp.	CO_2 photoreduction	5 cycles with photoactivity ≅80%.	Unrealized.	[324]
Biochar-templated g-C_3N_4/$Bi_2O_2CO_3$/$CoFe_2O_4$	B_g: 2.14; simulated solar visible-light irradiation from Xe lamp (800 W) and natural sun light illumination.	Degradation of paraquat in aqueous system, nitrophenol reduction and CO_2 conversion.	1° (99.3) - 5° (98.1) [c]	Unrealized.	[325]
Magnetic Fe_3O_4/$BiVO_4$ heterostructure supported by biochar	B_g: 2.12; solar light.	Degradation of methyl paraben and thiophanate methyl sorption in soil.	1° (70.17) - 5° (68.24) [d]	Unrealized.	[326]
TiO_2-modified biochar, by KOH (Ti-KBC) or $FeCl_3$ (Ti-FBC)	B_g Ti-KBC: 2.39 and B_g Ti-FBC: 2.48; 15 W UV lamp (254 nm) irradiation and visible-light irradiation.	Degradation of enrofloxacin in aqueous system.	1° (84.63) - 5° (77.14) [e]	Unrealized.	[327]
TiO_2 supported on biochar from miscanthus straw pellets (TiO_2/MSP700) and soft wood pellets (TiO_2/SWP700)	B_g TiO_2/MSP700: 2.50 B_g TiO_2/SWP700: 2.12; visible-light from xenon lamp (400-640 nm; ~60.6 W m^{-2}) and UV-light (220–400 nm, ~264.3 W m^{-2}).	Phenol degradation in the liquid phase and oxidation of methanol in the gas phase.	There was a loss of only ± 10% of phenol degradation activity after cycle 5. [f] There was a loss of only ± 10% photo-oxidation of methanol after execution 5. [f]	Leaching of titanium after photocatalytic assays was not observed in the aqueous solution.	[328]

[a] Not determined; [b] Study done only for ciprofloxacin; [c] Study done only for paraquat; [d] Study done only for methyl paraben; [e] Study done only for Ti-KBC; [f] Study done only for TiO_2/SWP700.

Table 8. Comparison between biochar and other carbon materials in the synthesis of TiO_2-based composites for photocatalytic degradation of methylene blue (MB)

Material	Syntheses do material	General degradation conditions	Main results	Ref.
Multiwalled carbon nanotubes (MWCNTs)	(1) oxidized MWCNTs were dispersed in a solution of Milli-Q water (100 mL) and ethanol (100 mL) and subjected to US for 10 min (2) (100 mL) of $Ti(OC_4H_9)_4$ and ethanol were added slowly to the suspension and stirred for 1 h. (3) Evaporation of the solvent at 90 ºC. (4) The system was calcined in vacuum at 600 ºC for 1 h.	Material dose: 0.5 g L^{-1}; [MB] = 10 mg L^{-1}. The suspension was stirred in the dark for 2 h to ensure the establishment of an adsorption-desorption balance. The system was irradiated with visible light using a cut filter (λ> 450 nm), mercury lamp (125 W).	76% of MB is degraded by MWCNT/TiO_2 (1:3) after less 100 min.	[329]
Graphene oxide (GO)	(1) Synthesis of graphene oxide by the Hummers method. (2) TiO_2 were added to a GO suspension (1:2 ration), which was previously dispersed for 1 h. After stirring for 30 min under US, the suspension was dried at 293K for 4 h. Finally, the sample was centrifuged at 6000 rpm for 20 min. The supernatant was discarded, while the solids were dried in an oven at 323K overnight.	Material dose: 0.2 g L^{-1}; [MB] = 5 mg L^{-1}; pH=10. The suspension was stirred for 30 min until it achieved an equilibrium. Time of reaction: 4h. The system was irradiated with xenon lamp (500 W).	~100% of removal.	[330]
Biochar from furniture industry (MDF)	(1) The MDF biomass was washed with water and dried at 60 ºC for 8 h. (2) The samples were ground; (3) TiO_2 was impregnated on the surface of MDF biomass in the proportion of 10% (B10T) (w/w) by immersion in isopropyl alcohol followed by US for 60 min at 50 ºC; (4) The sample was dried in an oven until complete evaporation of the alcohol, followed by pyrolysis at 500 ° C under a nitrogen atmosphere (N_2).	Material dose: 1.0 g L^{-1}; [MB] = 10 mg L^{-1}; pH=5.5. The suspension was stirred for 60 min until it achieved an equilibrium. Time of reaction: 180 min. The system was exposed to a source 10 mW m^{-2} of UV irradiation (15 W, wavelength range 380–480 nm).	~80% of removal.	[331]

3.4. Synthesis of fine chemicals

Biomass contains low energy density and a complex structural matrix, which can compromise its direct use as a fuel [332]. However, alternatives involving the synthesis of fine chemicals from biomass have attracted the attention of researchers. The valorization of biomass for the synthesis of value-added chemicals is a sustainable process in which produced chemicals can replace petrochemicals as building blocks for various consumer products [333]. Furfural and hydroxymethylfurfural (HMF) are obtained from lignocellulosic biomass and used as a platform chemical as shown in Fig. 20 [185], [334], [335]. Xia et al. (2018) published a review that highlighted the latest advances in catalytic conversion of HMF into value-added chemicals by some important reactions [336]. Another important review was written by Pileidis and Titirici (2016) in which they describe the production of levulinic acid from biomass. This molecule is also used as a platform in the synthesis of fine chemicals [337].

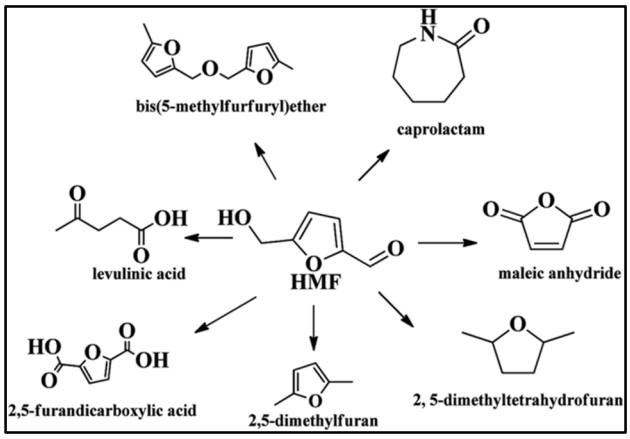

Fig. 20. HMF as a platform compound for diverse reactions. Reproduced from: Efficient conversion of 5-hydroxymethylfurfural to high-value chemicals by chemo- and bio-catalysis, 8, Xia, H. *et al.* Copyright (2018), with permission from Royal Society of Chemistry, https://doi.org/10.1039/c8ra05308a [336].

Acid-catalyzed fructose dehydration is the conventional method of production of HMF [332]. The reactions steps of the production of HMF from biomass are shown in Fig. 21.

To accelerate the conversion of biomass, two types of catalysts are used: (a) Brønsted acids that favor hydrolysis and dehydration through proton attack and (b) Lewis acids that promote isomerization through displacement of 1.2 hydrides [338], [333]. H_2SO_4, HCl and H_3PO_4 are the most used homogeneous catalytic reagents for the production of HMF through the dehydration of carbohydrates. They contribute to equipment corrosion and environmental pollution; however, product purification steps are necessary, and it is not possible to recycle the catalysts [339]. Heterogeneous

catalysis efficiently overcomes these disadvantages of homogeneous catalysis, but generally have low hydrolytic efficiency due to a mass transfer resistance between the solid catalyst and the water-insoluble cellulose [340]. Studies show that the incorporation of a Lewis acid metal species into porous support materials produces solids with high-performance catalysts for glucose isomerization to fructose [341].

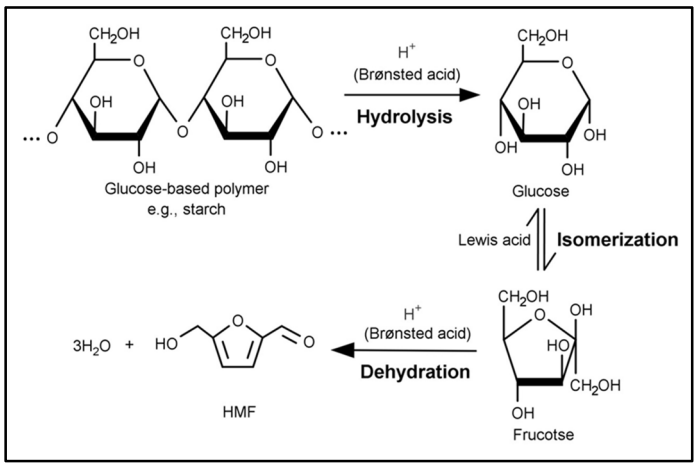

Fig. 21. Reaction steps and catalysts involved in the production of HMF from biomass. Reproduced from: Catalytic valorization of starch-rich food waste into hydroxymethylfurfural (HMF): Controlling relative kinetics for high productivity, 237, Iris, K. M. *et al.* Copyright (2019), with permission from Elsevier, License number: 4844661159641, https://doi.org/10.1016/j.biortech.2017.01.017 [338].

Fine chemicals obtained from biomass in reactions catalyzed by biochar are described in Table 9. This table describes the catalyst used, the start material, general conditions reactions, products obtained, yield and number of cycles.

Xiong and collaborators (2020) conducted a study of the isomerization from glucose to fructose. This reaction involves a critical intermediate step between many routes of chemical synthesis. The authors used biochar (BC), graphitic oxide (GIO) and graphene oxide (GO) as carbon supports to synthesize heterogeneous catalysts impregnated with Al. The conversions were performed via microwave heating, using a green solvent, in water, and moderate temperature (140 ºC). All materials showed useful catalytic activity in glucose isomerization with yields of 35, 34.3 and 29%, for GIO-Al200, GO-Al200 and BC-Al200, respectively. Comparatively, biochar-based catalysts showed similar catalytic performance and kinetic mode to graphene oxide-based catalysts [342].

Table 9. Fine chemicals obtained from biomass in reactions catalyzed by biochar.

Catalyst	Compound of origin	Conditions	Product obtained	Yields	Number of cycles (Yield %)	Ref
Ru-Re supported on biochar from rice straw	Furan	T=160 °C; P=30 bar H_2; weight ratio of feed/catalyst = 8; furan conversion = 80%.	Main products were: 1,4-butanediol (1,4-BD); tetrahydrofuran (THF),	1,4-BD ≅ 30% THF ≅ 50%	The catalyst showed loss of activity after the reaction.	[185]
Ru-ReOx supported on biochar from rice straw (RSB) by pyrolysis in an N_2 or CO_2 environment	Furan	T=160 °C; P= 30 bar de H_2; furan conversion = 80%.	1,4-butanediol (1,4-BD); tetrahydrofuran (THF)	Ru-ReOx/RSB-N_2: 1,4-BD ≅ 25% THF ≅ 55% Ru-ReOx/RSB-CO_2: 1,4-BD ≅ 15% THF ≅ 70%	Unrealized.	[186]
Phosphoric acid-activated wood biochar	Bread waste (BW); Rice waste (RW); Spaghetti waste (SW)	Food waste 0.5 g, catalyst 0.2 g, 180 °C, 20 min, DMSO/DIW * 10 mL (3/1, v/v)	5-hydroxymethylfurfural (HMF)	BW: 24.5 ; RW: 22.2 and SW:14.7 Cmol%	Unrealized.	[332]
Al supported on biochar from wood waste by N_2 (10%Al-700N2) or CO_2 (10%Al-700CO2) pyrolysis atmosphere	Glucose	Catalyst: 0.25 g, 0.5 g glucose in 10 mL water; T=160 °C; t=20 min; (microwave: 1900 W).	Fructose	10%Al-700N2: 14-16 Cmol% *** 10%Al-700CO2: 16-18 Cmol% ***	1° (21.5 mol%); 2° (13.5) and 3° (7.8 mol%). Conditions: 5 min, acetone/H_2O and 20% Al-500N2	[333]
Biochar-Supported Platinum Catalyst	Furfural	Catalyst: 0.025 mmol; T=210 °C for 2 h and 1500 psi, solvent: toluene; 3% w/w of Pt.	Furfuryl alcohol;	60.8%	≈ Same conversion and selectivity in two cycles. In the third, the conversion decrease 20%.	[334]
Bamboo-derived biochar sulfonic acid bearing polyamide	Cellulose	Catalyst: 0.1 g, cellulose: 0.2 g, water: 1.5 mL, microwave: 350 W, T:90 °C, t: 2 h.	5-hydroxymethylfurfural (HMF)	23%	Efficiency (20%) has been proven in 4 different cycles.	[335]

Sn supported on biochar from wood waste by N_2 (Sn-B750N) or CO_2 (Sn-B750C) pyrolysis atmosphere	Glucose	Catalyst: 0.25 g (Sn-B750N or Sn-B750C), glucose (10 mL; 5% w/v) at 160 °C for 20 min.	Fructose	Sn-B750N: 10.8 Cmol% Sn-B750C: 15.2 Cmol%	Sn-B750N: 1° (10.80)-3° (3.631) Sn-B750C: 1° (15.15)-3° (4.500)	[341]
Alloyed Cu–Ni Encapsulated in Biochar Catalysts (5%Cu-15%Ni/BC)	5-hydroxymethylfurfural (HMF)	T=220 °C, p(H_2)=4 MPa, t=12 h, catalyst=100 mg, HMF =250 mg, rating speed=500 rpm, and V_{THF} = 40 mL. Conversion ≅100 Cmol%	2,5-Dimethylfurfural (DMF), 5-methylfurfural (MFF) and 2,5-dihydroxymethylfuran (DHMF)	DMF ≅93.5% and ≅6.5% for other products	DMF yield decreased from 93.5% to 80.1% after the third run and stabilized until the fifth cycle.	[343]
Biochar-Mg-Sn	Corn stalk	T=100 °C, t=3 h in isopropanol/AMIMCl; catalyst dosage 20%**	5-hydroxymethylfurfural	63.57%	From 1-5° cycle the conversion decreased 10.67%, and the 5-HMF yield decreased 15.31%.	[344]
Aluminium oxide-silica/carbon from rice husk	Glucose	Catalyst: 100 mg, glucose 1.0 mmol, N-methylpyrrolidone (4 mL) 170 °C, 5 h. Conversion = 93%	5-hydroxymethylfurfural (HMF)	52%	≈ Same HMF yield after five cycles.	[345]

*dimethyl sulfoxide (DMSO) and deionized water (DIW); **AMIMCl: 1-allyl-3-methylimidazolium chloride; ***yield variation obtained for temperatures 500, 600 and 700 °C.

3.5. Syngas reforming reactions

Gases are generated in the incomplete degradation (syngas) during pyrolysis of biomass/gasification of biomass, which has several applications such as, for example, power generation using gas turbines or production of liquid fuels through the Fischer-Tropsch process [346]. Biomass gasification has several advantages over fossil fuels such as lower emissions of CO_2 and other flue gases, such as H_2S, SO_2, NO_x [347]. However, a major disadvantage that limits the use of syngas is the generation of tars, a complex mixture of aromatic and oxygenated condensed hydrocarbons with molecular weights greater than that of benzene [348].

Tars are produced together with syngas during biomass gasification and their content varies from about 0.5 to 100 g/m^3, depending on the type and design of the gasifier, the raw material used and the operating conditions [349]. Tars condense in pipes, filters or heat exchangers of downstream equipment and processes, which causes mechanical damage to the entire system [347]. There are several mechanical/physical gas cleanup systems that exist for removal of both particulates and tar from gases produced by biomass gasification. These processes will not be described here, and a review by Anis and Zainal (2011) is recommended [350].

Catalytic reforming is considered to be most promising in large scale applications, due to its fast reaction and reliability [349]. The catalysts for tar reduction are classified in six groups: (i) nickel-based, (ii) non-nickel metal, (iii) alkali metal, (iv) basic, (v) acid, and (vi) activated carbon catalysts [351], [350]. Noble metals such as Pt, Rh, Ru, etc. have an effect on tar reforming [317]. The nickel-based catalyst is the catalyst indicated for the cracking of tar, because it shows high tar conversion and gas production [352], [317]. However, the deactivation of the catalyst due to carbonaceous deposition, sintering of metals and the high costs of noble metals are still serious problems [353]. Carbon-based catalysts, such as coal char and biomass char, have received attention for tar cracking due to their low cost and good catalytic performance [352], [354], [355].

The thermal cracking of tar in a reactor using char as a catalyst has advantages over common mineral catalysts because: (1) char is produced in the pyrolysis and gasification system; (2) the coal surface is reactivated via gasification, avoiding deactivation; (3) coal is loaded with dispersed metal catalysts, increasing its catalytic capacity [356]. Besides, co-pyrolysis of coal and biomass is described as a way to increase the catalytic performance of coal in order to reduce tar [352], [351]. The

1 catalytic decomposition of tar using biochar from coal pyrolysis and/or biomass has
2 become valuable, because coal production and tar reduction are implemented
3 simultaneously within the gasifier [357].

4 The thermal cracking of tar proposed by Baker and Mudge, using NiO catalyst,
5 is described in Eqs. 53-57 [349].

6 $$\text{tars} \rightarrow C + C_nH_m + \text{gases} \qquad \text{(Eq. 53)}$$

7 $$C_nH_m + n\ H_2O \rightarrow n\ CO + (n+m/2)\ H_2 \qquad \text{(Eq. 54)}$$

8 $$C_nH_m + n\ CO_2 \rightarrow m/2\ H_2 + 2n\ CO \qquad \text{(Eq. 55)}$$

9 $$CH_4 + H_2O \rightleftharpoons CO + 3\ H_2 \qquad \text{(Eq. 56)}$$

10 $$CO_2 + H_2 \rightleftharpoons CO + H_2O \qquad \text{(Eq. 57)}$$

11 Other works that described the application of biochar-based materials in
12 reforming reactions are summarized in Table 10. In this table, the catalyst used, reactor
13 specifications and general reaction conditions, start compound, and main results are
14 briefly described.

15 For comparison, two works employing nickel-catalyzed methane reforming,
16 which was supported on two different supports, hydroxyapatite and biochar are shown
17 in Table 11. It can be seen that the yields of CH_4 and CO_2 conversion have seen very
18 similar, around 80% for each compound.

Table 10. Application of biochar-based materials in reforming reactions

Catalyst	Starting compound	Reactor specifications and some conditions	Principal results	Ref
Biochar from the pyrolysis (RC) of hardwood and activated carbon (AC)	Tar concentration = 20 g/Nm^3; benzene (61.34), toluene (23.13) and naphthalene (15.53%).	Reactor: *l*=47 cm; ϕ=2.66 cm. The bed area: h:7 cm. Gas permanence time in the bed: 0.5 s. P=atmospheric; T= 850 °C; t = 3 h.	The % of CO; CO_2; CH_4 and H_2, were respectively: RC: 32.7, 6.70; 27.6 and 33.0 AC: 33.6; 6.38; 33.0 and 27.0	[346]
Rice husk char-supported nickel-iron	Rice husk (0.125-0.5 mm)	Fast pyrolysis; T 800 °C; 5g of rice husk; carrier gas N_2; flow rate 1.0 L/min; catalyst 5 g	Conversion of 92.3 and 93% using Ni-Fe char (without calcination step) and Ni char (with calcination), respectively.	[347]
Bauxite residue-biochar mixed catalyst led. Biochar from sawdust by gasification (GBC) and bauxite activated with HCl and calcined at 600 °C	Naphthalene: 1.6 g/Nm^3	Reactor: quartz tube of $\phi_{internal}$=15 mm; *l*=600 mm; catalyst bed: *l*=50-60 mm; bed volume:5.3 cm^3; Catalyst particle size:180-210 μm; T 700; P=101.3 kPa; Space velocity: 4500 h^{-1}	The biochar acts as a reducer by increasing the catalytic activity of the bauxite residue, presenting high conversion (≅100%) in a humid syngas environment.	[348]
NiO supported on char from wood and coal (15% NiO loading)	Sawdust biomass feed	Reactor tube of quartz: ϕ: 1-in.; *l*: 24-in; vacuum-sealing; catalyst bed length: 9 cm; char particle size: 0.3-0.45 mm; catalysts: 18 g; gas residence time: 0.3 s; gas flow rate: 9.12 L/min; gasification agent: air; reforming time: 15 min; T= 800°C.	Conversion efficiency: 97% in the best conditions. Catalyst performance: Ni/coal char > Ni/Wood char > coal char > wood char > no catalyst.	[349]
Fe-rich char (with 10% Fe_2O_3 addition in the one-step method with microwave heating)	Methane reforming	Microwave reforming; quartz reactor; ϕ:4 cm; *l*=16 cm; catalyst: 3g; T: 800 °C; CH_4:CO_2:N_2 1:1:2, flow: 120 mL/min. Volumetric hourly space velocity: 2.4 L/(g h); t=160 min	Conversion > 95%. High material stability, evidenced by decrease in conversion <5% in 160 min.	[358]
Cr-promoted Ni/biochar (Ni and Cr were 5 and 2.6 wt% of the char, respectively)	Methane reforming	Quartz fixed-bed reactor: $\phi_{internal}$: 3 mm; atmospheric pressure, T: 850 °C; CH_4/CO_2 ration (3:2, 1:1 and 2:3); flow: 20 mL/ min	The main effect of Cr is the great enhance of the adsorption to CO_2.	[359]

Table 11. Comparison between biochar and other materials used as support for nickel catalysts for dry reforming of methane

Support material	General conditions for material synthesis	General reaction conditions	Overall results	Ref.
Hydroxyapatite: Ca-HA2 (S_{BET} = 60 m^2 g^{-1}, d_{50} = 6.1 µm)	(1) The material was doped with Ni by impregnation using $Ni(NO_3)_2$. (2) Drying at 105 ºC overnight. (3) The theoretical nickel content was 5.7% w/w.	The process was carried out in a fixed bed reactor ($\phi_{internal}$ = 8 mm). The catalyst (300 mg) was diluted twice with inert, non-porous alumina powder. The reactor was filled with the first layers of alumina powder, followed by the catalyst/alumina powder mixture, which was positioned in the center of the reactor, and finally with the second layer of alumina powder. The reactor was fed with a mixture of synthetic gas with the following composition: CH_4: 20 mol%, CO_2: 20 mol% and N_2: 60 mol% with space velocity per hour in weight (WHSV) of 15.9 L h^{-1} g cat $^{-1}$.	CH_4 conversion: 66-78% and CO_2 conversion: 73-84%, Time on stream: 90 h	[360]
Biochar produced from cotton stem (S_{BET} = 39 m^2 g^{-1})	The catalyst was prepared by impregnation using $Ni(NO_3)_2 \cdot 6H_2O$ with alumina (γ-Al_2O_3). The sample was heated under an N_2 atmosphere for 120 min, respectively at 800 ºC and 1000 ºC.	Reactor: quartz tube of $\phi_{internal}$=40 mm; l=200 mm; catalyst: 6 g; microwave: f=2450 MHz and P: 0- 3000 W; T: 800 °C; volume ratio of $CH_4/CO_2/N_2$ of 1:1:2 and flow: 120 mL/min.	10% of nickel content shown conversion > 80 and 88% for CH_4 and CO_2, respectively. The H_2/CO ratio are promoted in mixed reforming on Ni/biochar.	[361]

4. Final considerations

This review illustrates the fact that biochar, a by-product of the biomass carbonization process in energy production, is a promising material as catalyst support with unique characteristics. There are several processes leading to biochar. However, the hydrothermal carbonization has been highlighted due to lower energy consumption. In this process, quantum carbon dots are obtained with several catalytic applications. On the other hand, the pyrolysis process allows obtaining different products: biochar, bio-oil and syngas, enabling a sustainable procedure, with zero waste generation. One of the challenges in this regard is to produce the three products with adequate yields and quality for their different applications. In this sense, as seen in this review, the biochar generated in the pyrolysis process can be reused as support for different catalysts toward syngas reforming reactions and synthesis of fine products from biomass. In order to improve the catalytic activity of processes, chemical and/or physical activation can be used, as well as their functionalization. Then, it is believed that biochar use can mitigate environmental impacts, including the generation of greenhouse gases such as CO_2 and CH_4, being therefore a sustainable process of great economic and social value. The main components of biochar are graphene pieces or carbon quantum dots that stabilize transition metal nanoparticles and transition metal oxide nanoparticles by π-bonding to their surface. Peripheral OH and CO_2H groups bind the nanoparticles by H-bonding and O-metal site bonding that contribute to this stabilization, but leave a large number of open free sites for interaction with- and catalytic activation of substrates.

5. Prospects

As previously discussed, the excellent characteristics of biochar are notorious. Such characteristics allow applications that extend from its use as a soil additive to support catalysts for various applications. In this sense, new sustainable processes for the production of clean energy will be made possible from the carbonization of biomass and new destinations will be provided to the by-product, biochar. New energy conversion routes with zero waste generation are being implemented, as illustrated in Figure 22. Such practices will allow a significant advance in sustainable agriculture, enabling ecological and income improvements.

Catalyst supported by biochar are finding increasing use towards the production of fine chemicals involving a variety of nanocatalytic processes [362] also including the

remediation of organic [363] and inorganic [364] pollutants from water. The use of biochar as catalysis support, as that of carbon materials in general, now finds a significant place in the context of hydrothermal carbonization materials that open a spectrum of applications, not only as catalyst supports in heterogeneous catalysis and electrocatalysis, but also in other fields such as batteries and fluorescent nanomaterials [365].

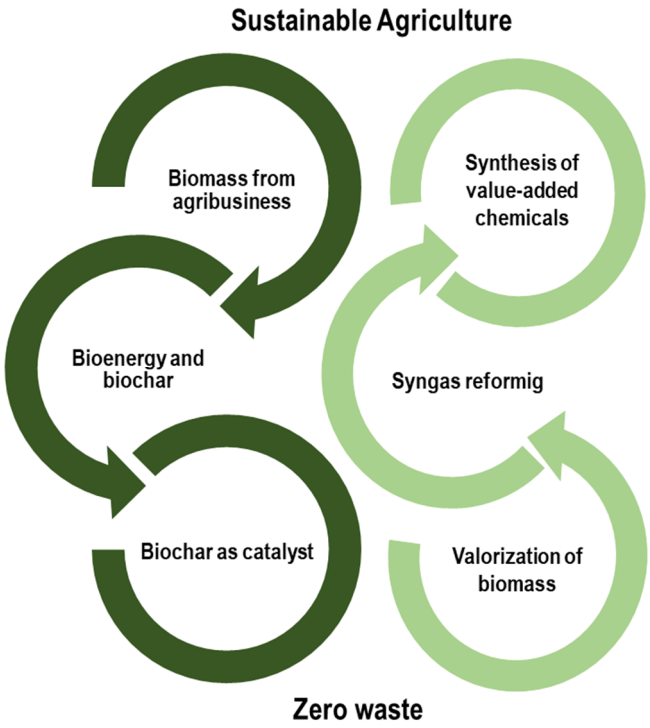

Fig. 22. Scheme illustrating the use of biomass in the conversion of bioenergy and value-added products: sustainable agriculture

6. Acknowledgment

Financial support from the Coordenação de Aperfeiçoamento de Pessoal de Nível Superior - Brazil (CAPES) for Process: 88881.337360/2019-01, CNPq/FAPEMIG (agreement recorded in SICONV: 793988/2013), the University of Bordeaux and the Centre National de la Recherche Scientifique (CNRS) and helpful suggestions of the referees are gratefully acknowledged.

7. References

[1] Agropecuária Brasileira em números, (2020). https://www.gov.br/agricultura/pt-br/assuntos/politica-agricola/todas-publicacoes-de-politica-agricola/agropecuaria-brasileira-em-numeros/agropecuaria-brasileira-em-numeros-abril-de-2020 (accessed June 30, 2020).

[2] N. Tripathi, C.D. Hills, R.S. Singh, C.J. Atkinson, Biomass waste utilisation in low-carbon products : harnessing a major potential resource, Npj Clim. Atmos. Sci. 2:35 (2019). https://doi.org/10.1038/s41612-019-0093-5.

[3] J. M. Encinar, A. Ramiro, J. F. Gonzalez, Pyrolysis/gasification of agricultural residues by carbon dioxide in the presence of different additives : influence of variables, Fuel Process. Technol. 55 (1998) 219–233.

[4] J. L. Santos, P. Mäki-arvela, A. Monzón, D.Y. Murzin, M. Ángel, Metal catalysts supported on biochars : Part I synthesis and characterization, Appl. Catal. B Environ. 268 (2020) 118423. https://doi.org/10.1016/j.apcatb.2019.118423.

[5] S. B. Montoro, J. L. Jr, D. F. L. Santos, M. S. S. M. Costa, Anaerobic co-digestion of sweet potato and dairy cattle manure : A technical and economic evaluation for energy and biofertilizer production, J. Clean. Prod. 226 (2019) 1082–1091. https://doi.org/10.1016/j.jclepro.2019.04.148.

[6] W. Tao, W. Duan, C. Liu, D. Zhu, X. Si, R. Zhu, P. Oleszczuk, B. Pan, Formation of persistent free radicals in biochar derived from rice straw based on a detailed analysis of pyrolysis kinetics, Sci. Total Environ. 715 (2020) 136575. https://doi.org/10.1016/j.scitotenv.2020.136575.

[7] D. Vamvuka, S. Sfakiotakis, Combustion behaviour of biomass fuels and their blends with lignite, Thermochim. Acta. 526 (2011) 192–199. https://doi.org/10.1016/j.tca.2011.09.021.

[8] F. Guo, K. Peng, S. Liang, X. Jia, X. Jiang, L. Qian, Evaluation of the catalytic performance of different activated biochar catalysts for removal of tar from biomass pyrolysis, Fuel. 258 (2019) 116204. https://doi.org/10.1016/j.fuel.2019.116204.

[9] M. Chen, C. Bao, D. Hu, X. Jin, Q. Huang, Facile and low-cost fabrication of ZnO/biochar nanocomposites from jute fibers for efficient and stable photodegradation of methylene blue dye, J. Anal. Appl. Pyrolysis. 139 (2019) 319–332. https://doi.org/10.1016/j.jaap.2019.03.009.

[10] A. Wahab, H. Sattar, A. Ashraf, S. N. Hussain, M. Saleem, S. Munir, Thermochemical, kinetic and ash characteristics behaviour of Thar Lignite , agricultural residues and synthetic polymer waste (EVA), Fuel. 266 (2020) 117151. https://doi.org/10.1016/j.fuel.2020.117151.

[11] H. Shahbeig, M. Nosrati, Pyrolysis of municipal sewage sludge for bioenergy production : Thermo-kinetic studies , evolved gas analysis , and techno-socio-economic assessment, Renew. Sustain. Energy Rev. 119 (2020) 109567. https://doi.org/10.1016/j.rser.2019.109567.

[12] J. Gutiérrez, C.A. Galán, R. Suárez, A. Álvarez-Murillo, J.F. González, Biofuels from cardoon pyrolysis : Extraction and application of biokerosene / kerosene mixtures in a self-manufactured jet engine, Energy Convers. Manag. 157 (2018) 246–256. https://doi.org/10.1016/j.enconman.2017.12.006.

[13] J. Plácido, S. Bustamante-López, K. E. Meissner, D. E. Kelly, S. L. Kelly, Microalgae biochar-derived carbon dots and their application in heavy metal sensing in aqueous systems, Sci. Total Environ. 656 (2019) 531–539. https://doi.org/10.1016/j.scitotenv.2018.11.393.

[14] X. Liu, L. Yang, H. Zhao, W. Wang, Pyrolytic production of zerovalent iron nanoparticles supported on rice husk-derived biochar : simple, in situ synthesis and use for remediation of Cr(VI)-polluted soils, Sci. Total Environ. 708 (2020) 134479. https://doi.org/10.1016/j.scitotenv.2019.134479.

[15] V. Benedetti, E. Cordioli, F. Patuzzi, M. Baratieri, CO2 Adsorption study on pure and chemically activated chars derived from commercial biomass gasifiers, J. CO2 Util. 33 (2019) 46–54. https://doi.org/10.1016/j.jcou.2019.05.008.

[16] J. S. Cha, S. H. Park, S. C. Jung, C. Ryu, J. K. Jeon, M. C. Shin, Y. K. Park, Production and utilization of biochar: A review, J. Ind. Eng. Chem. 40 (2016) 1–15. https://doi.org/10.1016/j.jiec.2016.06.002.

[17] N. Liu, A. B. Charrua, C. H. Weng, X. Yuan, F. Ding, Characterization of biochars derived from agriculture wastes and their adsorptive removal of atrazine from aqueous solution: A comparative study, Bioresour. Technol. 198 (2015) 55–62. https://doi.org/10.1016/j.biortech.2015.08.129.

[18] W. Chen, D. L. Mattern, E. Okinedo, J. C. Senter, A. A. Mattei, C. W. Redwine, Photochemical and Acoustic Interactions of Biochar with CO2 and H2O : Applications in Power Generation and CO2 Capture, Aiche J. 60 (2014) 1054-1065. https://doi.org/10.1002/aic.

[19] N. Zhou, H. Chen, J. Xi, D. Yao, Z. Zhou, Y. Tian, X. Lu, Biochars with excellent Pb (II) adsorption property produced from fresh and dehydrated banana peels via hydrothermal carbonization, Bioresour. Technol. 232 (2017) 204–210. https://doi.org/10.1016/j.biortech.2017.01.074.

[20] L. Beesley, E. Moreno-Jiménez, J. L. Gomez-Eyles, Effects of biochar and greenwaste compost amendments on mobility, bioavailability and toxicity of inorganic and organic contaminants in a multi-element polluted soil, Environ. Pollut. 158 (2010) 2282–2287. https://doi.org/10.1016/j.envpol.2010.02.003.

[21] A. F. N. Boss, F. L. Braghiroli, G. Amaral-Labat, A. A. T. Souza, M. R. Baldan, H. Bouafif, A. Koubaa, G. F. Silva, Dielectric characterization of white birch–activated biochar composites : A sustainable alternative to radar-absorbing materials, J. Compos. Mater. 54 (2020). https://doi.org/10.1177/0021998319877493.

[22] G. Fang, C. Zhu, D. D. Dionysiou, J. Gao, D. Zhou, Mechanism of hydroxyl radical generation from biochar suspensions : Implications to diethyl phthalate degradation, Bioresour. Technol. 176 (2015) 210–217. https://doi.org/10.1016/j.biortech.2014.11.032.

[23] Y. Shen, Chars as carbonaceous adsorbents/catalysts for tar elimination during biomass pyrolysis or gasification, Renew. Sustain. Energy Rev. 43 (2015) 281–295. https://doi.org/10.1016/j.rser.2014.11.061.

[24] L. J. Konwar, J. Boro, D. Deka, Review on latest developments in biodiesel production using carbon-based catalysts, Renew. Sustain. Energy Rev. 29 (2014) 546–564. https://doi.org/10.1016/j.rser.2013.09.003.

[25] A. H. Lone, G. R. Najar, M. A. Ganie, J. A. Sofi, T. Ali, Biochar for Sustainable Soil Health : A Review of Prospects and Concerns, Pedosphere 25 (2015) 639–653. https://doi.org/10.1016/S1002-0160(15)30045-X.

[26] M. Ahmad, A. U. Rajapaksha, J. E. Lim, M. Zhang, N. Bolan, D. Mohan, M. Vithanage, S. S. Lee, Y. S. Ok, Biochar as a sorbent for contaminant management in soil and water: A review, Chemosphere. 99 (2014) 19–23. https://doi.org/10.1016/j.chemosphere.2013.10.071.

[27] D. Mohan, A. Sarswat, Y. Sik, C.U. Pittman-Jr., Organic and inorganic contaminants removal from water with biochar, a renewable, low cost and sustainable adsorbent – A critical review, Bioresour. Technol. 160 (2014) 191–202. https://doi.org/10.1016/j.biortech.2014.01.120.

[28] H. Liu, L. Wang, M. Lei, Positive impact of biochar amendment on thermal balance during swine manure composting at relatively low ambient temperature, Bioresour. Technol. 273 (2019) 25–33. https://doi.org/10.1016/j.biortech.2018.10.033.

[29] A. B. Fuertes, G. A. Ferrero, N. Diez, M. Sevilla, A Green Route to High-Surface Area Carbons by Chemical Activation of Biomass-Based Products with Sodium Thiosulfate, ACS Sustain. Chem. Eng. 6 (2018). https://doi.org/10.1021/acssuschemeng.8b03264.

[30] C. A. Okonkwo, T. Lv, W. Hong, G. Li, J. Huang, J. Deng, L. Jia, M. Wu, H. Liu, M. Guo, The synthesis of micromesoporous carbon derived from nitrogen-rich spirulina extract impregnated castor shell based on biomass self- doping for highly ef fi cient supercapacitor electrodes, J. Alloys Compd. 825 (2020) 154009. https://doi.org/10.1016/j.jallcom.2020.154009.

[31] J. Yu, Y. Zhao, Y. Li, Utilization of corn cob biochar in a direct carbon fuel cell, J. Power Sources. 270 (2014) 312–317. https://doi.org/10.1016/j.jpowsour.2014.07.125.

[32] A. Elleuch, A. Boussetta, J. Yu, K. Halouani, Y. Li, Experimental investigation of direct carbon fuel cell fueled by almond shell biochar : Part I . Physico-chemical characterization of the biochar fuel and cell performance examination, Int. J. Hydrogen Energy. 38 (2013) 16590–16604.

https://doi.org/10.1016/j.ijhydene.2013.08.090.

[33] K. Preuss, V. Kumar, A. Marinovic, M. Isaacs, K. Wilson, I. Abrahams, M. M. Titirici, Bio-inspired carbon electro-catalysts for the oxygen reduction reaction, J. Energy Chem. 25 (2016) 228–235. https://doi.org/10.1016/j.jechem.2016.01.001.

[34] J. Jiang, L. Zhang, X. Wang, N. Holm, K. Rajagopalan, F. Chen, S. Ma, Highly ordered macroporous woody biochar with ultra-high carbon content as supercapacitor electrodes, Electrochim. Acta. 113 (2013) 481–489. https://doi.org/10.1016/j.electacta.2013.09.121.

[35] C. Liu, W. Chen, M. Li, S. Hong, W. Li, M. Pan, Q. Wu, C. Mei, Rapid microwave activation of waste palm into hierarchical porous carbons for supercapacitors using biochars from di ff erent carbonization temperatures as catalysts†, RSC Adv. 9 (2019) 19441–19449. https://doi.org/10.1039/c9ra03031j.

[36] S. Liu, M. Li, Y. Liu, N. Liu, X. Tan, L. Jiang, J. Wen, X. Hu, Z. Yin, Removal of 17β-estradiol from aqueous solution by graphene oxide supported activated magnetic biochar: Adsorption behavior and mechanism, J. Taiwan Inst. Chem. Eng. 102 (2019) 330–339. https://doi.org/10.1016/j.jtice.2019.05.002.

[37] L. Qian, W. Zhang, J. Yan, L. Han, Y. Chen, D. Ouyang, M. Chen, Nanoscale zero-valent iron supported by biochars produced at different temperatures : Synthesis mechanism and effect on Cr(VI) removal, Environ. Pollut. 223 (2017) 153–160. https://doi.org/10.1016/j.envpol.2016.12.077.

[38] D. Yao, Q. Hu, D. Wang, H. Yang, C. Wu, X. Wang, H. Chen, Hydrogen production from biomass gasification using biochar as a catalyst/support, Bioresour. Technol. 216 (2016) 159–164. https://doi.org/10.1016/j.biortech.2016.05.011.

[39] Y. Zu, P. Yang, J. Wang, X. Liu, J. Ren, G. Lu, Y. Wang, Efficient production of the liquid fuel 2,5-dimethylfuran from 5-hydroxymethylfurfural over Ru/Co3O4 catalyst, Appl. Catal. B Environ. 146 (2014) 244–248. https://doi.org/10.1016/j.apcatb.2013.04.026.

[40] X. Kong, Y. Zhu, H. Zheng, F. Dong, Y. Zhu, Y. W. Li, Switchable synthesis of 2,5-dimethylfuran and 2,5-dihydroxymethyltetrahydrofuran from 5-

hydroxymethylfurfural over Raney Ni catalyst, RSC Adv. 4 (2014) 60467–60472. https://doi.org/10.1039/c4ra09550b.

[41] M. Przydacza, M. Jędrzejczyka, M. Brzezińskaa, J. Rogowskia, N. Keller, A. M.Rupperta, Solvothermal hydrodeoxygenation of hydroxymethylfurfural derived from biomass towards added value chemicals on Ni/TiO 2 catalysts, J. Supercrit. Fluid. 163 (2020). https://doi.org/10.1016/j.supflu.2020.104827.

[42] P. V. F. Sousa, Y. M. Guimarães, G. C. Pinto, A. F. Oliveira, A. A. Silva, R. P. Lopes, Study of Cu NPs reactivity for compounds with different chemical structures: Black reactive dye 5, picric acid and 2,4-D herbicide, Chemosphere 235 (2019) 749–756. https://doi.org/10.1016/j.chemosphere.2019.06.210.

[43] M. F. Ourique, P. V. F. Sousa, A. F. Oliveira, R .P. Lopes, Comparative study of the direct black removal by Fe, Cu, and Fe/Cu nanoparticles, Environ. Sci. Pollut. R. 25 (2018) 28928-28941. https://doi.org/10.1007/s11356-018-2842-0

[44] M. A. Nascimento, R. P. Lopes, J. C. Cruz, A. A. Silva, C. F. Lima, Sulfentrazone dechlorination by iron-nickel bimetallic nanoparticles, Environ. Pollut. 211 (2016) 406–413. https://doi.org/10.1016/j.envpol.2015.12.043.

[45] J. C. Cruz, M. A. Nascimento, H. A. V. Amaral, D. S. D. Lima, A. P. C. Teixeira, R. P. Lopes, Synthesis and characterization of cobalt nanoparticles for application in the removal of textile dye, J. Environ. Manage. 242 (2019) 220–228. https://doi.org/10.1016/j.jenvman.2019.04.059.

[46] M. M. Titirici, R. J. White, N. Brun, V. L. Budarin, D. S. Su, F. del-Monte, J. H. Clark, M. J. MacLachlang, Sustainable carbon materials, Chem. Soc. Rev. 44 (2015) 250–290. https://doi.org/10.1039/c4cs00232f.

[47] D. W. Cho, S. Kim, Y. F. Tsang, H. Song, Preparation of nitrogen-doped Cu-biochar and its application into catalytic reduction of p-nitrophenol, Environ. Geochem. Health. 41 (2019) 1729–1737. https://doi.org/10.1007/s10653-017-9966-x.

[48] B. Sajjadi, J. W. Broome, W. Y. Chen, D. L. Mattern, N. O. Egiebor, N. Hammer, C. L. Smith, Urea functionalization of ultrasound-treated biochar : A feasible strategy for enhancing heavy metal adsorption capacity, Ultrason. Sonochem. 51

(2019) 20–30. https://doi.org/10.1016/j.ultsonch.2018.09.015.

[49] M. B. Ahmed, J. L. Zhou, H. H. Ngo, W. Guo, Insight into biochar properties and its cost analysis, Biomass. Bioenerg. 84 (2016) 76–86. https://doi.org/10.1016/j.biombioe.2015.11.002.

[50] H. Fu, S. Ma, P. Zhao, S. Xu, S. Zhan, Activation of peroxymonosulfate by graphitized hierarchical porous biochar and MnFe2O4 magnetic nanoarchitecture for organic pollutants degradation: Structure dependence and mechanism, Chem. Eng. J. 360 (2019) 157–170. https://doi.org/10.1016/j.cej.2018.11.207.

[51] D. V. Cuong, N. L. Liu, V. A. Nguyen, C. H. Hou, Meso/micropore-controlled hierarchical porous carbon derived from activated biochar as a high-performance adsorbent for copper removal, Sci. Total Environ. 692 (2019) 844–853. https://doi.org/10.1016/j.scitotenv.2019.07.125.

[52] K. Jindo, H. Mizumoto, Y. Sawada, M. A. Sanchez-Monedero, T. Sonoki, Physical and chemical characterization of biochars derived from different agricultural residues, Biogeosciences. 11 (2014) 6613–6621. https://doi.org/10.5194/bg-11-6613-2014.

[53] P. N. Y. Yek, W. Peng, C. C. Wong, R. K. Liew, Y. L. Ho, W. A. W. Mahari, E. Azwar, T. Q. Yuan, M. Tabatabaei, M. Aghbashlo, C. Sonne, S. S. Lam, Engineered biochar via microwave CO2 and steam pyrolysis to treat carcinogenic Congo red dye, J. Hazard. Mater. 395 (2020) 1226362. https://doi.org/10.1016/j.jhazmat.2020.122636.

[54] Y. Wei, C. Shen, J. Xie, Q. Bu, Science of the Total Environment Study on reaction mechanism of superior bamboo biochar catalyst production by molten alkali carbonates pyrolysis and its application for cellulose hydrolysis, Sci. Total Environ. 712 (2020) 136435. https://doi.org/10.1016/j.scitotenv.2019.136435.

[55] C. D. Blasi, Modeling chemical and physical processes of wood and biomass pyrolysis, Prog. Energ. Combust. 34 (2008) 47–90. https://doi.org/10.1016/j.pecs.2006.12.001.

[56] E. Pusceddu, S. F. Santilli, G. Fioravanti, A. Montanaro, F. Miglietta, P. U. Foscolo, Chemical-physical analysis and exfoliation of biochar-carbon matter :

from agriculture soil improver to starting material for advanced nanotechnologies, Mater. Res. Express 6 (2019) 115612. https://doi.org/10.1088/2053-1591/ab4ba8.

[57] H. Wu, Q. Feng, Fabrication of bimetallic Ag/Fe immobilized on modified biochar for removal of carbon tetrachloride, J. Environ. Sci. 54 (2016) 346–357. https://doi.org/10.1016/j.jes.2016.11.017.

[58] J. Park, S. Yoo, K. H. Lim, O. J. Rojas, M. A. Hubbe, S. Park, Impact of oxidative carbonization on structure development of loblolly pine- derived biochar investigated by nuclear magnetic resonance spectroscopy and X-ray photoelectron spectroscopy, Diam. Relat. Mater. 96 (2019) 140–147. https://doi.org/10.1016/j.diamond.2019.05.001.

[59] X. Xiao, B. Chen, A Direct Observation of the Fine Aromatic Clusters and Molecular Structures of Biochars, Environ. Sci. Technol. 51 (2017) 5473–5482. https://doi.org/10.1021/acs.est.6b06300.

[60] C. H. Chia, B. Gong, S. D. Joseph, C. E. Marjo, P. Munroe, A. M. Rich, Vibrational Spectroscopy Imaging of mineral-enriched biochar by FTIR, Raman and SEM–EDX, Vib. Spectrosc. 62 (2012) 248–257. https://doi.org/10.1016/j.vibspec.2012.06.006.

[61] Z. Li, Y. Sun, Y. Yang, Y. Han, T. Wang, J. Chen, D.C.W. Tsang, Biochar-supported nanoscale zero-valent iron as an e ffi cient catalyst for organic degradation in groundwater, J. Hazard. Mater. 383 (2020) 121240. https://doi.org/10.1016/j.jhazmat.2019.121240.

[62] S. Mandal, S. Pu, L. He, H. Ma, D. Hou, Biochar induced modi fi cation of graphene oxide & nZVI and its impact on immobilization of toxic copper in soil *, Environ. Pollut. 259 (2020) 113851. https://doi.org/10.1016/j.envpol.2019.113851.

[63] C. Sun, T. Chen, Q. Huang, M. Zhan, X. Li, J. Yan, Activation of persulfate by CO2-activated biochar for improved phenolic pollutant degradation : Performance and mechanism, Chem. Eng. J. 380 (2020) 122519. https://doi.org/10.1016/j.cej.2019.122519.

[64] B. Wang, Y. Li, L. Wang, Metal-free activation of persulfates by corn stalk biochar for the degradation of antibiotic nor fl oxacin : Activation factors and degradation

mechanism, Chemosphere. 237 (2019) 124454. https://doi.org/10.1016/j.chemosphere.2019.124454.

[65] J. He, Y. Xiao, J. Tang, H. Chen, H. Sun, Persulfate activation with sawdust biochar in aqueous solution by enhanced electron donor-transfer effect, Sci. Total Environ. 690 (2019) 768–777. https://doi.org/10.1016/j.scitotenv.2019.07.043.

[66] X. Zhou, Z. Zeng, G. Zeng, C. Lai, R. Xiao, S. Liu, D. Huang, L. Qin, X. Liu, B. Li, H. Yi, Y. Fu, L. Li, Z. Wang, Persulfate activation by swine bone char-derived hierarchical porous carbon : Multiple mechanism system for organic pollutant degradation in aqueous media, Chem. Eng. J. 383 (2020) 123091. https://doi.org/10.1016/j.cej.2019.123091.

[67] J. Yan, L. Yang, L. Qian, L. Han, M. Chen, Nano-magnetite supported by biochar pyrolyzed at different temperatures as hydrogen peroxide activator : Synthesis mechanism and the effects on ethylbenzene removal *, Environ. Pollut. 261 (2020) 114020. https://doi.org/10.1016/j.envpol.2020.114020.

[68] Z. Fan, Q. Zhang, B. Gao, M. Li, C. Liu, Y. Qiu, Removal of hexavalent chromium by biochar supported nZVI composite: Batch and fixed-bed column evaluations, mechanisms, and secondary contamination prevention, Chemosphere. 217 (2019) 85–94. https://doi.org/10.1016/j.chemosphere.2018.11.009.

[69] J. Yu, L. Tang, Y. Pang, G. Zeng, J. Wang, Y. Deng, Y. Liu, H. Feng, S. Chen, X. Ren, Magnetic nitrogen-doped sludge-derived biochar catalysts for persulfate activation: Internal electron transfer mechanism, Chem. Eng. J. 364 (2019) 146–159. https://doi.org/10.1016/j.cej.2019.01.163.

[70] K. Zhang, B. Chen, J. Mao, L. Zhu, B. Xing, Water clusters contributed to molecular interactions of ionizable organic pollutants with aromatized biochar via π-PAHB: Sorption experiments and DFT calculations, Environ. Pollut. 240 (2018) 342–352. https://doi.org/10.1016/j.envpol.2018.04.083.

[71] X. Cui, Q. Ni, Q. Lin, K. Y. Khan, T. Li, M. B. Khan, Z. He, X. Yang, Simultaneous sorption and catalytic oxidation of trivalent antimony by Canna indica derived biochars*, Environ. Pollut. 229 (2017) 394–402. https://doi.org/10.1016/j.envpol.2017.06.005.

[72] D. Wei, B. Li, L. Luo, Y. Zheng, L. Huang, J. Zhang, Y. Yang, H. Huang, Simultaneous adsorption and oxidation of antimonite onto nano zero-valent iron sludge-based biochar : Indispensable role of reactive oxygen species and redox-active moieties, J. Hazard. Mater. 391 (2020) 122057. https://doi.org/10.1016/j.jhazmat.2020.122057.

[73] Q. Wu, W. Li, Y. Wu, Z. Huang, S. Liu, Pentosan-derived water-soluble carbon nano dots with substantial fluorescence : Properties and application as a photosensitizer, Appl. Surf. Sci. 315 (2014) 66–72. https://doi.org/10.1016/j.apsusc.2014.06.127.

[74] Q. Wu, W. Li, J. Tan, Y. Wu, S. Liu, Hydrothermal carbonization of carboxymethylcellulose : One-pot preparation of conductive carbon microspheres and water-soluble fluorescent carbon nanodots, Chem. Eng. J. 266 (2015) 112–120. https://doi.org/10.1016/j.cej.2014.12.089.

[75] B. Zhang, Y. Liu, M. Ren, W. Li, X. Zhang, R. Vajtai, P. M. Ajayan, J. M. Tour, L. Wang, Sustainable Synthesis of Bright Green Fluorescent Nitrogen-Doped Carbon Quantum Dots from Alkali Lignin, ChemSusChem 12 (2019) 4202–4210. https://doi.org/10.1002/cssc.201901693.

[76] M. Zahedifar, N. Seyedi, M. Salajeghe, S. Shafiei, Nanomagnetic biochar dots coated silver NPs (BCDs-Ag / MNPs): A highly efficient catalyst for reduction of organic dyes, Mater. Chem. Phys. 246 (2020) 122789. https://doi.org/10.1016/j.matchemphys.2020.122789.

[77] N. K. Sahoo, G. C. Jana, M. N. Aktara, S. Das, S. Nayim, A. Patra, P. Bhattacharjee, K. Bhadra, M. Hossain, Carbon dots derived from lychee waste : Application for Fe3+ ions sensing in real water and multicolor cell imaging of skin melanoma cells, Mater. Sci. Eng. C. 108 (2020) 110429. https://doi.org/10.1016/j.msec.2019.110429.

[78] Y. Liu, C. Zhu, Y. Gao, L. Yang, J. Xu, X. Zhang, C. Lu, Y. Wang, Y. Zhu, Biomass-derived nitrogen self-doped carbon dots via a simple one-pot method : Physicochemical , structural , and luminescence properties, Appl. Surf. Sci. 510 (2020) 145437. https://doi.org/10.1016/j.apsusc.2020.145437.

[79] Z. Zhu, P. Yang, X. Li, M. Luo, W. Zhang, M. Chen, X. Zhou, Green preparation

of palm powder-derived carbon dots co-doped with sulfur/chlorine and their application in visible-light photocatalysis, Spectrochim. Acta Part A Mol. Biomol. Spectrosc. 227 (2020) 117659. https://doi.org/10.1016/j.saa.2019.117659.

[80] S. Kang, Y. K. Jeong, J. H. Ryu, Y. Son, W. R. Kim, B. Lee, K. H. Jung, K. M. Kim, Pulsed laser ablation based synthetic route for nitrogen-doped graphene quantum dots using graphite flakes, Appl. Surf. Sci. 506 (2020) 144998. https://doi.org/10.1016/j.apsusc.2019.144998.

[81] T. Yoshinaga, Y. Iso, T. Isobe, Particulate, Structural, and Optical Properties of D-Glucose-Derived Carbon Dots Synthesized by Microwave-Assisted Hydrothermal Treatment, Ecs. J. Solid State Sc. 7 (2018) R3034-R3039. https://doi.org/10.1149/2.0091801jss.

[82] S. Moradi, K. Sadrjavadi, N. Farhadian, L. Hosseinzadeh, M. Shahlaei, Easy synthesis , characterization and cell cytotoxicity of green nano carbon dots using hydrothermal carbonization of Gum Tragacanth and chitosan bio-polymers for bioimaging, J. Mol. Liq. 259 (2018) 284–290. https://doi.org/10.1016/j.molliq.2018.03.054.

[83] J. Wang, C. Wang, S. Chen, Amphiphilic Egg-Derived Carbon Dots : Rapid Plasma Fabrication, Pyrolysis Process, and Multicolor Printing Patterns** Angew. Chem. Int. 51 (2012) 9297–9301. https://doi.org/10.1002/anie.201204381.

[84] G. Wei, L. Wang, L. Huo, Y. Zhang, Economical green and rapid synthesis of CDs-Cu2O/CuO nanotube from the biomass waste reed as sensitive sensing platform for the electrochemical detection of hydrazine, Talanta. 209 (2020) 120431. https://doi.org/10.1016/j.talanta.2019.120431.

[85] H. Liu, J. Ding, K. Zhang, L. Ding, Fabrication of carbon dots@restricted access molecularly imprinted polymers for selective detection of metronidazole in serum, Talanta. 209 (2020) 120508. https://doi.org/10.1016/j.talanta.2019.120508.

[86] C. Wang, H. Shi, M. Yang, Y. Yan, E. Liu, Z. Ji, J. Fan, Facile synthesis of novel carbon quantum dots from biomass waste for highly sensitive detection of iron ions, Mater. Res. Bull. 124 (2020) 110730. https://doi.org/10.1016/j.materresbull.2019.110730.

[87] X. Wang, Y. Feng, P. Dong, J. Huang, A Mini Review on Carbon Quantum Dots : Preparation, Properties, and Electrocatalytic Application, Front. Chem. 7 (2019) 1–9. https://doi.org/10.3389/fchem.2019.00671.

[88] L. Zhang, W. Liu, H. Zhuang, J. Zhang, C. Chen, Environmentally friendly synthesis of photoluminescent biochar dots from waste soy residues for rapid monitoring of potentially toxic elements, RSC Adv. 9 (2019) 21653–21659. https://doi.org/10.1039/c9ra03001h.

[89] H. Luo, S. Dimitrov, M. Daboczi, J. Kim, Q. Guo, Y. Fang, M. Stoeckel, P. Samorì, O. Fenwick, A. B. J. Sobrido, X. Wang, M. M. Titirici, Nitrogen-Doped Carbon Dots/TiO2 Nanoparticle Composites for Photoelectrochemical Water Oxidation, Applield Nano Mater. 3 (2020). https://doi.org/10.1021/acsanm.9b02412.

[90] D. W. Zhang, N. Papaioannou, N. M. David, H. Luo, H. Gao, L. C. Tanase, T. Degouse, P. Samorì, A. Sapelkin, O. Fenwick, M. M. Titirici, S. Krause, Photoelectrochemical response of carbon dots (CDs) derived from chitosan and their use in electrochemical imaging, Mater. Horizons. 5 (2018) 423–428. https://doi.org/10.1039/c7mh00784a.

[91] S. Meyer, B. Glaser, P. Quicker, Technical, economical and climate related aspects of biochar production technologies: A literature review, Environ. Sci. Technol. 45 (2011) 110930141845009. https://doi.org/10.1021/es201792c.

[92] C. E. Brewer, K. Schmidt-Rohr, J. A. Satrio, R. C. Brown, Characterization of biochar from fast pyrolysis and gasification systems, Environ. Prog. Sustain. Energy 28 (2009) 386–396 https://doi.org/10.1002/ep.10378.

[93] E. A. Hirst, A. Taylor, R. Mokaya, A simple flash carbonization route for conversion of biomass to porous carbons with high CO2 storage capacity†, J. Mater. Chem. A. 6 (2018) 12393–12403. https://doi.org/10.1039/c8ta04409k.

[94] R. J. White, T. P. Fellinger, S. Kubo, N. Brun, M. M. Titirici, Porous Hydrothermal Carbons, in: M. Titirici (Eds) Sustainable Carbon Materials from Hydrothermal Processes, Wiley, 2013, pp 37-73. https://doi.org/10.1002/9781118622179.

[95] J. Fang, B. Gao, A. R. Zimmerman, K. S. Ro, J. Chen, Physically (CO2) activated hydrochars from hickory and peanut hull: preparation, characterization, and

sorption of methylene blue, lead, copper, and cadmium†, RSC Adv. 6 (2016) 24906–24911. https://doi.org/10.1039/c6ra01644h.

[96] M. Guiotoku, F. A. Hansel, E. H. Novotny, C. M .B. F. Maia, Molecular and morphological characterization of hydrochar produced by microwave-assisted hydrothermal carbonization of cellulose, Pesqui. Agropecu. Bras. 47 (2012) 687–692. https://doi.org/10.1590/S0100-204X2012000500008.

[97] N. Zhou, H. Chen, Q. Feng, D. Yao, H. Chen, H. Wang, Z. Zhou, H. Li, Y. Tian, X. Lu, Effect of phosphoric acid on the surface properties and Pb(II) adsorption mechanisms of hydrochars prepared from fresh banana peels, J. Clean. Prod. 165 (2017) 221–230. https://doi.org/10.1016/j.jclepro.2017.07.111.

[98] S. Kubo, R. Demir-Cakan, L. Zhao, R. J. White, M. M. Titirici, Porous Carbohydrate-Based Materials via Hard Templating, ChemSusChem. 3 (2010) 188–194. https://doi.org/10.1002/cssc.200900126.

[99] M. M. Titirici, R. J. White, C. Falco, M. Sevilla, Black perspectives for a green future: hydrothermal carbons for environment protection and energy storage, Energ. Environ. Sci. 5 (2012) 6796–6822. https://doi.org/10.1039/c2ee21166a.

[100] L. Wang, W. Jia, X. Liu, J. Li, M. M. Titirici, Sulphur-doped ordered mesoporous carbon with enhance d electrocatalytic activity for the oxygen reduction reaction, J. Energy Chem. 25 (2016) 566–570. https://doi.org/10.1016/j.jechem.2016.02.012.

[101] L. Yu, C. Falco, J. Weber, R. J. White, J. Y. Howe, M. M. Titirici, Carbohydrate-Derived Hydrothermal Carbons: A Thorough Characterization Study, Langmuir. 28 (2012) 12373–12383. https://doi.org/10.1021/la3024277.

[102] B.B. Hu, K. Wang, L. Wu, S. H. Yu, M. Antonietti, M. M. Titirici, Engineering Carbon Materials from the Hydrothermal Carbonization Process of Biomass, Adv. Mater. 22 (2010) 813–828. https://doi.org/10.1002/adma.200902812.

[103] H. Deng, L. Yang, G. Tao, J. Dai, Preparation and characterization of activated carbon from cotton stalk by microwave assisted chemical activation — Application in methylene blue adsorption from aqueous solution, J. Hazard. Mater. 166 (2009) 1514–1521. https://doi.org/10.1016/j.jhazmat.2008.12.080.

[104] L. Li, B. Meng, X. Qin, Z. Yang, J. Chen, K. Yan, F. Wang, Toluene microwave cracking and reforming over bio-char with in-situ activation and ex-situ impregnation of metal, Renew. Energy 149 (2020) 1205-1213. https://doi.org/10.1016/j.renene.2019.10.115

[105] W. Li, L. Zhang, J. Peng, N. Li, X. Zhu, Preparation of high surface area activated carbons from tobacco stems with K2CO3 activation using microwave radiation, Ind. Crop. Prod. 27 (2008) 341–347. https://doi.org/10.1016/j.indcrop.2007.11.011.

[106] P. N. Y. Yek, R. K. Liew, M. S. Osman, C. H. Lee, J. H. Chuah, Y. K. Park, S. S. Lam, Microwave steam activation, an innovative pyrolysis approach to convert waste palm shell into highly microporous activated carbon, J. Environ. Manage. 236 (2019) 245–253. https://doi.org/10.1016/j.jenvman.2019.01.010.

[107] R. K. Liew, C. Chai, P. N. Y. Yek, X. Y. Phang, M. Y. Chong, W. L. Nam, M. H. Su, W. H. Lam, N. L. Ma, S. S. Lam, Innovative production of highly porous carbon for industrial effluent remediation via microwave vacuum pyrolysis plus sodium-potassium hydroxide mixture activation, J. Clean. Prod. 208 (2021) 1436–1445. https://doi.org/10.1016/j.jclepro.2018.10.214.

[108] T. Guimarães, A. P..C. Teixeira, A. F. Oliveira, R. P. Lopes, Biochars obtained from arabica coffee husks by a pyrolysis process : characterization and application in Fe(II) removal in aqueous systems†, New J. Chem. 44 (2020) 3310-3322. https://doi.org/10.1039/c9nj04144c.

[109] L. Qin, Y. Wu, Z. Hou, E. Jiang, Influence of biomass components, temperature and pressure on the pyrolysis behavior and biochar properties of pine nut shells, Biores. Technol. 313 (2020) 123682. https://doi.org/10.1016/j.biortech.2020.123682

[110] J. H. Kim, S. Jung, Y. K. Park, E. E. Kwon, CO_2-cofed catalytic pyrolysis of tea waste over Ni/SiO2 for the enhanced formation of syngas, J. Hazard. Mater. 396 (2020) 122637. https://doi.org/10.1016/j.jhazmat.2020.122637

[111] Z. Liu, A. Quek, S. K. Hoekman, R. Balasubramanian, Production of solid biochar fuel from waste biomass by hydrothermal carbonization, Fuel. 103 (2013) 943–949. https://doi.org/10.1016/j.fuel.2012.07.069.

[112] X. Zhang, L. Zhang, A. Li, Eucalyptus sawdust derived biochar generated by combining the hydrothermal carbonization and low concentration KOH modification for hexavalent chromium removal, J. Environ. Manage. 206 (2018) 989–998. https://doi.org/10.1016/j.jenvman.2017.11.079.

[113] N. Zhou, H. Chen, J. Xi, D. Yao, Z. Zhou, Y. Tian, X. Lu, Biochars with excellent Pb(II) adsorption property produced from fresh and dehydrated banana peels via hydrothermal carbonization, Bioresour. Technol. 232 (2017) 204–210. https://doi.org/10.1016/j.biortech.2017.01.074.

[114] W. T. Tsai, P. C. Huang, Y. Q. Lin, Reusing Cow Manure for the Production of Activated Carbon Using Potassium Hydroxide (KOH) Activation Process and Its Liquid-Phase Adsorption Performance, Processes. 7 (2019) 737. https://doi.org/doi:10.3390/pr7100737.

[115] O. Oginni, K. Singh, G. Oporto, B. Dawson-Andoh, L. Mcdonald, E. Sabolsky, Reports Influence of one-step and two-step KOH activation on activated carbon characteristics, Bioresour. Technol. Reports. 7 (2019) 100266. https://doi.org/10.1016/j.biteb.2019.100266.

[116] H. Ma, Z. Xu, W. Wang, Xiang Gao, H. Ma, Adsorption and regeneration of leaf-based biochar for p-nitrophenol adsorption from aqueous solution, RSC Adv. 9 (2019) 39282–39293. https://doi.org/10.1039/c9ra07943b.

[117] X. Zhang, X. Mao, L. Pi, T. Wu, Y. Hu, Adsorptive and capacitive properties of the activated carbons derived from pig manure residues, J. Environ. Chem. Eng. 7 (2019) 103066. https://doi.org/10.1016/j.jece.2019.103066.

[118] H. M. Jang, S. Yoo, Y. K. Choi, S. Park, E. Kan, Adsorption isotherm, kinetic modeling and mechanism of tetracycline on Pinus taeda -derived activated biochar, Bioresour. Technol. 259 (2018) 24–31. https://doi.org/10.1016/j.biortech.2018.03.013.

[119] A. F. Hassan, A. M. Youssef, Preparation and characterization of microporous NaOH- activated carbons from hydrofluoric acid leached rice husk and its application for lead(II) adsorption, Carbon Lett. 15 (2014) 57–66. https://doi.org/10.5714/CL.2014.15.1.057.

[120] F. Suo, X. You, Y. Ma, Y. Li, Rapid removal of triazine pesticides by P doped biochar and the adsorption mechanism, Chemosphere. 235 (2019) 918–925. https://doi.org/10.1016/j.chemosphere.2019.06.158.

[121] O. Oginni, K. Singh, G. Oporto, B. Dawson-Andoh, L. Mcdonald, E. Sabolsky, Effect of one-step and two-step H3PO4 activation on activated carbon characteristics, Bioresour. Technol. Reports. 8 (2019) 100307. https://doi.org/10.1016/j.biteb.2019.100307.

[122] Y. Fu, N. Zhang, Y. Shen, X. Ge, M. Chen, Micro-mesoporous carbons from original and pelletized rice husk via one- step catalytic pyrolysis, Bioresour. Technol. 269 (2018) 67–73. https://doi.org/10.1016/j.biortech.2018.08.083

[123] G. Chu, J. Zhao, Y. Huang, D. Zhou, Y. Liu, M. Wu, H. Peng, Q. Zhao, B. Pan, C.E.W. Steinberg, Phosphoric acid pretreatment enhances the speci fi c surface areas of biochars by generation of micropores*, Environ. Pollut. 240 (2018) 1–9. https://doi.org/10.1016/j.envpol.2018.04.003.

[124] Y. Luo, R. Li, X. Sun, X. Liu, D. Li, The roles of phosphorus species formed in activated biochar from rice husk in the treatment of landfill leachate, Bioresour. Technol. 288 (2019) 121533. https://doi.org/10.1016/j.biortech.2019.121533.

[125] Q. Yang, P. Wu, J. Liu, S. Rehman, Z. Ahmed, B. Ruan, N. Zhu, Batch interaction of emerging tetracycline contaminant with novel phosphoric acid activated corn straw porous carbon: Adsorption rate and nature of mechanism, Environ. Res. 181 (2020) 108899. https://doi.org/10.1016/j.envres.2019.108899.

[126] H. Peng, P. Gao, G. Chu, B. Pan, J. Peng, B. Xing, Enhanced adsorption of Cu(II) and Cd(II) by phosphoric acid-modified biochars, Environ. Pollut. 229 (2017) 846–853. https://doi.org/10.1016/j.envpol.2017.07.004.

[127] L. Liu, Y. Li, S. Fan, Preparation of KOH and H3PO4 Modified Biochar and Its Application in Methylene Blue Removal from Aqueous Solution, Processes. 7 (2019) 891. https://doi.org/10.3390/pr7120891.

[128] Y. Shi, G. Liu, L. Wang, H. Zhang, Activated carbons derived from hydrothermal impregnation of sucrose with phosphoric acid : remarkable adsorbents for sulfamethoxazole removal, RSC Adv. 9 (2019) 17841–17851.

https://doi.org/10.1039/c9ra02610j.

[129] N. Zhou, Y. Wang, L. Huang, J. Yu, H. Chen, J. Tang, F. Xu, X. Lu, M. Zhong, Z. Zhou, In situ modification provided by a novel wet pyrolysis system to enhance surface properties of biochar for lead immobilization, Colloids Surf, A Physicochem Eng Asp. 570 (2019) 39–47. https://doi.org/10.1016/j.colsurfa.2019.03.012.

[130] M. A. Islam, M. J. Ahmed, W. A. Khanday, M. Asif, B.H. Hameed, Mesoporous activated coconut shell-derived hydrochar prepared via hydrothermal carbonization-NaOH activation for methylene blue adsorption, J. Environ. Manage. 203 (2017) 237–244. https://doi.org/10.1016/j.jenvman.2017.07.029.

[131] D. L. Castelló, J. M. Calo, D. C. Amorós, A. L. Solano, Carbon activation with KOH as explored by temperature programmed techniques , and the effects of hydrogen, Carbon 45 (2007) 2529–2536. https://doi.org/10.1016/j.carbon.2007.08.021.

[132] X. Yao, L. Ji, J. Guo, S. Ge, W. Lu, L. Cai, Y. Wang, W. Song, H. Zhang, Magnetic activated biochar nanocomposites derived from wakame and its application in methylene blue adsorption, Bioresour. Technol. 302 (2020) 122842. https://doi.org/10.1016/j.biortech.2020.122842.

[133] C. Zhao, J. Ma, Z. Li, H. Xia, H. Liu, Y. Yang, Highly enhanced adsorption performance of tetracycline antibiotics on KOH-activated biochar derived from reed plants†, RSC Adv. 10 (2020) 5066–5076. https://doi.org/10.1039/c9ra09208k.

[134] I. S. Ismail, G. Singh, P. Smith, S. Kim, J. Yang, S. Joseph, S. Yusup, M. Singh, V. Bansal, S. N. Talapaneni, A. Vinu, Oxygen functionalized porous activated biocarbons with high surface area derived from grape marc for enhanced capture of CO2 at elevated-pressure, Carbon 160 (2020) 113–124. https://doi.org/10.1016/j.carbon.2020.01.008.

[135] D. Hsu, C. Lu, T. Pang, Y. Wang, G. Wang, Adsorption of Ammonium Nitrogen from Aqueous Solution on Chemically Activated Biochar Prepared from Sorghum Distillers Grain, Appl. Sci. 9 (2019) 5249. https://doi.org/10.3390/app9235249.

[136] Y. Shen, Y. Zhou, Y. Fu, N. Zhang, Activated carbons synthesized from unaltered and pelletized biomass wastes for bio-tar adsorption in different phases, Renew. Energy. 146 (2020) 1700–1709. https://doi.org/10.1016/j.renene.2019.07.167.

[137] S. Ding, Y. Liu, Adsorption of CO2 from flue gas by novel seaweed-based KOH-activated porous biochars, Fuel. 260 (2020) 116382. https://doi.org/10.1016/j.fuel.2019.116382.

[138] Y. Ding, T. Wang, D. Dong, Y. Zhang, Using Biochar and Coal as the Electrode Material for Supercapacitor Applications, Front. Energy Res. 7 (2020) 1–11. https://doi.org/10.3389/fenrg.2019.00159.

[139] N. Liu, Y. Liu, G. Zeng, J. Gong, X. Tan, J. Wen, S. Liu, L. Jiang, M. Li, Z. Yin, Adsorption of 17 β -estradiol from aqueous solution by raw and direct / pre / post-KOH treated lotus seedpod biochar, J. Environ. Sci. 87 (2019) 10–23. https://doi.org/10.1016/j.jes.2019.05.026.

[140] H. Wang, H. Wang, H. Zhao, Q. Yan, Adsorption and Fenton-like removal of chelated nickel from Zn-Ni alloy electroplating wastewater using activated biochar composite derived from Taihu blue algae, Chem. Eng. J. 379 (2020) 122372. https://doi.org/10.1016/j.cej.2019.122372.

[141] N. S. Trivedi, R.A. Kharkar, S. A. Mandavgane, 2,4-Dichlorophenoxyacetic acid adsorption on adsorbent prepared from groundnut shell : Effect of preparation conditions on equilibrium adsorption capacity, Arab. J. Chem. 12 (2019) 4541–4549. https://doi.org/10.1016/j.arabjc.2016.07.022.

[142] B. Zhao, X. Xu, S. Xu, X. Chen, H. Li, F. Zeng, Surface characteristics and potential ecological risk evaluation of heavy metals in the bio-char produced by co-pyrolysis from municipal sewage sludge and hazelnut shell with zinc chloride, Bioresour. Technol. 243 (2017) 375–383. https://doi.org/10.1016/j.biortech.2017.06.032.

[143] G. Singh, K. S. Lakhi, I. Y. Kim, S. Kim, P. Srivastava, R. Naidu, A. Vinu, Highly Efficient Method for the Synthesis of Activated Mesoporous Biocarbons with Extremely High Surface Area for High-Pressure CO2 Adsorption, ACS Appl. Mater. Interfaces. 9 (2017) 29782–29793. https://doi.org/10.1021/acsami.7b08797.

[144] L. Yan, Y. Liu, Y. Zhang, S. Liu, C. Wang, W. Chen, C. Liu, Z. Chen, Y. Zhang, ZnCl2 modified biochar derived from aerobic granular sludge for developed microporosity and enhanced adsorption to tetracycline, Bioresour. Technol. 297 (2020) 122381. https://doi.org/10.1016/j.biortech.2019.122381.

[145] S. Uçar, M. Erdem, T. Tay, S. Karagöz, Preparation and characterization of activated carbon produced from pomegranate seeds by ZnCl2 activation, Appl. Surf. Sci. 255 (2009) 8890–8896. https://doi.org/10.1016/j.apsusc.2009.06.080.

[146] N.R. Khalili, M. Campbell, G. Sandi, J. Golas, Production of micro- and mesoporous activated carbon from paper mill sludge: I . Effect of zinc chloride activation, Carbon 38 (2000) 1905–1915. https://doi.org/10.1016/S0008-6223(00)00043-9

[147] F. Caturla, M. Molina-Sabio, F. Rodriguez-Reinoso, Preparation of activated carbon by chemical activation with ZnCl2, Carbon 29 (1991) 999–1007. https://doi.org/10.1016/0008-6223(91)90179-M.

[148] Y. Shi, R. Shan, L. Lu, H. Yuan, H. Jiang, Y. Zhang, Y. Chen, High-efficiency removal of Cr(VI) by modified biochar derived from glue residue, J. Clean. Prod. 254 (2020) 119935. https://doi.org/10.1016/j.jclepro.2019.119935.

[149] K. Sun, Q. Huang, Y. Chi, J. Yan, Effect of ZnCl2-activated biochar on catalytic pyrolysis of mixed waste plastics for producing aromatic-enriched oil, Waste Manag. 81 (2018) 128–137. https://doi.org/10.1016/j.wasman.2018.09.054.

[150] B. Wang, M. Ran, G. Fang, T. Wu, Y. Ni, Biochars from Lignin-rich Residue of Furfural Manufacturing Process for Heavy Metal, Materials. 13 (2020) 1037. https://doi.org/10.3390/ma13051037.

[151] J. Zhang, J. Shao, Q. Jin, Z. Li, X. Zhang, Y. Chen, S. Zhang, H. Chen, Sludge-based biochar activation to enhance Pb(II) adsorption, Fuel. 252 (2019) 101–108. https://doi.org/10.1016/j.fuel.2019.04.096.

[152] X. Zhang, W. Xiang, B. Wang, J. Fang, W. Zou, F. He, Y. Li, D.C.W. Tsang, Y. S. Ok, B. Gao, Adsorption of acetone and cyclohexane onto CO2 activated hydrochars, Chemosphere. 245 (2020) 125664. https://doi.org/10.1016/j.chemosphere.2019.125664.

[153] F. L. Braghiroli, H. Bouafif, C .M. Neculita, A. Koubaa, Performance of Physically and Chemically Activated Biochars in Copper Removal from Contaminated Mine Effluents, Air Water Soil Pollut. 230:178 (2019) 1–14. https://doi.org/10.1007/s11270-019-4233-7.

[154] R. Chatterjee, B. Sajjadi, D.L. Mattern, W. Chen, T. Zubatiuk, D. Leszczynska, J. Leszczynski, N. O. Egiebor, N. Hammer, Ultrasound cavitation intensified amine functionalization: A feasible strategy for enhancing CO2 capture capacity of biochar, Fuel. 225 (2018) 287–298. https://doi.org/10.1016/j.fuel.2018.03.145.

[155] B. Sajjadi, W. Chen, D. L. Mattern, N. Hammer, A. Dorris, Engineering Low-temperature acoustic-based activation of biochar for enhanced removal of heavy metals, J. Water Process Eng. 34 (2020) 101166. https://doi.org/10.1016/j.jwpe.2020.101166.

[156] R. Chatterjee, B. Sajjadi, W. Chen, D. L. Mattern, N. O. Egiebor, N. Hammer, V. Raman, Low Frequency Ultrasound Enhanced Dual Amination of Biochar: A Nitrogen-Enriched Sorbent for CO2 Capture, Energy Fuels 33 (2019) 2366-2380. https://doi.org/10.1021/acs.energyfuels.8b03583.

[157] C. Wang, H. Wang, Y. Cao, Pb(II) sorption by biochar derived from Cinnamomum camphora and its improvement with ultrasound-assisted alkali activation, Colloids Surf. A Physicochem. Eng. Asp. 556 (2018) 177–184. https://doi.org/10.1016/j.colsurfa.2018.08.036.

[158] Y. Shan, W. Yang, Y. Li, Y. Liu, J. Pan, Preparation of microwave-activated magnetic bio-char adsorbent and study on removal of elemental mercury from fl ue gas, Sci. Total Environ. 697 (2019) 134049. https://doi.org/10.1016/j.scitotenv.2019.134049.

[159] O. Paunovic, S. Pap, S. Maletic, M. A. Taggart, N. Boskovic, M. T. Sekulic, Ionisable emerging pharmaceutical adsorption onto microwave functionalised biochar derived from novel lignocellulosic waste biomass, J. Colloid Interface Sci. 547 (2019) 350–360. https://doi.org/10.1016/j.jcis.2019.04.011.

[160] S. Liu, Y. Liu, X. Tan, G. Zeng, Y. Zhou, S. Liu, Z. Yin, L. Jiang, M. Li, J. Wen, The effect of several activated biochars on Cd immobilization and microbial community composition during in-situ remediation of heavy metal contaminated

sediment, Chemosphere. 208 (2018) 655–664. https://doi.org/10.1016/j.chemosphere.2018.06.023.

[161] S. Tang, N. Shao, C. Zheng, F. Yan, Z. Zhang, Amino-functionalized sewage sludge-derived biochar as sustainable efficient adsorbent for Cu(II) removal, Waste Manage. 90 (2019) 17–28. https://doi.org/10.1016/j.wasman.2019.04.042.

[162] D. P. Narayanan, S. K. Cherikallinmel, S. Sankaran, B. N. Narayanan, Functionalized carbon dot adorned coconut shell char derived green catalysts for the rapid synthesis of amidoalkyl naphthols, J. Colloid Interface Sci. 520 (2018) 70–80. https://doi.org/10.1016/j.jcis.2018.02.077.

[163] H. Urakami, A. G. Yilmaz, P. Osiceanu, Y. Yagci, F. Vilela, M. M. Titirici, Facile Polymer Functionalization of Hydrothermal-Carbonization-Derived Carbons, Macromol. Rapid Commun. 34 (2013) 1080–1084. https://doi.org/DOI: 10.1002/marc.201300209.

[164] S. Ye, G. Zeng, X. Tan, H. Wu, J. Liang, B. Song, N. Tang, P. Zhang, Y. Yang, Q. Chen, X. Li, Nitrogen-doped biochar fiber with graphitization from Boehmeria nivea for promoted peroxymonosulfate activation and non-radical degradation pathways with enhancing electron transfer, Appl. Catal. B Environ. 269 (2020) 118850. https://doi.org/10.1016/j.apcatb.2020.118850.

[165] Z. Guo, R. Chen, R. Yang, F. Yang, J. Chen, Y. Li, R. Zhou, J. Xu, Synthesis of amino-functionalized biochar / spinel ferrite magnetic composites for low-cost and ef fi cient elimination of Ni(II) from wastewater, Sci. Total Environ. 722 (2020) 137822. https://doi.org/10.1016/j.scitotenv.2020.137822.

[166] G. Yang, H. Jiang, Amino modification of biochar for enhanced adsorption of copper ions from synthetic wastewater, Water Res. 48 (2014) 396–405. https://doi.org/10.1016/j.watres.2013.09.050.

[167] H. Bamdad, K. Hawboldt, S. Macquarrie, Nitrogen Functionalized Biochar as a Renewable Adsorbent for Efficient CO2 Removal, Energy Fuels 32 (2018) 11742−11748. https://doi.org/10.1021/acs.energyfuels.8b03056.

[168] W. Cai, J. Wei, Z. Li, Y. Liu, J. Zhou, B. Han, Preparation of amino-functionalized magnetic biochar with excellent adsorption performance for Cr(VI) by a mild one-

step hydrothermal method from peanut hull, Colloids Surf. A Physicochem. Eng. Asp. 563 (2019) 102–111. https://doi.org/10.1016/j.colsurfa.2018.11.062

[169] Faheem, J. Bao, H. Zheng, H. Tufail, S. Irshad, J. Du, Adsorption-assisted decontamination of Hg(II) from aqueous solution by multi-functionalized corncobderived biochar, RSC Adv. 8 (2018) 38425–38435. https://doi.org/10.1039/c8ra06622a.

[170] B. Wang, Y. Jiang, F. Li, D. Yang, Preparation of biochar by simultaneous carbonization, magnetization and activation for norfloxacin removal in water, Bioresour. Technol. 233 (2017) 159–165. https://doi.org/10.1016/j.biortech.2017.02.103.

[171] M. Yang, W. Tong, J. Lee, E. Kwon, K. A. Lin, CO2 as a reaction medium for pyrolysis of lignin leading to magnetic cobalt-embedded biochar as an enhanced catalyst for Oxone activation, J. Colloid Interface Sci. 545 (2019) 16–24. https://doi.org/10.1016/j.jcis.2019.02.090.

[172] M. Yang, Y. Du, W. Tong, A .C. K. Yip, K.A. Lin, Cobalt-impregnated biochar produced from CO2-mediated pyrolysis of Co/lignin as an enhanced catalyst for activating peroxymonosulfate to degrade acetaminophen, Chemosphere. 226 (2019) 924–933. https://doi.org/10.1016/j.chemosphere.2019.04.004.

[173] N. M. Mubarak, J. N. Sahu, E. C. Abdullah, N. S. Jayakumar, Plam oil empty fruit bunch based magnetic biochar composite comparison for synthesis by microwave-assisted and conventional heating, J. Anal. Appl. Pyrolysis. 120 (2016) 521–528. https://doi.org/10.1016/j.jaap.2016.06.026.

[174] S. Jiang, L. Ling, Z. Xu, W. Liu, H. Jiang, Enhancing the Catalytic Activity and Stability of Noble Metal Nanoparticles by the Strong Interaction of Magnetic Biochar Support, Ind. Eng. Chem. Res. 57 (2018) 13055–13064. https://doi.org/10.1021/acs.iecr.8b02777.

[175] T. Han, X. Lu, Y. Sun, J. Jiang, W. Yang, P. G. Jönsson, Magnetic bio-activated carbon production from lignin via a streamlined process and its use in phosphate removal from aqueous solutions, Sci. Total Environ. 708 (2020) 135069. https://doi.org/10.1016/j.scitotenv.2019.135069.

[176] D. H. K. Reddy, S. Lee, Magnetic biochar composite: Facile synthesis, characterization , and application for heavy metal removal, Colloids Surf. A Physicochem. Eng. Asp. 454 (2014) 96–103. https://doi.org/10.1016/j.colsurfa.2014.03.105.

[177] Y. Zhai, Y. Dai, J. Guo, L. Zhou, M. Chen, H. Yang, L. Peng, Novel biochar@CoFe2O4/Ag3PO4 photocatalysts for highly efficient degradation of bisphenol a under visible-light irradiation, J. Colloid Interf. Sci. 560 (2020) 111–121. https://doi.org/10.1016/j.jcis.2019.08.065.

[178] S. Jiang, K. Xi, J. Yang, H. Jiang, Biochar-supported magnetic noble metallic nanoparticles for the fast recovery of excessive reductant during pollutant reduction, Chemosphere. 227 (2019) 63–71. https://doi.org/10.1016/j.chemosphere.2019.04.044.

[179] H. Li, D. Jiang, Z. Huang, K. He, G. Zeng, A. Chen, L. Yuan, M. Peng, T. Huang, G. Chen, Preparation of silver-nanoparticle-loaded magnetic biochar/poly (dopamine) composite as catalyst for reduction of organic dyes, J. Colloid Interface Sci. 555 (2019) 460–469. https://doi.org/10.1016/j.jcis.2019.08.013.

[180] R. K. Liew, M. Y.Chong, O. U. Osazuwa, W. L. Nam, X. Y. Phang, M. H. Su, C. K. Cheng, C. T. Chong, S. S. Lam, Production of activated carbon as catalyst support by microwave pyrolysis of palm kernel shell : a comparative study of chemical versus physical activation, Res. Chem. Intermed. 44 (2018) 3849–3865. https://doi.org/10.1007/s11164-018-3388-y.

[181] Y. Huang, K. Zheng, X. Liu, X. Meng, D. Astruc, Optimization of Cu catalysts for nitrophenol reduction , click reaction and alkyne coupling†, Inorg. Chem. Front. 7 (2020) 939–945. https://doi.org/10.1039/c9qi01449g.

[182] D. Wang, L. Salmon, J. Ruiz, D. Astruc, A recyclable ruthenium(II) complex supported on magnetic nanoparticles: a regioselective catalyst for alkyne–azide cycloaddition†, ChemComm. 49 (2013) 6956–6958. https://doi.org/10.1039/c3cc43048k.

[183] A. Nasser, L. Guo, H. Elnaggar, Y. Wang, X. Guo, A. AbdelMoneim, N. Tsubaki, Mn-Fe nanoparticles on a reduced graphene oxide catalyst for enhanced ole fi n production from syngas in a slurry reactor †, RSD Adv. 8 (2018) 14854–14863.

https://doi.org/10.1039/c8ra02193g.

[184] M. E. Ali, M. Rahman, M. S. M. Sarkar, S. Bee, A. Hamid, Heterogeneous Metal Catalysts for Oxidation Reactions, J. Nanomater. 2014 (2014). https://doi.org/10.1155/2014/192038.

[185] Y. Lee, Y. T. Kim, E. E. Kwon, J. Lee, Biochar as a catalytic material for the production of 1,4-butanediol and tetrahydrofuran from furan, Environ. Res. 184 (2020) 109325. https://doi.org/10.1016/j.envres.2020.109325.

[186] Y. Lee, S. W. Lee, Y. F. Tsang, Y. T. Kim, J. Lee, Engineered rice-straw biochar catalysts for the production of value-added chemicals from furan, Chem. Eng. J. 387 (2020) 124194. https://doi.org/10.1016/j.cej.2020.124194.

[187] L. Zhu, S. Yin, Q. Yin, H. Wang, S. Wang, Biochar: a new promising catalyst support using methanation as a probe reaction, Energy Sci. Eng. 3(2) (2015) 126–134. https://doi.org/10.1002/ese3.58.

[188] J. Gao, D. Han, Y. Xu, Y. Liu, J. Shang, Persulfate activation by sulfide-modified nanoscale iron supported by biochar (S-nZVI/BC) for degradation of ciprofloxacin, Sep. Purif. Technol. 235 (2020) 116202. https://doi.org/10.1016/j.seppur.2019.116202.

[189] J. Wu, Y. Yi, Y. Li, Z. Fang, E. P. Tsang, Excellently reactive Ni/Fe bimetallic catalyst supported by biochar for the remediation of decabromodiphenyl contaminated soil: Reactivity, mechanism, pathways and reducing secondary risks, J. Hazard. Mater. 320 (2016) 341–349. https://doi.org/10.1016/j.jhazmat.2016.08.049.

[190] C. M. Navarathna, N. B. Dewage, A. G. Karunanayake, E. L. Farmer, F. Perez, E. B.Hassan, T. E. Mlsna, C. U. Pittman Jr. Rhodamine B Adsorptive Removal and Photocatalytic Degradation on MIL-53-Fe MOF/Magnetic Magnetite/Biochar Composites, J. Inorg. Organomet. Polym. Mater. 30, (2020) 214–229. https://doi.org/10.1007/s10904-019-01322-w

[191] M. M. Mian, G. Liu, B. Fu, Y. Song, Facile synthesis of sludge-derived MnOx-N-biochar as an efficient catalyst for peroxymonosulfate activation, Appl. Catal. B: Environ. 255 (2019) 117765. https://doi.org/10.1016/j.apcatb.2019.117765.

[192] J. Qin, J. Wang, J. Yang, Y. Hu, M. Fu, D. Ye, Metal organic framework derivative-TiO2 composite as efficient and durable photocatalyst for the degradation of toluene, Appl. Catal. B Environ. 267 (2020) 118667. https://doi.org/10.1016/j.apcatb.2020.118667.

[193] Y. Qiu, X. Xu, Z. Xu, J. Liang, Y. Yu, X. Cao, Contribution of different iron species in the iron-biochar composites to sorption and degradation of two dyes with varying properties, Chem. Eng. J. 389 (2020) 124471. https://doi.org/10.1016/j.cej.2020.124471.

[194] H. Xia, Z. Peng, W. Wang, F. Tan, X. Wang, X. Qiao, One-pot preparation of magnetic Fe@Ag bimetallic catalyst for the catalytic reduction of 4-nitrophenol Desalin. Water Treat. 141 (2019) 124–132. https://doi.org/10.5004/dwt.2019.23437.

[195] W. S. Pereira, R. S. Freire, Azo dye degradation by recycled waste zero-valent iron powder, J. Braz. Chem. Soc. 17 (2006) 832–838. https://doi.org/10.1590/S0103-50532006000500003.

[196] T. Li, J. Farrell, Reductive dechlorination of trichloroethene and carbon tetrachloride using iron and palladized-iron cathodes, Environ. Sci. Technol. 34 (2000) 173–179. https://doi.org/10.1021/es9907358.

[197] A. Ghauch, A. Tuqan, H. A. Assi, Antibiotic removal from water: Elimination of amoxicillin and ampicillin by microscale and nanoscale iron particles, Environ. Pollut. 157 (2009) 1626–1635. https://doi.org/10.1016/j.envpol.2008.12.024.

[198] X. Zhang, Y. Lin, Z. Chen, 2,4,6-Trinitrotoluene reduction kinetics in aqueous solution using nanoscale zero-valent iron, J. Hazard. Mater. 165 (2009) 923–927. https://doi.org/10.1016/j.jhazmat.2008.10.075.

[199] C. D. Raman, S. Kanmani, Textile dye degradation using nano zero valent iron: A review, J. Environ. Manage. 177 (2016) 341–355. https://doi.org/10.1016/j.jenvman.2016.04.034.

[200] D. O'Carroll, B. Sleep, M. Krol, H. Boparai, C. Kocur, Nanoscale zero valent iron and bimetallic particles for contaminated site remediation, Adv. Water Resour. 51 (2013) 104–122. https://doi.org/10.1016/j.advwatres.2012.02.005.

[201] W. J. Liu, T. T. Qian, H. Jiang, Bimetallic Fe nanoparticles: Recent advances in synthesis and application in catalytic elimination of environmental pollutants, Chem. Eng. J. 236 (2014) 448–463. https://doi.org/10.1016/j.cej.2013.10.062.

[202] D. Zhang, J. Shen, H. Shi, G. Su, X. Jiang, J. Li, X. Liu, Y. Mu, L. Wang, Substantially enhanced anaerobic reduction of nitrobenzene by biochar stabilized sulfide-modi fi ed nanoscale zero-valent iron: Process and mechanisms, Environ. Int. 131 (2019) 105020. https://doi.org/10.1016/j.envint.2019.105020.

[203] K. Wang, Y. Sun, J. Tang, J. He, H. Sun, Aqueous Cr(VI) removal by a novel ball milled Fe 0 -biochar composite : Role of biochar electron transfer capacity under high pyrolysis temperature, Chemosphere. 241 (2020) 125044. https://doi.org/10.1016/j.chemosphere.2019.125044.

[204] J. Wang, G. Liu, C. Zhou, T. Li, J. Liu, Synthesis , characterization and aging study of kaolinite-supported zero-valent iron nanoparticles and its application for Ni(II) adsorption, Mater. Res. Bull. 60 (2014) 421–432. https://doi.org/10.1016/j.materresbull.2014.09.016.

[205] N. Ezzatahmadi, G. A. Ayoko, G. J. Millar, R. Speight, C. Yan, J. Li, S. Li, J. Zhu, Y. Xi, Clay-supported nanoscale zero-valent iron composite materials for the remediation of contaminated aqueous solutions : A review, Chem. Eng. J. 312 (2017) 336–350. https://doi.org/10.1016/j.cej.2016.11.154.

[206] L. Wu, L. Liao, G. Lv, F. Qin, Stability and pH-independence of nano-zero-valent iron intercalated montmorillonite and its application on Cr(VI) removal, J. Contam. Hydrol. 179 (2015) 1–9. https://doi.org/10.1016/j.jconhyd.2015.05.001.

[207] S. Froehner, M. Maceno, E. C. Da Luz, K. S. Machado, F. Falcão (2010) Degradation of Organochlorine Compounds using Zero Valent Iron (ZVI) Nanopartles Impregnated in Hydrophobic Modified Bentonite. In: Xu J., Huang PM (eds) Molecular Environmental Soil Science at the Interfaces in the Earth's Critical Zone. Springer, Berlim, Heidelberg. https://doi.org/10.1007/978-3-642-05297-2_73

[208] S. A. Kim, S. Kamala-kannan, K. J. Lee, Y. Park, P. J. Shea, W. Lee, H. Kim, B. Oh, Removal of Pb(II) from aqueous solution by a zeolite – nanoscale zero-valent iron composite, Chem. Eng. J. 217 (2013) 54–60.

https://doi.org/10.1016/j.cej.2012.11.097.

[209] Z. Li, L. Wang, J. Meng, X. Liu, J. Xu, F. Wang, P. Brookes, Zeolite-supported nanoscale zero-valent iron: New findings on simultaneous adsorption of Cd(II), Pb(II), and As(III) in aqueous solution and soil, J. Hazard. Mater. 344 (2018) 1–11. https://doi.org/10.1016/j.jhazmat.2017.09.036.

[210] Y. Guo, W. Huang, B. Chen, Y. Zhao, D. Liu, Y. Sun, B. Gong, Removal of tetracycline from aqueous solution by MCM-41-zeolite A loaded nano zero valent iron: Synthesis, characteristic, adsorption performance and mechanism, J. Hazard. Mater. 339 (2017) 22–32. https://doi.org/10.1016/j.jhazmat.2017.06.006.

[211] M. Ahmadi, M. Foladivanda, N. Jaafarzadeh, Z. Ramezani, B. Ramavandi, S. Jorfi, B. Kakavandi, Synthesis of chitosan zero-valent iron nanoparticles-supported for cadmium removal: characterization, optimization and modeling approach, J. Water Supply Res. Technol. 66 (2017) 116–130. https://doi.org/10.2166/aqua.2017.027.

[212] F. Su, H. Zhou, Y. Zhang, G. Wang, Three-dimensional honeycomb-like structured zero-valent iron/chitosan composite foams for effective removal of inorganic arsenic in water, J. Colloid Interface Sci. 478 (2016) 421–429. https://doi.org/10.1016/j.jcis.2016.06.035.

[213] H. Wu, Q. Feng, H. Yang, P. Lu, B. Gao, A. Alansari, Enhanced phenanthrene removal in aqueous solution using modified biochar supported nano zero-valent iron, Environ. Technol. 40 (2019) 3114–3123. https://doi.org/10.1080/09593330.2018.1549104.

[214] H. Lyu, J. Tang, M. Cui, B. Gao, B. Shen, Biochar/iron (BC/Fe) composites for soil and groundwater remediation : Synthesis, applications, and mechanisms, Chemosphere. 246 (2020) 125609. https://doi.org/10.1016/j.chemosphere.2019.125609.

[215] H. Woo, J. Park, S. Lee, S. Lee, Effects of washing solution and drying condition on reactivity of nano-scale zero valent irons (nZVIs) synthesized by borohydride reduction, Chemosphere. 97 (2014) 146–152. https://doi.org/10.1016/j.chemosphere.2013.11.010.

[216] S. Machado, J. G. Pacheco, H. P. A. Nouws, J. T. Albergaria, C. D. Matos, Green zero-valent iron nanoparticles for the degradation of amoxicillin, Int. J. Environ. Sci. Technol. 14 (2017) 1109–1118. https://doi.org/10.1007/s13762-016-1197-7.

[217] J. Liu, T. Mwamulima, Y. Wang, Y. Fang, S. Song, C. Peng, Removal of Pb(II) and Cr(VI) from aqueous solutions using the flyash-based adsorbent material-supported zero-valent iron, J. Mol. Liq. 243 (2017) 205–211. https://doi.org/10.1016/j.molliq.2017.08.004.

[218] C. Yu, D. Zhang, X. Dong, Q. Lin, Pyrolytic behavior of a zero-valent iron biochar composite and its Cu(II) removal mechanism, RSC Adv. 8 (2018) 34151–34160. https://doi.org/10.1039/c8ra05676e.

[219] Y. Sun, I.K.M. Yu, D.C.W. Tsang, X. Cao, D. Lin, L. Wang, N.J.D. Graham, D.S. Alessi, M. Komárek, Y. S. Ok, Y. Feng, X. D. Li, Multifunctional iron-biochar composites for the removal of potentially toxic elements, inherent cations, and hetero-chloride from hydraulic fracturing wastewater, Environ. Int. 124 (2019) 521–532. https://doi.org/10.1016/j.envint.2019.01.047.

[220] L. Kong, H. Zhang, K. Shih, M. Su, Z. Diao, J. Long, L. Hou, G. Song, D. Chen, Synthesis of FC-supported Fe through a carbothermal process for immobilizing uranium, J. Hazard. Mater. 357 (2018) 168–174. https://doi.org/10.1016/j.jhazmat.2018.05.067.

[221] M. Lawrinenko, D. A. Laird, J. H. Van Leeuwen, Sustainable Pyrolytic Production of Zerovalent Iron, ACS Sustain. Chem. Eng. 5 (2017) 767–773. https://doi.org/10.1021/acssuschemeng.6b02105.

[222] M. Lawrinenko, Z. Wang, R. Horton, D. Mendivelso-Perez, E. A. Smith, T. E. Webster, D. A. Laird, J. H. Van Leeuwen, Macroporous Carbon Supported Zerovalent Iron for Remediation of Trichloroethylene, ACS Sustain. Chem. Eng. (2017) 1586–1593. https://doi.org/10.1021/acssuschemeng.6b02375.

[223] P. Devi, A. K. Saroha, Synthesis of the magnetic biochar composites for use as an adsorbent for the removal of pentachlorophenol from the effluent, Bioresour. Technol. 169 (2014) 525–531. https://doi.org/10.1016/j.biortech.2014.07.062.

[224] Y. Yi, J. Wu, Y. Wei, Z. Fang, E. P. Tsang, The key role of biochar in the rapid

removal of decabromodiphenyl ether from aqueous solution by biochar-supported Ni/Fe bimetallic nanoparticles, J. Nanopart. Res. 19 (2017) 245. https://doi.org/10.1007/s11051-017-3927-2.

[225] H. Wu, Q. Feng, H. Yang, E. Alam, B. Gao, D. Gu, Modified biochar supported Ag/Fe nanoparticles used for removal of cephalexin in solution: Characterization, kinetics and mechanisms, Colloids Surf, A. Physicochem. Eng. Asp. 517 (2017) 63–71. https://doi.org/10.1016/j.colsurfa.2017.01.005.

[226] P. Li, K. Lin, D. Ph, Z. Fang, D. Ph, K. Wang, Enhanced nitrate removal by novel bimetallic Fe/Ni nanoparticles supported on biochar, J. Clean. Prod. 151 (2017) 21-33. http://dx.doi.org/10.1016/j.jclepro.2017.03.042.

[227] Y. Xiang, H. Liu, J. Yang, Z. Shi, Y. Tan, J. Jin, R. Wang, S. Zhang, J. Wang, Biochar decorated with gold nanoparticles for electrochemical sensing application, Electrochim. Acta. 261 (2018) 464–473. https://doi.org/10.1016/j.electacta.2017.12.162.

[228] J. Wang, J. Yang, P. Xu, H. Liu, L. Zhang, S. Zhang, L. Tian, Gold nanoparticles decorated biochar modi fi ed electrode for the high- performance simultaneous determination of hydroquinone and catechol, Sens. Actuators B Chem. 306 (2020) 127590. https://doi.org/10.1016/j.snb.2019.127590.

[229] P. Moradi, M. Hajjami, F. Valizadeh-Kakhki, Biochar as heterogeneous support for immobilization of Pd as efficient and reusable biocatalyst in C–C coupling reactions, Appl. Organomet. Chem. 33 (2019) 1-13. https://doi.org/10.1002/aoc.5205.

[230] M. L. N. Lobos, J. M. Sieben, V. Comignani, M. Duarte, M. A. Volpe, E. L. Moyano, Biochar from pyrolysis of cellulose : An alternative catalyst support for the electro-oxidation of methanol, Int. J. Hydrogen. Energ. 41 (2016) 10695-10706. https://doi.org/10.1016/j.ijhydene.2016.04.041.

[231] W. Liu, L. Ling, Y. Wang, H. He, Y. He, H. Yu, H. Jiang, One-pot high yield synthesis of Ag nanoparticle-embedded biochar hybrid materials from waste biomass for catalytic Cr(VI) reduction, Environ. Sci. Nano 3 (2016) 745–753. https://doi.org/10.1039/c6en00109b.

[232] N. Sahiner, N. Karakoyun, D. Alpaslan, N. Aktas, Biochar-Embedded Soft Hydrogel and Their Use in Ag Nanoparticle Preparation and Reduction of 4-Nitro Phenol, Int. J. Polym. Mater. 62 (2013) 590–595. https://doi.org/10.1080/00914037.2013.769163.

[233] H. Wu, Q. Feng, P. Lu, M. Chen, H. Yang, Degradation mechanisms of cefotaxime using biochar supported Co/Fe bimetallic, Environ. Sci-Wat Res. 4 (2018) 964–975. https://doi.org/10.1039/c8ew00163d.

[234] H. Li, Y. Qiu, X. Wang, J. Yang, Y. Yu, Y. Chen, Y. Liu, Biochar supported Ni/Fe bimetallic nanoparticles to remove 1,1,1-trichloroethane under various reaction conditions, Chemosphere. 169 (2017) 534–541. https://doi.org/10.1016/j.chemosphere.2016.11.117.

[235] H. Zhang, Y. Ruan, A. Liang, K. Shih, Z. Diao, M. Su, L. Hou, D. Chen, H. Lu, L. Kong, Carbothermal reduction for preparing nZVI/BC to extract uranium: Insight into the iron species dependent uranium adsorption behavior, J. Clean. Prod. 239 (2019) 117873. https://doi.org/10.1016/j.jclepro.2019.117873.

[236] Y. Liu, S. P. Sohi, S. Liu, J. Guan, J. Zhou, J. Chen, Adsorption and reductive degradation of Cr(VI) and TCE by a simply synthesized zero valent iron magnetic biochar, J. Environ. Manage. 235 (2019) 276–281. https://doi.org/10.1016/j.jenvman.2019.01.045.

[237] S. Bakshi, C. Banik, S. J. Rathke, D. A. Laird, Arsenic sorption on zero-valent iron-biochar complexes, Water Res. 137 (2018) 153–163. https://doi.org/10.1016/j.watres.2018.03.021

[238] S. Oh, Y. Seo, K. Ryu, D. Park, S. Lee, Redox and catalytic properties of biochar-coated zero-valent iron for the removal of nitro explosives and halogenated phenols†, Environ. Sci.: Process. Impacts 19 (2017) 711–719. https://doi.org/10.1039/c7em00035a.

[239] C. Zhang, J. Lu, J. Wu, One-step green preparation of magnetic seaweed biochar/sulfidated Fe0 composite with strengthen adsorptive removal of tetrabromobisphenol A through in situ reduction, Bioresour. Technol. 307 (2020) 123170. https://doi.org/10.1016/j.biortech.2020.123170.

[240] X. Shang, L. Yang, D. Ouyang, B. Zhang, W. Zhang, M. Gu, J. Li, M. Chen, L. Huang, L. Qian, Enhanced removal of 1,2,4-trichlorobenzene by modi fi ed biochar supported nanoscale zero-valent iron and palladium, Chemosphere. 249 (2020) 126518. https://doi.org/10.1016/j.chemosphere.2020.126518.

[241] L. Liu, X. Liu, D. Wang, H. Lin, L. Huang, Removal and reduction of Cr(VI) in simulated wastewater using magnetic biochar prepared by co-pyrolysis of nano-zero-valent iron and sewage sludge, J. Clean. Prod. 257 (2020) 120562. https://doi.org/10.1016/j.jclepro.2020.120562.

[242] L. Han, J. Yan, L. Qian, W. Zhang, M. Chen, Multifunctional Pd/Fe-biochar composites for the complete removal of trichlorobenzene and its degradation products, J. Environ. Manage. 245 (2019) 238–244. https://doi.org/10.1016/j.jenvman.2019.05.079.

[243] L. Qian, S. Liu, W. Zhang, Y. Chen, D. Ouyang, L. Han, J. Yan, M. Chen, Enhanced reduction and adsorption of hexavalent chromium by palladium and silicon rich biochar supported nanoscale zero-valent iron, J. Colloid Interface Sci. 533 (2019) 428–436. https://doi.org/10.1016/j.jcis.2018.08.075.

[244] Y. Yin, C. Shen, X. Bi, T. Li, Removal of hexavalent chromium from aqueous solution by fabricating novel heteroaggregates of montmorillonite microparticles with nanoscale zero-valent iron, Sci. Rep. (2020) 1–12. https://doi.org/10.1038/s41598-020-69244-z.

[245] M. Jang, B. Park, H. Lee, T. Kim, Y. Kim, Removal of hexavalent chromium ion from aqueous solution using nanoscale zero-valent iron particles immobilized on porous silica support prepared by polymer template method, Environ. Eng. 35 (2018) 2015–2023. https://doi.org/10.1007/s11814-018-0113-x.

[246] J. Huang, Y. Li, J. Wu, P. Cao, Y. Liu, G. Jiang, Floatable, macroporous structured alginate sphere supporting iron nanoparticles used for emergent Cr(VI) spill treatment, Carbohydr. Polym. 146 (2016) 115–122. https://doi.org/10.1016/j.carbpol.2016.03.035.

[247] A. Toli, K. Chalastara, C. Mystrioti, A. Xenidis, N. Papassiopi, Incorporation of zero valent iron nanoparticles in the matrix of cationic resin beads for the remediation of Cr(VI) contaminated waters, Environ. Pollut. 214 (2016) 419–429.

https://doi.org/10.1016/j.envpol.2016.04.034

[248] Y. Zhang, X. Jiao, N. Liu, J. Lv, Y. Yang, Enhanced removal of aqueous Cr(VI) by a green synthesized nanoscale zero-valent iron supported on oak wood biochar, Chemosphere 245 (2020) 125542. https://doi.org/10.1016/j.chemosphere.2019.125542.

[249] J. Yang, B. Pan, H. Li, S. Liao, D. Zhang, M. Wu, B. Xing, Degradation of p - Nitrophenol on Biochars: Role of Persistent Free Radicals, Rev. Chem. Eng. 35(7) (2016) 777–815. https://doi.org/10.1021/acs.est.5b04042.

[250] Z. Jiang, J. Li, D. Jiang, Y. Gao, Y. Chen, W. Wang, B. Cao, Y. Tao, L. Wang, Y. Zhang, Removal of atrazine by biochar-supported zero-valent iron catalyzed persulfate oxidation: Reactivity, radical production and transformation pathway, Environ. Res. 184 (2020) 109260. https://doi.org/10.1016/j.envres.2020.109260.

[251] F. Zhu, Y. Wu, Y. Liang, H. Li, W. Liang, Degradation mechanism of norfloxacin in water using persulfate activated by BC@nZVI/Ni, Chem. Eng. J. 389 (2020) 124276. https://doi.org/10.1016/j.cej.2020.124276.

[252] L. Chen, S. Yang, X. Zuo, Y. Huang, T. Cai, D. Ding, Biochar modification significantly promotes the activity of Co3O4 towards heterogeneous activation of peroxymonosulfate, Chem. Eng. J. 354 (2018) 856–865. https://doi.org/10.1016/j.cej.2018.08.098

[253] Y. Du, M. Dai, J. Cao, C. Peng, I. Ali, I. Naz, J. Li, Efficient removal of acid orange 7 using a porous adsorbent-supported zero-valent iron as a synergistic catalyst in advanced oxidation process, Chemosphere. 244 (2020) 125522. https://doi.org/10.1016/j.chemosphere.2019.125522.

[254] H. Fu, P. Zhao, S. Xu, G. Cheng, Z. Li, Y. Li, K. Li, S. Ma, Fabrication of Fe3O4 and graphitized porous biochar composites for activating peroxymonosulfate to degrade p-hydroxybenzoic acid: Insights on the mechanism, Chem. Eng. J. 375 (2019) 121980. https://doi.org/10.1016/j.cej.2019.121980.

[255] E. Magioglou, Z. Frontistis, J. Vakros, I.D. Manariotis, D. Mantzavinos, Activation of Persulfate by Biochars from Valorized Olive Stones for the Degradation of Sulfamethoxazole, Catalysts 9 (2019) 419. https://doi:10.3390/catal9050419

[256] G. Fang, J. Gao, C. Liu, D. D. Dionysiou, Y. Wang, D. Zhou, Key Role of Persistent Free Radicals in Hydrogen Peroxide Activation by Biochar: Implications to Organic Contaminant Degradation, Environ. Sci. Technol. 48 (2014) 1902–1910. https://doi.org/10.1021/es4048126.

[257] J. Liu, S. Jiang, D. Chen, G. Dai, D. Wei, Y. Shu, Activation of persulfate with biochar for degradation of bisphenol A in soil, Chem. Eng. J. 381 (2020) 122637. https://doi.org/10.1016/j.cej.2019.122637.

[258] S. Yao, X. Chen, M. A. Gomez, X. Ma, H. Wang, S. Zang, One-step synthesis of zerovalent-iron-biochar composites to activate persulfate for phenol degradation, Water Sci. Technol. 80(10) (2019) 1851–1860. https://doi.org/10.2166/wst.2020.001.

[259] J. Wei, Y. Liu, Y. Zhu, J. Li, Enhanced catalytic degradation of tetracycline antibiotic by persulfate activated with modified sludge bio-hydrochar, Chemosphere. 247 (2020) 125854. https://doi.org/10.1016/j.chemosphere.2020.125854.

[260] T.A. Nguyen, S. Oh, Biochar-mediated oxidation of phenol by persulfate activated with zero-valent iron, J. Chem. Technol. Biot. 94 (2019) 3932–3940. https://doi.org/10.1002/jctb.6194.

[261] K. Masaru , M. Ikuko, Discovery of the Activated-Carbon Radical AC+ and the Novel Oxidation-Reactions Comprising the AC/AC+ Cycle as a Catalyst in an Aqueous Solution, Bull. Chem. Soc. Jpn. 67 (1994) 2357-2360. https://doi.org/10.1246/bcsj.67.2357

[262] I. Hussain, Y. Zhang, S. Huang, Degradation of aniline with zero-valent iron as an activator of persulfate in aqueous solution†, RSC Adv. 4(7) (2014) 3502–3511. https://doi.org/10.1039/c3ra43364a.

[263] J. Chen, X. Yu, C. Li, X. Tang, Y. Sun, Removal of tetracycline via the synergistic e ff ect of biochar adsorption and enhanced activation of persulfate, Chem. Eng. J. 382 (2020) 122916. https://doi.org/10.1016/j.cej.2019.122916.

[264] Z. Pi, X. Li, D. Wang, Q. Xu, Z. Tao, X. Huang, F. Yao, Y. Wu, L. He, Q. Yang, Persulfate activation by oxidation biochar supported magnetite particles for

tetracycline removal :Performance and degradation pathway, J. Clean. Prod. 235 (2019) 1103-1115. https://doi.org/10.1016/j.jclepro.2019.07.037.

[265] C. Lai, F. Huang, G. Zeng, D. Huang, L. Qin, M. Cheng, C. Zhang, B. Li, H. Yi, S. Liu, L. Li, L. Chen, Fabrication of novel magnetic MnFe2O4/bio-char composite and heterogeneous photo-Fenton degradation of tetracycline in near neutral pH, Chemosphere. 224 (2019) 910–921. https://doi.org/10.1016/j.chemosphere.2019.02.193.

[266] J. Yu, L. Tang, Y. Pang, G. Zeng, H. Feng, J. Zou, J, Wang, C. Feng, X. Zhu, X. Ouyang, J. Tan, Hierarchical porous biochar from shrimp shell for persulfate activation : A two-electron transfer path and key impact factors, Appl. Catal. B Environ. 260 (2020) 118160. https://doi.org/10.1016/j.apcatb.2019.118160.

[267] J. Yu, Z. Zhu, H. Zhang, T. Chen, Y. Qiu, Z. Xu, D. Yin, Efficient removal of several estrogens in water by Fe-hydrochar composite and related interactive effect mechanism of H2O2 and iron with persistent free radicals from hydrochar of pinewood, Sci. Total Environ. 658 (2019) 1013–1022. https://doi.org/10.1016/j.scitotenv.2018.12.183.

[268] H. Xu, Y. Zhang, J. Li, Q. Hao, X. Li, F. Liu, Heterogeneous activation of peroxymonosulfate by a biochar-supported Co3O4 composite for efficient degradation of, Environ. Pollut. 257 (2020) 113610. https://doi.org/10.1016/j.envpol.2019.113610.

[269] X. Rong, M. Xie, L. Kong, V. Natarajan, L. Ma, J. Zhan, The magnetic biochar derived from banana peels as a persulfate activator for organic contaminants degradation, Chem. Eng. J. 372 (2019) 294–303. https://doi.org/10.1016/j.cej.2019.04.135.

[270] J. Wang, M. Shen, Q. Gong, X. Wang, J. Cai, S. Wang, Z. Chen, One-step preparation of ZVI-sludge derived biochar without external source of iron and its application on persulfate activation, Sci. Total Environ. 714 (2020) 136728. https://doi.org/10.1016/j.scitotenv.2020.136728.

[271] S. Wang, J. Wang, Peroxymonosulfate activation by Co9S8@S and N co-doped biochar for sulfamethoxazole degradation, Chem. Eng. J. 385 (2020) 123933. https://doi.org/10.1016/j.cej.2019.123933.

[272] P. Zhang, X. Tan, S. Liu, Y. Liu, G. Zeng, S. Ye, Z. Yin, X. Hu, N. Liu, Catalytic degradation of estrogen by persulfate activated with iron-doped graphitic biochar : Process variables effects and matrix effects, Chem. Eng. J. 378 (2019) 122141. https://doi.org/10.1016/j.cej.2019.122141.

[273] H. Li, F. Zhu, S. He, The degradation of decabromodiphenyl ether in the e-waste site by biochar supported nanoscale zero-valent iron/persulfate, Ecotoxicol. Environ. Saf. 183 (2019) 109540. https://doi.org/10.1016/j.ecoenv.2019.109540.

[274] C. Dong, C. Chen, C. Hung, Persulfate activation with rice husk-based magnetic biochar for degrading PAEs in marine sediments, Environ. Sci. Pollut. Res. (2019) 33781–33790. https://doi.org/10.1007/s11356-018-2423-2.

[275] Q. Mao, Y. Zhou, Y. Yang, J. Zhang, L. Liang, H. Wang, S. Luo, L. Luo, P. Jeyakumar, Y. S. Ok, M. Rizwang, Experimental and theoretical aspects of biochar-supported nanoscale zero- valent iron activating H2O2 for ciprofloxacin removal from aqueous solution, J. Hazard. Mater. 380 (2019) 120848. https://doi.org/10.1016/j.jhazmat.2019.120848.

[276] L. Li, C. Lai, F. Huang, M. Cheng, G. Zeng, D. Huang, B. Li, S. Liu, M. M. Zhang, L. Qin, M. Li, J. He, Y. Zhang, L. Chen, Degradation of naphthalene with magnetic bio-char activate hydrogen peroxide: Synergism of bio-char and Fe e Mn binary oxides, Water Res. 160 (2019) 238–248. https://doi.org/10.1016/j.watres.2019.05.081

[277] Z. Li, D. Liu, W. Huang, X. Wei, W. Huang, Biochar supported CuO composites used as an efficient peroxymonosulfate activator for highly saline organic wastewater treatment, Sci. Total Environ. 721 (2020) 137764. https://doi.org/10.1016/j.scitotenv.2020.137764.

[278] L. Gan, Q. Zhong, A. Geng, L. Wang, C. Song, S. Han, J. Cui, L. Xu, Cellulose derived carbon nanofiber : A promising biochar support to enhance the catalytic performance of CoFe2O4 in activating peroxymonosulfate for recycled dimethyl phthalate degradation, Sci. Total Environ. 694 (2019) 1–9. https://doi.org/10.1016/j.scitotenv.2019.133705

[279] V. Nguyen, T. Nguyen, C. Chen, C. Hung, C. P. Huang, C. Dong, Cobalt-impregnated biochar (Co-SCG) for heterogeneous activation of

peroxymonosulfate for removal of tetracycline in water, Bioresour. Technol. 292 (2019) 121954. https://doi.org/10.1016/j.biortech.2019.121954.

[280] J. Deng, H. Dong, C. Zhang, Z. Jiang, Y. Cheng, K. Hou, L. Zhang, C. Fan, Nanoscale zero-valent iron / biochar composite as an activator for Fenton- like removal of sulfamethazine, Sep. Purif. Technol. 202 (2018) 130–137. https://doi.org/10.1016/j.seppur.2018.03.048

[281] Y. Yang, L. Xu, W. Li, W. Fan, S. Song, J. Yang, Adsorption and degradation of sulfadiazine over nanoscale zero-valent ironencapsulated in three-dimensional graphene network through oxygen-driven heterogeneous Fenton-like reactions, Appl. Catal. B Environ. (2019) 118057. https://doi.org/10.1016/j.apcatb.2019.118057.

[282] A. Fujishima, K. Honda, Electrochemical Photolysis of Water at a Semiconductor Electrode, Nature, 238 (1972) 37–38. https://doi.org/10.1038/238037a0.

[283] M. Umar, H. A. Aziz, Photocatalytic degradation of organic pollutants in water. In: Rashed MN (ed) Organic pollutants-monitoring, risk and treatment. InTech, London, pp 195–208.

[284] M. R. Hoffmann, S. T. Martin, W. Choi, D. W. Bahnemann, Environmental Applications of Semiconductor Photocatalysis, Chem. Rev. 95 (1995) 69–96. https://doi.org/10.1021/cr00033a004.

[285] M. N. Chong, B. Jin, C. W. K. Chow, C. Saint, Recent developments in photocatalytic water treatment technology : A review, Water Res. 44 (2010) 2997–3027. https://doi.org/10.1016/j.watres.2010.02.039.

[286] K. Hashimoto, H. Irie, A. Fujishima, TiO2 Photocatalysis : A Historical Overview and Future Prospects, Jpn. J. Appl. Phys. 44 (2006) 8269–8285. https://doi.org/10.1143/JJAP.44.8269.

[287] S. Wang, Y. Zhou, S. Han, N. Wang, W. Yin, X. Yin, B. Gao, X. Wang, J. Wang, Carboxymethyl cellulose stabilized ZnO/biochar nanocomposites : Enhanced adsorption and inhibited photocatalytic degradation of methylene blue, Chemosphere. 197 (2018) 20–25. https://doi.org/10.1016/j.chemosphere.2018.01.022.

[288] R. T. Bueno, O. F. Lopes, K. T. G. Carvalho, C. Ribeiro, H. A. J. L. Mourão, Semicondutores heteroestruturados: uma abordagem sobre os principais desafios para a obtenção e aplicação em processos fotoquímicos ambientais e energéticos, Quim. Nova. XY (2019) 1–15. http://dx.doi.org/10.21577/0100-4042.20170372.

[289] X. Yuan, L. Jiang, J. Liang, Y. Pan, J. Zhang, H. Wang, L. Leng, Z. Wu, R. Guan, G. Zeng, In-situ synthesis of 3D microsphere-like In2S3/InVO4 heterojunction with efficient photocatalytic activity for tetracycline degradation under visible light irradiation, Chem. Eng. J. 356 (2019) 371–381. https://doi.org/10.1016/j.cej.2018.09.079.

[290] Y. Lv, S. Duan, R. Wang, Structure design, controllable synthesis, and application of metal- semiconductor heterostructure nanoparticles, Prog. Nat. Sci. Mater. Int. 30 (2020) 1–12. https://doi.org/10.1016/j.pnsc.2019.12.005.

[291] M. Fang, C. Tsao, Y. Hsu, Semiconductor nanoheterostructures for photoconversion applications, J. Phys. D Appl. Phys. 53 (2020) 143001. https://doi.org/10.1088/1361-6463/ab5f25.

[292] B. Wang, J. Cao, Y. Liu, Recent progress of heterostructure-based photoelectrodes in photoelectrochemical biosensing : a mini review, Analyst. 145 (2020) 1121–1128. https://doi.org/10.1039/c9an02448d.

[293] X. Peng, M. Wang, F. Hu, F. Qiu, H. Dai, Z. Cao, Facile fabrication of hollow biochar carbon-doped TiO2/CuO composites for the photocatalytic degradation of ammonia nitrogen from aqueous solution, J. Alloys Compd. 770 (2019) 1055–1063. https://doi.org/10.1016/j.jallcom.2018.08.207.

[294] X. Xie, S. Li, H. Zhang, Z. Wang, H. Huang, Promoting charge separation of biochar-based Zn-TiO2/pBC in the presence of ZnO for ef fi cient sulfamethoxazole photodegradation under visible light irradiation, Sci. Total Environ. 659 (2019) 529–539. https://doi.org/10.1016/j.scitotenv.2018.12.401.

[295] M. M. Mian, G. Liu, Sewage sludge-derived TiO2/Fe/Fe3C-biochar composite as an ef fi cient heterogeneous catalyst for degradation of methylene blue, Chemosphere 215 (2019) 101-114. https://doi.org/10.1016/j.chemosphere.2018.10.027.

[296] H. Zhang, Z. Wang, R. Li, J. Guo, Y. Li, J, Zhu, X. Xie, TiO2 supported on reed straw biochar as an adsorptive and photocatalytic composite for the efficient degradation of sulfamethoxazole in aqueous matrices, Chemosphere. 185 (2017) 351–360. https://doi.org/10.1016/j.chemosphere.2017.07.025.

[297] J. Hu, L. Zhang, B. Lu, X. Wang, H. Huang, LaMnO3 nanoparticles supported on N doped porous carbon as e ffi cient photocatalyst, Vacuum 159 (2019) 59–68. https://doi.org/10.1016/j.vacuum.2018.10.021.

[298] L. Lu, R. Shan, Y. Shi, S. Wang, H. Yuan, A novel TiO2/biochar composite catalysts for photocatalytic degradation of methyl orange, Chemosphere. 222 (2019) 391–398. https://doi.org/10.1016/j.chemosphere.2019.01.132.

[299] J. R. Kim, E. Kan, Heterogeneous photocatalytic degradation of sulfamethoxazole in water using a biochar-supported TiO2 photocatalyst, J. Environ. Manage. 180 (2016) 94–101. https://doi.org/10.1016/j.jenvman.2016.05.016.

[300] H. Li, J. Hu, X. Wang, L. An, Development of a bio-inspired photo-recyclable feather carbon adsorbent towards removal of amoxicillin residue in aqueous solutions, Chem. Eng. J. 373 (2019) 1380–1388. https://doi.org/10.1016/j.cej.2019.03.160.

[301] X. Cai, J. Li, Y. Liu, Z. Yan, X. Tan, S. Liu, G. Zeng, Y. Gu, X. Hu, L. Jiang, Titanium dioxide-coated biochar composites as adsorptive and photocatalytic degradation materials for the removal of aqueous organic, J. Chem. Technol. Biot. 93 (2018) 783–791. https://doi.org/10.1002/jctb.5428.

[302] S. Zhang, X. Lu, Treatment of wastewater containing Reactive Brilliant Blue KN-R using TiO2/BC composite as heterogeneous photocatalyst and adsorbent, Chemosphere. 206 (2018) 777–783. https://doi.org/10.1016/j.chemosphere.2018.05.073.

[303] R. Shan, L. Lu, J. Gu, Y. Zhang, H. Yuan, Y. Chen, B. Luo, Materials Science in Semiconductor Processing Photocatalytic degradation of methyl orange by Ag/TiO2/biochar composite catalysts in aqueous solutions, Mater. Sci. Semicond. Process. 114 (2020) 105088. https://doi.org/10.1016/j.mssp.2020.105088.

[304] A. A. El-Bindary, S. M. El-Marsafy, A. A. El-Maddah, Enhancement of the

photocatalytic activity of ZnO nanoparticles by silver doping for the degradation of AY99 contaminants, J. Mol. Struct. 1191 (2019) 76–84. https://doi.org/10.1016/j.molstruc.2019.04.064.

[305] K. Guan, P. Zhou, J. Zhang, L. Zhu, Synthesis and characterization of ZnO@RSDBC composites and their Photo-Oxidative degradation of Acid Orange 7 in water, J. Mol. Struct. 1203 (2020) 127425. https://doi.org/10.1016/j.molstruc.2019.127425.

[306] Y. Zhang, P. Su, D. Weathersby, Q. Zhang, J. Zheng, R. Fan, J. Zhang, Q. Dai, Synthesis of γ-Fe2O3-ZnO-biochar nanocomposites for Rhodamine B removal, Appl. Surf. Sci. 501 (2020) 144217. https://doi.org/10.1016/j.apsusc.2019.144217.

[307] K. Hayat, S.S. Shah, M. Yousaf, M.J. Iqbal, M. Ali, S. Ali, M. Ajmal, Y. Iqbal, Processing, device fabrication and electrical characterization of LaMnO3 nanofibers, Mater Sci Semicond Process. 41 (2016) 364–369. https://doi.org/10.1016/j.mssp.2015.10.009.

[308] M. Shaterian, M. Enhessari, D. Rabbani, M. Asghari, M. Salavati-Niasari, Synthesis , characterization and photocatalytic activity of LaMnO3 nanoparticles, Appl. Surf. Sci. 318 (2014) 213–217. https://doi.org/10.1016/j.apsusc.2014.03.087.

[309] L. Meng, W. Yin, S. Wang, X. Wu, J. Hou, W. Yin, K. Feng, Y. Sik, X. Wang, Photocatalytic behavior of biochar-modified carbon nitride with enriched visible-light reactivity, Chemosphere. 239 (2020) 124713. https://doi.org/10.1016/j.chemosphere.2019.124713.

[310] F. Li, M. Lin, Synthesis of Biochar-Supported K-doped g-C3N4 Photocatalyst for Enhancing the Polycyclic Aromatic Hydrocarbon Degradation Activity, Int. J. Environ. Res. Public Health 17(6): (2020) 2065. https://doi.org/10.3390/ijerph17062065.

[311] M. Chen, Y. Dai, J. Guo, H. Yang, D. Liu, Y. Zhai, Solvothermal synthesis of biochar@ZnFe2O4/BiOBr Z-scheme heterojunction for efficient photocatalytic ciprofloxacin degradation under visible light, Appl. Surf. Sci. 493 (2019) 1361–1367. https://doi.org/10.1016/j.apsusc.2019.04.160.

[312] A. Geng, L. Xu, L. Gan, C. Mei, L. Wang, X. Fang, M. Li, M. Pan, S. Han, J. Cui, Using wood flour waste to produce biochar as the support to enhance the visible-light photocatalytic performance of BiOBr for organic and inorganic contaminants removal, Chemosphere. 250 (2020) 126291. https://doi.org/10.1016/j.chemosphere.2020.126291.

[313] S. Li, Z. Wang, X. Xie, G. Liang, X. Cai, X. Zhang, Z. Wang, Fabrication of vessel-like biochar-based heterojunction photocatalyst Bi2S3/BiOBr/BC for diclofenac removal under visible LED light irradiation : Mechanistic investigation and intermediates analysis, J. Hazard. Mater. 391 (2020) 121407. https://doi.org/10.1016/j.jhazmat.2019.121407.

[314] M. F. Arkaan, R. F. Ekaputri, I. Fatimah, A. Kamari, Physicochemical and photocatalytic activity of hematite/biochar nanocomposite prepared from Salacca skin waste, Sustain. Chem. Pharm. 16 (2020) 100261. https://doi.org/10.1016/j.scp.2020.100261.

[315] T. Fazal, A. Razzaq, F. Javed, A. Hafeez, N. Rashid, U. S. Amjad, M. S. U. Rehman, A. Faisal, F. Rehman, Integrating adsorption and photocatalysis: A cost effective strategy for textile wastewater treatment using hybrid biochar-TiO2 composite, J. Hazard. Mater. 390 (2020) 121623. https://doi.org/10.1016/j.jhazmat.2019.121623.

[316] T. Wang, S. Liu, W. Mao, Y. Bai, K. Chiang, K. Shah, J. Paz-Ferreiro, Novel Bi2WO6 loaded N-biochar composites with enhanced photocatalytic degradation of rhodamine B and Cr(VI), J. Hazard. Mater. 389 (2020) 121827. https://doi.org/10.1016/j.jhazmat.2019.121827.

[317] N. Zhu, C. Li, L. Bu, C. Tang, S. Wang, P. Duan, L. Yao, J. Tang, D. D. Dionysiou, Y. Wu, Bismuth impregnated biochar for efficient estrone degradation : The synergistic effect between biochar and Bi/Bi2O3 for a high photocatalytic performance, J. Hazard. Mater. 384 (2020) 121258. https://doi.org/10.1016/j.jhazmat.2019.121258.

[318] M. Thiruppathi, K. Leeladevi, C. Ramalingan, K. Chen, E. R. Nagarajan, Processing Construction of novel biochar supported copper tungstate nanocomposites : A fruitful divergent catalyst for photocatalysis and

electrocatalysis, Mater. Sci. Semicond. Process. 106 (2020) 104766. https://doi.org/10.1016/j.mssp.2019.104766.

[319] P. Gholami, A. Khataee, R. D. C. Soltani, L. Dinpazhoh, A. Bhatnagar, Photocatalytic degradation of gemifloxacin antibiotic using Zn-Co-LDH@biochar nanocomposite, J. Hazard. Mater. 382 (2020) 121070. https://doi.org/10.1016/j.jhazmat.2019.121070

[320] Y. Yu, Q. An, L. Jin, N. Luo, Z. Li, J. Jiang, Unraveling sorption of Cr(VI) from aqueous solution by FeCl3 and ZnCl2 - modified corn stalks biochar : Implicit mechanism and application, Bioresour. Technol. 297 (2020) 122466. https://doi.org/10.1016/j.biortech.2019.122466.

[321] A. Khataee, D. Kalderis, P. Gholami, A. Fazli, M. Moschogiannaki, V. Binas, M. Lykakig, M. Konsolakisg, Cu2O-CuO@biochar composite : Synthesis, characterization and its efficient photocatalytic performance, Appl. Surf. Sci. 498 (2019) 143846. https://doi.org/10.1016/j.apsusc.2019.143846.

[322] Q. Men, T. Wang, C. Ma, L. Yang, Y. Liu, P. Huo, Y. Yan, In-suit preparation of CdSe quantum dots / porous channel biochar for improving photocatalytic activity for degradation of tetracycline, J Taiwan Inst. Chem. E. 99 (2019) 180–192. https://doi.org/10.1016/j.jtice.2019.03.019

[323] T. Wang, X. Liu, Q. Men, C. Ma, Y. Liu, W. Ma, Z. Liu, Ma. Wei, C. Li, Y. Yan, Surface plasmon resonance effect of Ag nanoparticles for improving the photocatalytic performance of biochar quantum-dot/Bi4Ti3O12 nanosheets, Chinese J. Catal. 40 (2019) 886–894. https://doi.org/10.1016/S1872-2067(19)63330-9.

[324] T. Kulandaivalu, S. A. Rashid, N. Sabli, T. L. Tan, Visible light assisted photocatalytic reduction of CO2 to ethane using CQDs/Cu2O nanocomposite photocatalyst, Diam. Relat. Mater. 91 (2019) 64–73. https://doi.org/10.1016/j.diamond.2018.11.002.

[325] A. Kumar, A. Kumar, G. Sharma, A.H. Al-muhtaseb, M. Naushad, A.A. Ghfar, C. Guo, F.J. Stadler, Biochar-templated g-C3N4/Bi2O2CO3/CoFe2O4 nano-assembly for visible and solar assisted photo-degradation of paraquat, nitrophenol reduction and CO2 conversion, Chem. Eng. J. 339 (2018) 393–410.

https://doi.org/10.1016/j.cej.2018.01.105.

[326] A. Kumar, Shalini, G. Sharma, M. Naushad, A. Kumar, S. Kalia, C. Guo, G. T. Mola, Facile hetero-assembly of superparamagnetic Fe3O4/BiVO4 stacked on biochar for solar photo-degradation of methyl paraben and pesticide removal from soil, J. Photochem. Photobiol. A 337 (2017) 118–131. https://doi.org/10.1016/j.jphotochem.2017.01.010.

[327] W. Wang, J. Zhang, T. Chen, J. Sun, X. Ma, Y. Wang, J. Wang, X. Z. Xie, Preparation of TiO2-modified Biochar and its Characteristics of Photo-catalysis Degradation for Enrofloxacin, Sci. Rep. 10:6588 (2020) 1–12. https://doi.org/10.1038/s41598-020-62791-5.

[328] P. Lisowski, J. C. Colmenares, O. Mašek, W. Lisowski, D. Lisovytskiy, A. Kamińska, D. Łomot, Dual Functionality of TiO2/Biochar Hybrid Materials: Photocatalytic Phenol Degradation in the Liquid Phase and Selective Oxidation of Methanol in the Gas Phase, ACS Sustain. Chem. Eng. 5 (2017) 274–6287. https://doi.org/10.1021/acssuschemeng.7b01251.

[329] Donglin Zhao, Xin Yang, Changlun Chen, Xiangke Wang, Enhanced photocatalytic degradation of methylene blue on multiwalled carbon nanotubes-TiO2, J. Colloid Interface Sci. 398 (2013) 234–239. https://doi.org/10.1016/j.jcis.2013.02.017.

[330] T. A. Kurniawan, Z. Mengting, D. Fu, S. K. Yeap, M. Hafiz, M. H. D. Othman, R. Avtar, T. Ouyang, Functionalizing TiO2 with graphene oxide for enhancing photocatalytic degradation of methylene blue (MB) in contaminated wastewater, J. Environ. Manage. 270 (2020) 110871. https://doi.org/10.1016/j.jenvman.2020.110871.

[331] S. Silvestri, N. Stefanello, A. A. Sulkovski, E. L. Folleto, Preparation of TiO2 supported on MDF biochar for simultaneous removal of methylene blue by adsorption and photocatalysis, J. Chem. Technol. Biot. (2019). https://doi.org/10.1002/jctb.6279.

[332] L. Cao, I. K. M. Yu, D. C. W. Tsang, S. Zhang, Y. S. Ok, E. E. Kwon, H. Song, C. S. Poon, Phosphoric acid-activated wood biochar for catalytic conversion of starch- rich food waste into glucose and 5-hydroxymethylfurfural, Bioresour.

Technol. 267 (2018) 242–248. https://doi.org/10.1016/j.biortech.2018.07.048.

[333] I. K. M. Yu, X. Xiong, D. C. W. Tsang, L. Wang, A. J. Hunt, H. Song, J. Shang, Y. S. Ok, C. S. Poon, Aluminium-biochar composites as sustainable heterogeneous catalysts for glucose isomerisation in a biorefinery, Green Chem. 21 (2019) 1267-1281. https://doi.org/10.1039/c8gc02466a.

[334] A. Fuente-Hernández, R. Lee, N. Béland, I. Zamboni, J. Lavoie, Reduction of Furfural to Furfuryl Alcohol in Liquid Phase over a Biochar-Supported Platinum Catalyst, Energies 10 (2017) 286. https://doi.org/10.3390/en10030286.

[335] Z. Chen, Q. Li, Y. Xiao, C. Zhang, Z. Fu, Y. Liu, X. Yi, A. Zheng, C. Li, D. Yin, Acid–base synergistic catalysis of biochar sulfonic acid bearing polyamide for microwave-assisted hydrolysis of cellulose in water, Cellulose. 26 (2019) 751–762. https://doi.org/10.1007/s10570-018-2098-3.

[336] H. Xia, S. Xu, H. Hu, J. An, C. Li, Efficient conversion of 5-hydroxymethylfurfural to high-value chemicals by chemo- and bio-catalysis RSC Adv. 8 (2018) 30875–30886. https://doi.org/10.1039/c8ra05308a.

[337] F. D. Pileidis, M. M. Titirici, Levulinic Acid Biorefineries: New Challenges for Efficient Utilization of Biomass, ChemSusChem. 9 (2016) 562–582. https://doi.org/10.1002/cssc.201501405.

[338] I. K. M. Yu, D. C. W. Tsang, A. C. K. Yip, S. S. Chen, L. Wang, Y. S. Ok, C. S. Poon, Catalytic valorization of starch-rich food waste into hydroxymethylfurfural (HMF): Controlling relative kinetics for high productivity, Bioresour. Technol. 237 (2017) 222–230. https://doi.org/10.1016/j.biortech.2017.01.017.

[339] L. Cao, I.K.M. Yu, S.S. Chen, D.C.W. Tsang, L. Wang, X. Xiong, S. Zhang, Y. S. Ok, E.E. Kwon, H. Song, C. S. Poon, Production of 5-hydroxymethylfurfural from starch-rich food waste catalyzed by sulfonated biochar, Bioresour. Technol. 252 (2018) 76–82. https://doi.org/10.1016/j.biortech.2017.12.098.

[340] C. Zhang, Z. Cheng, Z. Fu, Y. Liu, X. Yi, A. Zheng, S. R. Kirk, D. Yin, Effective transformation of cellulose to 5-hydroxymethyl- furfural catalyzed by fluorine anion-containing ionic liquid modified biochar sulfonic acids in water, Cellulose. 24 (2017) 95–106. https://doi.org/10.1007/s10570-016-1118-4.

[341] X. Yang, I. K. M. Yu, D. Cho, S. S. Chen, D. C. W. Tsang, J. Shang, A. C. K. Yip, L. Wang, Y. S. Ok, Tin-Functionalized Wood Biochar as a Sustainable Solid Catalyst for Glucose Isomerization in Biorefinery, 7 (2019) 4851–4860. https://doi.org/10.1021/acssuschemeng.8b05311.

[342] X. Xiong, I. K. M. Yu, D. C. W. Tsang, L. Chen, Z. Su, C. Hu, G. Luo, S. Zhang, Y. S. Ok, J. H. Clark, Study of glucose isomerisation to fructose over three heterogeneous carbon-based aluminium-impregnated catalysts, J. Clean. Prod. 268 (2020) 122378. https://doi.org/10.1016/j.jclepro.2020.122378.

[343] C. Zhu, H. Wang, H. Li, B. Cai, W. Lv, C. Cai, C. Wang, L. Yan, Q. Liu, L. Ma, Selective Hydrodeoxygenation of 5-Hydroxymethylfurfural to 2,5-Dimethylfuran over Alloyed Cu–Ni Encapsulated in Biochar Catalysts, Acs Sustain. Chem. Eng. 7 (2019) 19556–19569. https://doi.org/10.1021/acssuschemeng.9b04645.

[344] L. Liu, X. Yang, Q. Hou, S. Zhang, M. Ju, Corn stalk conversion into 5-hydroxymethylfurfural by modi fi ed biochar catalysis in a multi-functional solvent, J. Clean. Prod. 187 (2018) 380–389. https://doi.org/10.1016/j.jclepro.2018.03.234.

[345] S.M. Al-amsyar, F. Adam, E. Ng, Aluminium oxide-silica / carbon composites from rice husk as a bi-functional heterogeneous catalyst for the one-pot sequential reaction in the conversion of glucose, Surf. Interfaces. 9 (2017) 1–8. https://doi.org/10.1016/j.surfin.2017.06.011.

[346] D. Buentello-Montoya, X. Zhang, J. Li, V. Ranade, S. Marques, M. Geron, Performance of biochar as a catalyst for tar steam reforming : Effect of the porous structure, Appl. Energy 259 (2020) 114176. https://doi.org/10.1016/j.apenergy.2019.114176.

[347] Y. Shen, P. Zhao, Q. Shao, D. Ma, F. Takahashi, K. Yoshikawaa, In-situ catalytic conversion of tar using rice husk char-supported nickel-iron catalysts for biomass pyrolysis/gasification, Appl. Catal. B-Environ. 153 (2014) 140–151. https://doi.org/10.1016/j.apcatb.2014.01.032

[348] L. Cheng, Z. Wu, Z. Zhang, C. Guo, N. Ellis, X. Bi, A. P. Watkinson, J. R. Grace, Tar elimination from biomass gasification syngas with bauxite residue derived catalysts and gasification char, Appl. Energy. 258 (2020) 114088.

https://doi.org/10.1016/j.apenergy.2019.114088.

[349] D. Wang, W. Yuan, W. Ji, Char and char-supported nickel catalysts for secondary syngas cleanup and conditioning, Appl. Energy 88 (2011) 1656–1663. https://doi.org/10.1016/j.apenergy.2010.11.041.

[350] S. Anis, Z.A. Zainal, Tar reduction in biomass producer gas via mechanical , catalytic and thermal methods: A review, Renew. Sustain. Energy Rev. 15 (2011) 2355–2377. https://doi.org/10.1016/j.rser.2011.02.018.

[351] S. Krerkkaiwan, A. Tsutsumi, P. Kuchonthara, Biomass derived tar decomposition over coal char bed, Sci Asia 39 (2013) 511–519. https://doi.org/10.2306/scienceasia1513-1874.2013.39.511.

[352] S. Mueangta, P. Kuchonthara, S. Krerkkaiwan, Catalytic Steam Reforming of Biomass-Derived Tar over the Coal/Biomass Blended Char:Effect of Devolatilization Temperature and Biomass Type, Energ. Fuel 33 (2019) 3290–3298. https://doi.org/10.1021/acs.energyfuels.9b00320.

[353] T. He, Z. Sun, J. Wu, Z. Xu, D. Zhang, D. Han, Catalytic Performance of Coal Char for theMethane Reforming Process, Chem. Eng. Technol. 38 (2015) 68–74. https://doi.org/10.1002/ceat.201400124.

[354] L. Burhenne, T. Aicher, Benzene removal over a fixed bed of wood char: The effect of pyrolysis temperature and activation with CO2 on the char reactivity, Fuel Process. Technol. 127 (2014) 140–148. https://doi.org/10.1016/j.fuproc.2014.05.034.

[355] Z. A. El-Rub, E. A. Bramer, G. Brem, Experimental comparison of biomass chars with other catalysts for tar reduction, Fuel 87 (2008) 2243–2252. https://doi.org/10.1016/j.fuel.2008.01.004.

[356] Q. Sun, S. Yu, F. Wang, J. Wang, Decomposition and gasification of pyrolysis volatiles from pine wood through a bed of hot char, Fuel. 90 (2011) 1041–1048. https://doi.org/10.1016/j.fuel.2010.12.015.

[357] B. Lai, Y. Zhang, Y. Yuan, Z. Chen, P. Yang, Influence of Preparation Conditions on Characteristics, Reactivity, and Operational Life of Microsized Fe/Cu Bimetallic

Particles, Ind. Eng. Chem. Res. 53 (2014) 12295–12304. https://doi.org/10.1021/ie501756m.

[358] L. Li, K. Yan, J. Chen, T. Feng, F. Wang, J. Wang, Z. Song, C. Ma, Fe-rich biomass derived char for microwave-assisted methane reforming with carbon dioxide, Sci. Total Environ. 657 (2019) 1357–1367. https://doi.org/10.1016/j.scitotenv.2018.12.097.

[359] L. Xu, L. Duan, M. Tang, P. Liu, X. Ma, Y. Zhang, H. G. Harris, M. Fan, Catalytic CO2 reforming of CH4 over Cr-promoted Ni/char for H2 production, Int. J. Hydrogen Energ. 9 (2014) 10141-10153. https://doi.org/10.1016/j.ijhydene.2014.04.172.

[360] B. R. Vasconcelos, D. P. Minh, E. Martins, A. Germeau, P. Sharrock, A. Nzihou, Highly-efficient hydroxyapatite-supported nickel catalysts for dry reforming of methane, Int. J. Hydrog. Energy 5 (2019) 18502-18518. https://doi.org/10.1016/j.ijhydene.2019.08.068.

[361] L. Li, X. Jiang, H. Wang, J. Wang, Z. Song, X. Zhao, C. Ma, Methane dry and mixed reforming on the mixture of bio-char and nickel-based catalyst with microwave assistance, J. Anal. Appl. Pyrol. 125 (2017) 318–327. https://doi.org/10.1016/j.jaap.2017.03.009.

[362] D. Astruc, Introduction: Nanoparticles in Catalysis. Chem. Rev. 120 (2020) 461-463. https://doi.org/10.1021/acs.chemrev.8b00696.

[363] F. Lu, D. Astruc. Nanocatalysts and other nanomaterials for water remediation from organic pollutants. Coord. Chem. Rev. 120 (2020) 213180. https://doi.org/10.1016/j.ccr.2020.213180.

[364] F. Lu, D. Astruc. Nanomaterials for removal of toxic elements from water. Coord. Chem. Rev. 356 (2018) 147-164. https://doi.org/10.1016/j.ccr.2017.11.003.

[365] S. A. Nicolae, H. Au, P. Modugno, H. Luo, A. E. Szego, M. Qiao, L. Li, W. Yin, H. J. Heeres, N. Berge, M. M. Titirici. Recent advances in hydrothermal carbonisation: from tailored carbon materials and biochemicals to applications

and bioenergy. Green Chem. 22 (2020) 4747-4800. https://doi.org/10.1039/d0gc00998a.

Agro-industrial waste

Syngas, Bio-oil and Biochar

Biomass Carbonization

Biochar: Catalyst and support